This is a preprint, the final version is subject to change, of the American Mineralogist (MSA)
Cite as Authors (Year) Title. American Mineralogist, in press.
(DOI will not work until issue is live.) DOI: http://dx.doi.org/10.2138/am-2016-5402

Revision 4

Review Article

Rates and Styles of Planetary Cooling on Earth, Moon, Mars and Vesta, Using New Models for Oxygen Fugacity, Ferric-Ferrous Ratios, Olivine-liquid Fe-Mg Exchange, and Mantle Potential Temperature

Keith Putirka

Department of Earth and Environmental Sciences, California State University - Fresno, 2345 E. San Ramon Ave, MS/MH24, Fresno, CA 93720, kputirka@csufresno.edu

ABSTRACT

Mantle potential temperatures (T_p) provide insights into mantle circulation, and tests of whether Earth is the only planet to exhibit thermally bi-modal volcanism—a distinctive signature of modern plate tectonics. Planets that have a stagnant lid, for example, should exhibit volcanism that is uni-modal with T_p, since mantle plumes would have a monopoly on the genesis of volcanism. But new studies of magmatic ferric-ferrous ratios ($X_{Fe2O3}^{liq}/X_{FeO}^{liq}$) (Cottrell and Kelley 2011) and the olivine-liquid Fe-Mg exchange coefficient, $K_D(Fe\text{-}Mg)^{ol\text{-}liq}$ (or K_D) (Matzen et al. 2011) indicate that re-evaluations of T_p are needed. New tests and calibrations are thus presented for oxygen fugacity (fO_2), $X_{Fe2O3}^{liq}/X_{FeO}^{liq}$, potential temperature (T_p), melt fraction (F), K_D, and peridotite enthalpies of fusion (ΔH_{fus}) and heat capacities (C_p). The new models for $X_{Fe2O3}^{liq}/X_{FeO}^{liq}$ and fO_2 reduce error by 25-30%, and residual error for all models appears random; this last observation supports the common, but mostly untested, assumption that equilibrium is the most probable of states obtained by experiment, and perhaps in nature as well. Aggregate 1σ error on T_p is as high as ~±77ºC, and estimates of F, and mantle olivine composition, are the greatest sources of error. Pressure and ΔH_{fus} account for smaller, but systematic

uncertainties (a constant ΔH_{fus} can under-predict $T_{excess} = T_p^{plume} - T_p^{ambient}$; assumptions of 1-atm can under-predict T_p). However, assumptions about whether parental magmas are incremental, accumulated, or isobaric batch melts induces no additional systematic error.

The new models show that maximum T_p estimates on the oldest samples from Earth, Mars, Moon, and Vesta, decrease as planet size decreases. This may be expected since T_p should scale with accretion energy, and reflect the Clausius-Clapeyron slope for the melting of silicates and Fe-Ni alloys. This outcome, however, occurs only if shergottites (from Mars) are 4.3 Ga (e.g., Bouvier et al. 2009; Werner et al. 2014), and the highest MgO komatiites from Earth's Archean era (27-30% MgO; Green et al. 1975) are used to estimate T_p. With these assumptions, Earth and Mars exhibit monotonic cooling, and support for Stevenson's (2003) idea that smaller planets cool at similar rates (~90-135ºC/Ga), but at lower absolute temperatures. T_p estimates for Mars and Earth are also important in two other ways: Mars exhibits non-linear cooling, with rates as high as 275-550ºC/Ga in its first 0.5 Ga. Archean volcanism on Earth was thermally bi-modal; several hundred Archean volcanic compositions are in equilibrium with Fo92-94 olivine, and yield T_p modes at 1940ºC and 1720ºC, possibly representing plume and ambient mantle respectively. These compare to modern T_p values of 1560-1670ºC at Mauna Loa (plume) and 1330-1450ºC at MORB (ambient). We conclude that plate tectonics were thus active in some manner in the Archean, and that assertions of an Archean "thermal catastrophe" are exaggerated. Our new models also show that the modern Hawaiian source, when compared at the same T, has a lower fO_2 compared to MORB, which would discount a Hawaiian source rich in recycled pyroxenite.

INTRODUCTION

The rate at which a planet cools may control whether or how plate tectonics develop (e.g., Stevenson 2003), and consequently how life might evolve. Numerical models allow us to explore possible cooling scenarios (e.g., Stevenson 2003; O'Rourke and Korenaga 2012; Nakagawa and Tackley 2012; 2014). But a clearer understanding of planetary thermal history requires knowledge of mantle potential temperatures (T_p), which delimit convection style, cooling-rates and "thermal budgets" (Korenaga 2008).

The idea of a potential temperature has long been used in meteorology, to compare the thermal energy of air masses (e.g., Saunders 1957; Bolton 1980). The concept is implicit in Cawthorn's (1975) analysis of mantle adiabatic paths, but was formally introduced by McKenzie and Bickle (1988), to compare the thermal energies of mantle parcels. By their definition, T_p is the temperature a parcel of mantle would have if it rises adiabatically (isentropically) to a planetary surface without melting (Fig. 1A). The "adaibatic" assumption (Turcotte and Oxburgh 1972; Brown and Shankland 1981) means that a parcel rises quickly enough so as not to lose heat by conduction to its surroundings. If ascent is along an isentropic adiabat (S = entropy, and $dS = 0$), temperature will decrease, and the T drop for adiabatic cooling (ΔT_{ac}), from a source pressure P_1 to a surface pressure, P_o,. is $\Delta T_{ac} = (P_1 - P_o)\left(\frac{dT}{dP}\right)$. For our purposes, $P_o \approx 0$, so with $\left.\frac{\partial T}{\partial P}\right|_S = \frac{V\alpha T}{C_p}$ (see Ramburg 1971; Turcotte and Oxburgh 1972), then $\Delta T_{ac} \approx P_1\left(\frac{V\alpha T}{C_p}\right)$, where V = molar volume, α = the coefficient of thermal expansion, C_p = heat capacity, and T is the mean temperature along the adiabat.

Mantle convection, however, may be neither isentropic nor adiabatic. For example, due to radiogenic heat production, convection may be sub-adiabatic (Bunge 2005; Mattern et al. 2005; Davies 2009; here, T decreases less than along an adiabat) and the lower mantle may be superadiabatic (DaSilva et al. 2000). Moreover, Ganguly (2005) and Tirone (2015) suggest that the mantle adiabat is isenthalpic (H = enthalpy, and dH = 0), rather than isentropic, in which case T might actually increase upon ascent (see also Cawthorn 1975). When T_p is used *to compare thermal energies*, corrections for adiabatic cooling are not critical, if consistently applied. But the corrections are critical when T_p is used to obtain a geotherm. Fortunately, within present uncertainties, an isentropic adiabat serves well as an approximation (Brown and Shankland 1981; Deschamps and Trampert 2004; Mattern et al. 2005; Katsura et al. 2010). So we define T_p as:

$$T_p = T^{sol} - \Delta T_{ac} \qquad (1)$$

where T^{sol} is the temperature of solid, un-melted mantle at pressure P_1, and $\Delta T_{ac} \approx P_1 \left.\frac{\partial T}{\partial P}\right|_S$, where $\left.\frac{\partial T}{\partial P}\right|_S$ is ~1-2°C/kbar (McKenzie and Bickle 1988; Putirka 2005) (Fig. 1A). If the mantle intersects the solidus on its way to the surface, then to recover T_p, we must

account for the loss of thermal energy, ΔT_{fus}, due to the heat of fusion, ΔH_{fus} (Fig. 1A): $\Delta T_{fus} = F(\Delta H_{fus}/C_p)$ (Cawthorn 1975), where F is the fraction of melt created. If we let T^m be a magmatic T at P_1, so $T^{sol} = T^m + F(\Delta H_{fus}/C_p)$, then by substitution into (1) we have,

$$T_p = T^m + F\left(\frac{\Delta H_{fus}}{C_p}\right) - \Delta T_{ac} \quad \text{(2a) or}$$

$$T_p = T^m + F\left(\frac{\Delta H_{fus}}{C_p}\right) - P_1\left(\frac{V\alpha T}{C_p}\right) \quad \text{(2b).}$$

Figure 1A illustrates these relationships (without considering conductive cooling).

Comparisons of mantle thermal energies, through T_p, are important as they have tectonic implications. A higher T_p, may reflect active upwelling—plumes that obtain thermal buoyancy from near the core-mantle boundary (Morgan 1971; but see also Hess 1962)—whereas a lower T_p may reflect passive upwelling of cooler, shallower mantle, as at spreading ridges (McKenzie 1967) or arc or back-arc systems (e.g., Lee et al. 2009) (Fig. 1B). We should also expect interplanetary contrasts in T_p: Earth exhibits a bi-modal T_p distribution (e.g., Putirka et al. 2007; Lee et al. 2009) (Fig. 1C, top). But Mars is thought to have a "stagnant lid" (e.g., Stevenson 2003), which means that its brittle lithosphere does not participate in convection (Fig. 1c). Under a stagnant lid, there are no arcs or ridges, and thus no passive upwelling. Planets such as Mars should thus yield a uni-modal T_p distribution, reflecting the monopoly that thermal plumes exert in effecting planetary volcanism (Fig. 1a, c).

From the above, it should be clear that T_p only has meaning at Earth's surface. But numerical modelers have need of a measure of average mantle temperature, T_{avg} (e.g., Nakagawa and Tackley 2012). For example, Korenaga (2008) calculates T_{avg} as T_i in his Eqns. 8-9 (but plots T only as T_p). To convert T_p to T_{avg}, we must apply a mantle-wide adiabat. Using Katsura et al.'s (2010) adiabat, a T_p of 1400ºC (for modern MORB, or ambient mantle) translates to T_{avg} = 1992ºC (averaged over the depth range 100-2889 km). It so happens that T_{avg} is the T obtained at 1,400 km (essentially mid-mantle); T_{1400km} thus approximates "average" mantle and so provides a useful reference for numerical modelers and petrologists.

Absent an understanding of model error, though, T_p values are, of course, meaningless. And the possible sources of error are many, forming something of an Indra's net: T^m is often obtained from olivine-liquid equilibria ($T^{ol\text{-}liq}$; so $T^m = T^{ol\text{-}liq}$), which are in turn

affected by oxygen fugacity (fO_2), magmatic ferric-ferrous ratios ($X_{Fe2O3}^{liq}/X_{FeO}^{liq}$), the Fe-Mg exchange coefficient ($K_D(Fe\text{-}Mg)^{xtl\text{-}liq}$, or simply K_D, where Fe is Fe^{2+}) and P_1. This interdependence can be expected given the Gibbs-Duhem equation (see Castellan 1971):

$$\sum_{i=1}^{I} n_i \, d\mu_i = -SdT + VdP \qquad (3)$$

where n_i is the number of moles of component i in a given system (of i different components), and μ_i is the chemical potential of component i. The Gibbs-Duhem equation shows that any one estimate of T^m, P, fO_2, F etc., necessarily reflects the value of all the others. Here we examine which parts of the T_p calculation contain significant error, which can be made approximately independent of others, and how such errors propagate. We also show that models that translate $fO_2 \rightarrow X_{Fe2O3}^{liq}/X_{FeO}^{liq}$ often disagree, yielding very different experimental predictions of K_D—the foundation on which equilibrium is assessed in natural systems. To rectify these issues, new calibrations are offered for fO_2, $X_{Fe2O3}^{liq}/X_{FeO}^{liq}$, K_D and F, which are applied to determine T_p for Earth, Moon, Mars and Vesta.

METHODS

Experimental data are used to test and calibrate models involving fO_2, $X_{Fe2O3}^{liq}/X_{FeO}^{liq}$, K_D, , F, and T_p. Data are from the Library of Experimental Phase Relations (LEPR; Hirschmann et al. 2008), which reports 1,629 partial melting experiments that yield olivine (with or without other phases). Of these, 1,270 experiments [when data from Matzen et al. (2011) are added] provide constraints on fO_2, reporting either $\log[fO_2]$ or an oxygen buffer (e.g., quartz + fayalite + magnetite, or QFM; Ni + NiO or NNO) from which $\log[fO_2]$ can be calculated. For nearly all these experiments, Fe_2O_3/FeO ratios in glasses are not measured, and so Fe_2O_3/FeO ratios are calculated for the experimental glasses (liquids) using Kilinc et al. (1983), Kress and Carmichael (1988), Kress and Carmichael (1991; their Eqns. 6, 7), Jayasuriya et al. (2004; their Eqn. 12) and Borisov (2010). Because of the apparent role of Fe_2O_3/FeO estimates in determining equilibrium values of K_D, the effect of using different models to calculate $\log[fO_2]$ for a given O_2 buffer (Hewitt 1978; Schwab and Kustner 1981; Myers and Eugster 1983; Fegley 2013) is also examined. Also used are 380 experimental studies of silicate liquids, where Fe_2O_3

and FeO are measured, and from which fO_2 – Fe_2O_3/FeO relationships have been calibrated (Table 1).

Published parental magma compositions are mostly used for T_p estimation, with the assumption that these represent isobaric batch melts. However, new parental magma compositions are estimated for Mauna Loa, to illustrate how error on Tp evolves from such calculations. And a re-evaluation of Archean parental magmas is presented, to illustrate how such calculations affect inferences of secular cooling rates. As shown below (Errors on Mantle Potential Temperatures), this assumption has no discernable affect on the T_p. However, when using Eqns. 2a, b, it is important to include the effect of T on $\Delta H_{fus}^{peridotite}$, and a new model is calibrated, using data from Stebbins et al. (1984), Richet and Bottinga (1986), Navrotsky et al. (1989), Robie and Hemingway (1995), and Kojitani and Akaogi (1997). Mantle peridotite is assumed to be 55% olivine (ol), 20% each of clinopyroxene (cpx) and orthopyroxene (opx), and 5% garnet (gt). But calculated on a per-oxygen basis, the value of ΔH_{fus} would only be 3.3% higher for a mantle source with 15% ol, 5% gt and 40% each of cpx and opx, so source mineralogy can mostly be ignored. For all parental magmas, two different computational approaches are used, depending upon whether Fe_2O_3 contents are measured or must be estimated (Table 2). For terrestrial T_p estimates, 1. MORB from Cottrell and Kelley (2011) was used. The high T end of this group agrees with East Pacific Rise T_p estimates from Putirka et al. (2007). 2. Hawaiian parental magmas compositions (Mauna Loa) are estimated here; and 3. Archean to Cretaceous parental magma compositions are from Hole (2015), Herzberg and Gazel (2009) and Herzberg et al. (2010). Archean T_p estimates are also re-evaluated by examining a 3.5 Ga composition (Green et al. 1975), and high MgO compositions from GEOROC (http://georoc.mpch-mainz.gwdg.de/georoc/) in equilibrium with olivine having forsterite (Fo) contents of 91-94% at F = 0.4-0.5 (see Bernstein et al. 2007). For all these samples, fO_2 is assumed to be at QFM (Carmichael 1991), but is varied for Hawaiian magmas (Table 2) to test for fO_2 effects on T_p. For Mars, we use primitive compositions from Longhi and Pan (1989), Musselwhite et al. (2006), Monders et al. (2007), Filberto et al. (2008), and Goodrich et al. (2010), and apply the martian chronology of Bouvier et al (2009), age dates of Greeley et al. (2005), and fO_2 conditions of Herd (2006) (and also Righter et al. 2008 as a test). Some controversy surrounds age

dates for shergottite meteorites, which we assume are 4.3 Ga, based on Werner et al. (2014) and Bouvier et al. (2009). For Vesta, the putative parent body for the HED family of meteorites, we use primitive compositions from Treiman (1997) and Mandler and Elkins-Tanton (2013), and assume that fO_2 is similar to that for Mars (Herd 2006). For Earth's Moon, we use Apollo 15 green glass compositions from Delano (1986) and Barr and Grove (2013), and "Mg suite" magmas from McCallum and Schwartz (2001) and Ariskin (2007), with fO_2 from Wadhwa (2008).

In calculating T_p, we use thermometers from Putirka et al. (2007), Beattie (1993) with the Herzberg and O'Hara (2002) pressure correction, and the Si-activity barometer of Putirka (2008). Tests of PRIMELT3 (Herzberg and Asimow 2015) are also presented, where we input experimental peridotite partial melt compositions, experimental P and peridotite MgO and FeO contents, into the "PRIMELT3 MEGA" spreadsheet; Fe^{2+}/Fe^{3+} is set to 1.0 and we examine the predicted T and F for the case of 0% olivine addition.

We also apply new expressions that simplify the translation of $T^{ol\text{-}liq} \rightarrow T_p$ from knowledge of P and melt fraction (F). Additional new expressions predict F, $\log[fO_2]$, $X_{Fe2O3}^{liq}/X_{FeO}^{liq}$ and K_D, which are applied to all terrestrial parental melt compositions. Melt fraction models, though, are imprecise at best and appear not to apply to extraterrestrial systems. For Apollo 15 lunar compositions, we thus use $F = 0.2$, based on parent liquid-cumulate modeling of Barr and Grove (2013), and $F = 0.2$ is applied to high Mg# lunar samples, based on McCallum and Schwartz (2001). For martian samples we calibrate a new equation for F using the Ding and Dasgupta (2015) solidus. For eucrite parent compositions, we use $P = 0.05$ GPa, and $F = 0.35$, the latter being a middle value of estimates provided by Mandler and Elkins-Tanton (2013) for their calculated parental liquid compositions. Table 2 and the Discussion section provide further details regarding calculation procedures.

BACKGROUND ON K_D, AND fO_2

Most modern estimates of T_p derive from olivine-liquid equilibria (e.g., Herzberg and O'Hara 2002; Putirka et al. 2007; Lee et al. 2009; Herzberg et al. 2010). These approaches begin with Roeder and Emslie (1970), who recognized the usefulness of the Fe-Mg exchange reaction between olivine and silicate liquid,

$$MgSi_{0.5}O_2^{olivine} + FeO^{liq} = FeSi_{0.5}O_2^{olivine} + MgO^{liq} \quad (4a)$$

or as in their work:

$$MgO^{olivine} + FeO^{liq} = FeO^{olivine} + MgO^{liq} \quad (4b)$$

where FeO is not total Fe, but refers only to Fe in the 2^+ state. Rather than use an equilibrium constant (K_{eq}) for Eqn. (4a), they instead express Eqn. (4a) as an exchange coefficient, K_D:

$$K_D = (X_{FeO}^{olivine}/X_{MgO}^{olivine})/(X_{FeO}^{liquid}/X_{MgO}^{liquid}) \quad (5)$$

where X_i are the mole fractions of i in the indicated phases. In Roeder and Emslie (1970), X_{MgO}^{ol} and X_{FeO}^{ol} act as proxies for the activities of forsterite and fayalite (i.e., a(Fo) and a(Fa) respectively). Although there is no clear meaning for the activities of FeO or MgO in olivine, if X_{Fo} and X_{Fa} are defined respectively as $X_{MgO}/(X_{MgO} + X_{FeO})$, and $X_{FeO}/(X_{MgO} + X_{FeO})$, then K_D is numerically equivalent to K_{eq}^{4a} since $(X_{MgO} + X_{FeO})$ cancels in both expressions.

Roeder and Emslie (1970) found that K_D is independent of T, fO_2, or liquid composition and recommended a mean value of 0.30 (K_D ranges from 0.26 to 0.36 in their study) as a constant, characteristic of equilibrium. Implicit in their argument was that deviations from the mean are random. In support of their result, they cited Bradley's (1962) report of very similar heats of fusion for both Fo and Fa, and so the enthalpy of reaction (ΔH_r) for Eqn. 4a, and by implication, 4b, were expected to be small. Later studies showed that Eqn. (5) is somewhat sensitive to composition (e.g., Gee and Sack 1988; Toplis 2005), and P (Herzberg and O'Hara 1998).

Matzen et al. (2011), however, show that K_D, for Hawaiian compositions, is 0.34-0.36, and Filberto and Dasgupta (2011) and Barr and Grove (2013) arrive at a $K_D = 0.35$ for martian and lunar compositions respectively. High K_D results are not new; values of 0.33 to 0.36 were reported for komatiites previously (Bickle et al. (1977). The ~13%

difference between the canonical 0.30 of Roeder and Emslie (1974) and Matzen et al. (2011) $K_D = 0.34$ is not negligible. Consider a basalt with 9.9 % FeOt (total Fe as FeO) and 7.6% MgO that falls on an olivine control line (meaning that it has fractionated only olivine since being removed from its mantle source). If we reconstruct a parental magma from this composition, at 2 GPa, and in equilibrium Fo91.5, then using $K_D = 0.30$, the parental magma has 17.3% MgO, but using $K_D = 0.34$, it would have 21.4% MgO. The latter yields a T estimate that is 69-78ºC higher than the former (using Matzen et al. 2011; Beattie 1993; and Putirka et al. 2007). A difference of 70ºC is more than twice model error (±30ºC) (Putirka 2008), but the significance here is only that we misapprehend equilibrium.

RESULTS – MODEL TESTS AND NEW CALIBRATIONS

Models for Predicting Magmatic Fe_2O_3/FeO ratios and fO_2

The data of Roeder and Emslie (1970) are mostly not available, so cannot be compared to Matzen et al. (2011), but certain contrasts likely derive from an accounting of $X_{Fe2O3}^{liq}/X_{FeO}^{liq}$ (where $X_{Fe2O3}^{liq} = [X_{FeOt}^{liq}][X_{Fe2O3}^{liq}/X_{FeO}^{liq}]/(1+2[X_{Fe2O3}^{liq}/X_{FeO}^{liq}])$; $X_{FeO}^{liq} = X_{FeOt}^{liq} - 2[X_{Fe2O3}^{liq}]$). Figure 1 illustrates the problem. The mean K_D for 1,270 experimental data using Jayasuriya et al. (2005; Eqn. 12) (0.342±0.055) and Kress and Carmichael (1991; Eqn. 7) (0.331±0.050) are quite close. But the use of Jayasuriya et al. (2005) yields a higher K_D for 90% of these experiments (Fig. 1A), with differences of >20% in some cases. Both the Jayasuriya et al. (2005) and Kress and Carmichael (1991) models yield quite similar results for Matzen et al. (2011), who applied Jayasuriya et al. (2005), so this systematic error does not explain Matzen et al.'s higher K_D. But more importantly, the higher K_D using Jayasuriya et al. (2005; Eqn. 12) is due to their higher predicted values for $X_{Fe2O3}^{liq}/X_{FeO}^{liq}$ (Fig.1B).

Even more interesting is that Jayasuriya et al. (2005), and Kress and Carmichael (1988; 1991) predict quite different T— $X_{Fe2O3}^{liq}/X_{FeO}^{liq}$ or fO_2—$X_{Fe2O3}^{liq}/X_{FeO}^{liq}$ relationships (Fig. 2A), with the intriguing result that K_D may either increase or decrease with T (Fig. 2B). The magnitudes of the contrasts are low at the fO_2 ranges below NNO, but increase with increasing fO_2 (Fig. 2C). This contrasting behavior is perhaps not unexpected: the

operative equilibrium is often expressed as $Fe_2O_3 = FeO + 0.5O_2$, but is perhaps more revealingly expressed by Mysen (1991):

$$4SiO_2 + Si_2O_5^{2-} + 4Fe(IV)O_2^{1-} = 5SiO_3^{2-} + SiO_4^{4-} + 4Fe(VI)^{2+} + O_2 \qquad (6a).$$

In (6a), each molecular unit is a dissolved silicate liquid species, roman numerals indicate Fe coordination and Fe(IV) is Fe^{3+} and Fe(VI) is Fe^{2+}. Silicates on the right hand side of Eqn. 6a are more depolymerized than on the left, and O_2 represents possibly unbounded O, so entropy appears to be greater on the right hand side of 6a. This means that the equilibrium should shift to the right, to lower Fe^{3+}/Fe^{2+}, with increasing T, and perhaps also with increasing P if, as in crystalline silicates, more highly polymerized units have higher molar volumes. And there is a leftward shift to higher Fe^{3+}/Fe^{2+}, when fO_2 is increased at constant T. Fortunately, though, the choice of model used to translate an oxygen buffer (e.g., QFM) to $\log[fO_2]$ has a trivial effect on $X_{Fe2O3}^{liq}/X_{FeO}^{liq}$ or K_D (Fig. 3).

To determine which model better predicts $X_{Fe2O3}^{liq}/X_{FeO}^{liq}$, the data were divided into 3 data sets based on the calibration and methods used to determine $X_{Fe2O3}^{liq}/X_{FeO}^{liq}$ (Table 1). Of the six published models illustrated (ignored are models where X_{Fe2O3}^{liq} inappropriately appears as an independent variable in regression analysis, e.g., Jayasuria et al.'s (2005) Eqn. 14), the Jayasuriya et al. (2005) and Kress and Carmichael (1991) models perform best. The Kress and Carmichael (1991) model has a bit less systematic error (slope and intercepts for predicted vs. measured values are closer to 1 and 0 respectively) but both models yield similar standard errors of estimate (Figs. 4d, e). Two new calibrations, though (using DS1 and DS3) reduce error by 20-30% (Figs. 4g, h):

$$\ln[X_{Fe2O3}^{liq}/X_{FeO}^{liq}] = -6.53 + 10813.8/T(\mathrm{K}) + 0.19\ln[fO_2] + 12.4[X_{Na2O}^{liq} + X_{K2O}^{liq}] - 3.44\,[X_{Al2O3}^{liq}/(X_{Al2O3}^{liq} + X_{SiO2}^{liq})] + 4.15[X_{CaO}^{liq}] \qquad (6b)$$

$$\ln[X_{Fe2O3}^{liq}/X_{FeO}^{liq}] = -6.75 + 10634.9/T(\mathrm{K}) + 0.195\ln[fO_2] + 7.9[X_{Na2O}^{liq} + X_{K2O}^{liq}] - 4.6[X_{MgO}^{liq}] + 0.54[X_{MgO}^{liq}/(X_{MgO}^{liq} + X_{FeOt}^{liq})] \quad -53.4[X_{P2O5}^{liq}] + 1.07[\mathrm{NBO/T}] \qquad (6c)$$

In Eqns. 6b and 6c, the X_i are mole fractions of i in silicate liquids, expressed as traditional oxides (Al_2O_3, Na_2O), to allow comparison of the new coefficients with prior models. In Eqn. 6c, NBO/T is the ratio of non-bridging oxygens (NBO) to tetrahedrally coordinated cations (T), calculated using cation fractions ($AlO_{1.5}$, $NaO_{0.5}$, etc.), and purposefully excluding Fe^{3+}(IV) so as to avoid a circular regression model. The use of NBO/T in Eqn. 6c partially eliminates residual error that varies with X_{Fe2O3}^{liq}, which,

cannot properly be used as an independent regression variable. *NBO/T* is calculated as follows: After calculating oxides on a cation fraction basis (where oxides are expressed as SiO_2, TiO_2, $AlO_{1.5}$, FeO^{total}, MnO, MgO, CaO, $NaO_{0.5}$, and $KO_{0.5}$, and written below, as Si, Ti, Al, Fe, etc.; see Putirka (2008) for examples):

1) Al^{IV} = the lesser of Al^{total} or Na + K + 2(Ca + Mg)

2) T = Si + Ti + Al^{IV}

3) O^T (Total Oxygens) = 2[Si + Ti] + 1.5[Al] + Fe^{total} + Mn + Mg + Ca + 0.5[Na + K]

4) NBO = 2[O^T] – 4[T]

5) NBO/T = (2[O^T] – 4[T])/T

The log-scale so often used to portray $X_{Fe2O3}^{liq}/X_{FeO}^{liq}$, hides significant error (Fig. 4h. For Eqn. 6b, error is ~25% across the range of predicted ratios, so increases as: $[X_{Fe2O3}^{liq}/X_{FeO}^{liq}]^{measured} - [X_{Fe2O3}^{liq}/X_{FeO}^{liq}]^{predicted} = 0.02 + 0.2[X_{Fe2O3}^{liq}/X_{FeO}^{liq}]^{predicted}$.

Interestingly, $\log[fO_2]$ has yet to be calibrated as a dependent variable when $X_{Fe2O3}^{liq}/X_{FeO}^{liq}$ is known, leaving the prediction of fO_2 to the numerically problematic rearrangement of expressions such as Eqn. 6b. As Galton (1886) shows, regression lines have a slope that is less than slope of an ellipse's major axis that encompasses a given set of data. In our present case, this means that regression is not symmetric with respect to fO_2 and $X_{Fe2O3}^{liq}/X_{FeO}^{liq}$. The following model resolves this issue (using DS1 only):

$$\log[fO_2] = 14.45 - 24200.5/T(\mathrm{K}) + 2.17\ln[X_{Fe2O3}^{liq}/X_{FeO}^{liq}] - 19.6[X_{Na2O}^{liq} + X_{K2O}^{liq}] - 35.6\,[X_{Fe2O3}^{liq}] - 10.09[X_{CaO}^{liq}] + 2.27[X_{MgO}/(X_{FeO} + X_{MgO})] \quad (7).$$

Here, X_i are mole fractions as in Eqn. 6b, and Eqn. 7 reduces error by ~25% compared to rearrangement of Kilinc et al. (1983), Kress and Carmichael (1991; Eqn. 7) and Jayasuriya et al. (2005; Eqn. 12) (in Fig. 5, statistics are on $\log[fO_2]$). Published models successfully predict fO_2 for data not used in their respective calibrations (e.g., DS2), but only Eqn. 7 predicts $\log[fO_2]$ for the Mossbauer data (DS3) without systematic error (Fig. 5). Since Eqn. 7 is calibrated only from wet chemistry experiments, there appears to be no systematic error relative to the method used to determine $X_{Fe2O3}^{liq}/X_{FeO}^{liq}$.

Models for Predicting K_D

Most erupted lavas at Earth's surface are not in equilibrium with mantle olivine. Thus, to estimate T_p, it is common to reconstruct a parental magma that is mantle equilibrated

(e.g., Herzberg and O'Hara 2002; Putirka et al. 2007), and which through differentiation, gives rise to observed magma compositions. The details of how to calculate a parental magma are taken up in a later section, but some aspects are relevant here. A common approach (e.g., Herzberg and O'Hara 2002; Putirka 2005; Lee et al. 2009) is to add or subtract olivine from a natural composition until a calculated liquid is in equilibrium with mantle olivine. A key problem, besides determining a mantle source olivine composition, is the test for equilibrium. Models for K_D, such as Roeder and Emslie (1970), are needed. K_D, while largely independent of T and P, varies with composition (Fig. 6; see also Toplis (2005; Fig. 7a)) and usually requires knowledge of Fe_2O_3, which is rarely measured in either experimental or natural systems. Here, two sets of models for K_D are proposed, one where X_{Fe2O3}^{liq} is "known" (i.e., calculated using Eqn. 6b), and another where Fe^{liq} is treated as FeO^{total}. For the former, we recommend:

$$K_D = 0.33 \pm 0.044 \quad (8a),$$

$$K_D = 0.21 + 0.008[P(GPa)] + 0.0025[SiO_2] - 3.63x10^{-4}[Na_2O+K_2O]^2 \quad (8b),$$

and

$$K_D = 0.25 + 0.0018[SiO_2] - 3.27x10^{-4}[Na_2O+K_2O]^2 \quad (8c)$$

where SiO_2, Na_2O and K_2O are weight % values of liquid compositions. Equations 8b (Fig. 7b) and 8c describe 1,199 experimental data with an error of ±0.040. Equation 8b is only needed at P >1 GPa. Compared to Eqn. 8a, the additional variation described by Eqns. 8b and 8c is quite small: 5% (Fig. 7b) and 10% respectively. Data from Gee and Sack (1980) are here excluded from this analysis, as their very unusual compositions (SiO_2<45%; Na_2O+K_2O>8%) are untypical of oceanic basalts. To describe the Gee and Sack (1980) data, several additional terms are needed:

$$K_D = 0.6 + 0.013[P(GPa)] + 0.016[SiO_2] - 1.73x10^{-4}[SiO_2]^2 + 0.0179[Al_2O_3] - 2.6[Al\#] + 0.211\ln[Al\#] - 3.19x10^{-5}[Na_2O+K_2O]^3 \quad (8d)$$

Here, Al# = $(Al_2O_3/(Al_2O_3 + SiO_2)$, and all terms are again in weight %. Equation 8d reduces SEE to ±0.038 (n = 1,210; Fig. 7c) but Eqn. 8d need only be used when both SiO_2 and Na_2O+K_2O are < 45% and > 8% by weight respectively.

An alternative approach is to make the dependency of K_D on fO_2 explicit, i.e., treat all Fe^{liq} as FeO^{total}, which can be useful when Fe_2O_3 is unknown:

$$K_D^{FeOt} = 0.29 \pm 0.051 \quad (9a)$$

$$K_D^{FeOt} = 0.0583 + 0.00252[SiO_2(wt.\ \%)] + 0.028[P(GPa)]$$

$$- 0.0091[Na_2O+K_2O\ (wt.\ \%)] - 0.013383[\log(fO_2)] \qquad (9b)$$

Equation 9a is simply a mean and a standard deviation of experimental observations with no correction for ferric-ferrous ratios. With Eqn. 9a, the user accepts a greater level of uncertainty compared to K_D in Eqn. 8a. But it's great advantage is its independence of T, P, X_i and fO_2; it thus makes for an excellent starting point for calculating parental magma compositions. In Eqn. 9b, $R^2 = 0.52$, the SEE = ±0.035 (n = 1223; Fig. 7d) and the last term accounts for variations X_{Fe2O3}^{liq} indirectly, using fO_2 (base-10 log) as a proxy. The residuals of Eqn. 9b are uncorrelated with T ($R^2 = 0.005$), but K_D is sensitive to T, through the T-sensitivity of fO_2. By coincidence only, the K_D^{FeOt} in Eqn. 9a comes quite close to the Roeder and Emslie (1970) K_D value, which was intended for use when Fe_2O_3 is known.

In contrast to these new models, the Toplis (2005) model captures the Gee and Sack (1980) compositions and predicts K_D for the remaining data with similar uncertainties: R^2 = 0.25 and SEE = ±0.038 (n = 129; Fig. 7a); here, the lower R^2 for Toplis is a virtue, in that it's intent, as in Eqns. 9a, b above, is to include the effects of fO_2 within the computation of K_D itself. But the Toplis (2005) model requires an equilibrium olivine composition as input. Filberto and Dasgupta (2011) find a Fe-Mg exchange coefficient of 0.35 for martian compositions, which can be reproduced if Fe is treated as FeO^{total} (so they calculate K_D^{FeOt}, not K_D). By applying Eqn. 6b, we find that K_D for ~100 experiments on martian compositions does not vary with fO_2, or other compositional parameters, so we have:

$$K_D(\text{martian}) = 0.37 \pm 0.04 \qquad (10a)$$

$$K_D(\text{martian; } Fe^{liq} \text{ as } FeO^{total}) = 0.35 \pm 0.03 \qquad (10b)$$

Models for Predicting Mantle Potential Temperatures (T_p)

Most recent T_p estimates (e.g, Herzberg and O'Hara 2002; Putirka 2005; Herzberg and Asimow 2008; Lee et al. 2009) begin with a T estimate of olivine-liquid equilibration: $T^{ol\text{-}liq}$. The strategy is useful because olivine is a dominant phase in peridotite and its $D_{MgO}^{ol\text{-}liq}$ is highly T-sensitive. So in Eqn. 2b, $T^m = T^{ol\text{-}liq}$:

$$T_p = T^{ol-liq} + F\left(\frac{\Delta H_{fus}}{C_p}\right) - P_1\left(\frac{V\alpha T}{C_p}\right) \qquad (2c)$$

Published estimates of T_p disagree less because of the $T^{ol\text{-}liq}$ or $P_1\left(\frac{V\alpha T}{C_p}\right)$ terms, but instead because of the choice of mantle olivine composition, or because $F(\Delta H_{fus}/C_p)$ is calculated in contrasting ways (see section 8 of Putirka et al. 2007). For example, Lee et al. (2009) report T_p^{MORB} in the range 1300-1400ºC. But only T_p^{MORB} in the range 1375-1400ºC works well as a *mean value* for MORB, since only these adiabats fall to the high-T side of Lee et al.'s (2009) mean P-$T^{ol\text{-}liq}$ estimates (their Fig. 2A); otherwise, the implication is that $\Delta H_{fus} = 0$. Their implicit T_p^{MORB}, for $\Delta H_{fus} > 0$, is ~1330-1450ºC.

Herzberg and Gazel (2009) provide an empirical equation to translate $T^{ol\text{-}liq}$ to T_p, which condenses certain thermodynamic assumptions; while possibly useful, our goal is to evaluate all inputs, especially those responsible for substantial uncertainty in T_p. In Putirka et al. (2007), ΔH_{fus} for peridotite is 130 kJ/mole (using ΔH_{fus}^{Fo} = 142 kJ/mole from Richet et al. 1993), but a re-evaluation here indicates that this value is too high for all but the highest P-T conditions of partial melting, leading to overestimates of T_p. Reports for the entropy of fusion, ΔS_{fus}, range from 0.3 J/K·g (Hirschmann et al. 1999) to 0.4 J/K·g (Kojitani and Akaogi 1997), which at 1773 K (and for a peridotite with 167 g/mole), translate to ΔH_{fus} of 88 and 118 kJ/mole respectively ($\Delta H_{fus} = T\Delta S_{fus}$). These different values likely represent not just measurement error, but real variation in ΔH_{fus} as $\Delta H_{fus} = f(T)$ (e.g., Navrotsky et al. 1989; Kojitani and Akagoi 1997); this T-dependency is systematic, so as to underestimate excess temperatures, $T_{ex} = T_p^{Plume} - T_p^{MORB}$.

The thermal variation ΔH_{fus}, though, can be simply modeled. For the minerals pyrope, diopside, forsterite and anorthite, values for ΔH_{fus} can be expressed on a per-oxygen basis, which varies smoothly with T_{fus} (the pure phase melting temperature). So for forsterite, Mg_2SiO_4 becomes $Mg_{0.5}Si_{0.25}O$, and $\Delta H_{fus}^{Fo\ 1\text{-}Ox}$ = (114kJ/mole)/4 = 28.5 kJ/mole, at 2163 K (Navrotsky et al. 1989). For these silicate minerals:

$$\Delta H_{fus}^{mineral\ 1\text{-}Ox} = 1.48 + 0.0131T(\mathrm{K}) - 1.66[T(\mathrm{K}) - 1881]^2 \qquad (11a)$$

which likely reflects mean bonding strength in Ca-Mg-Al silicates. To the extent that this model is valid, it also disallows the larger ΔH_{fus} for Fo of Richet et al. (1993) as it falls well off an otherwise coherent trend. Equation 11a allows one to calculate ΔH_{fus} for any rock where the heat of mixing is near zero (Kojitani and Akaogi 1997), using:

$$\Delta H_{\text{fus}}^{\text{rock}} = \sum_i X_i (\Delta H_{fus}^{mineral\ 1-Ox}) N_i \quad (11b)$$

where for each mineral i, X_i is its weight fraction in the rock, $\Delta H_{fus}^{mineral\ 1-Ox}$ is the heat of fusion of mineral i when expressed with one oxygen, and N_i is the number of oxygens in the mineral formula when used to express a rock composition (e.g., 4 for Mg_2SiO_4; 6 for $CaMgSi_2O_6$; 3 for $MgSiO_3$, etc.). Equations 11a, and 11b reproduce the 1.1, 3 and 4 GPa values of ΔH_{fus} from Kojitani and Akaogi (1997) within their experimental error (±20-40 J/g or ±4-8 kJ/mole). For an average peridotite composition (Putirka et al. 2011):

$\Delta H_{\text{fus}}^{\text{peridotite}}$(kJ/mole) 1 atm =

$$\begin{cases} \text{T(°C)} = 1150 \text{ to } 1890^{\circ}\text{C};\ 21.1 + 0.061T(^{\circ}\text{C}) - 7.6\times10^{-5}[T(^{\circ}\text{C})-1600]^2 \\ \text{T(°C)} > 1890^{\circ}\text{C};\ 130 \text{ kJ/mole} \end{cases} \quad (12a).$$

Equation 12a predicts ΔH_{fus} to within ±15 kJ/mole and yields $\Delta H_{\text{fus}}^{\text{peridotite}}$ of 88-128 kJ/mole for temperatures of 1250-1800°C. This treatment does not account for P, but while a P-correction can be derived, it must be used with caution. An empirical regression of Kojitani and Akaogi's (1997) results yields $d\Delta H_{\text{fus}}/dP \approx 7.5$ kJ/mole·GPa, which is half the 1σ error on 12a. But the derivative might become negative at P>3 GPa. The pressure derivative for enthalpy is $\left.\frac{\partial \Delta H_{fus}}{\partial P}\right|_T = \Delta V_{fus} - \Delta V_{fus}\alpha T$, where ΔV_{fus} is the molar volume of fusion, and α is the weighted coefficient of thermal expansion of the system in question. Using data and expressions from Lange and Carmichael (1990) and Holland and Powell (1998) for a system of 50% Fo, 20% Di and 30% En at 1800 K, then $\left.\frac{\partial \Delta H_{fus}}{\partial P}\right|_T$ is 6.6 kJ/GPa at P = 1 GPa. This value approximates that obtained from Kojitani and Akaogi (1997). But at 3 GPa, the derivative reverses sign, and $\left.\frac{\partial \Delta H_{fus}}{\partial P}\right|_T$ = -4.0 kJ/GPa. Since decreases in ΔV_{fus} are quite viable over the 1-5 GPa P range of interest (Agee and Walker 1993), the small and uncertain P-correction is not applied here.

As to heat capacity, data from, Robie and Hemingway (1995), Gillet et al. (1991), and Thieblot et al. 1999) yield a mean value for peridotite of C_p = 212 J/K·mole. This is probably acceptable, but C_p for peridotite can be calculated as:

$$C_p = 130 + 11.4\ln[T(^{o}C)] \quad (12b)$$

which predicts C_p to within ± 12 J/K·mole, and errors are < ±2 kJ/mole for >10% ranges in mineral mode and composition. We thus recommend using:

$$T_p = T^{\text{ol-liq}} + \frac{A}{B}F - 13.3P_1 \qquad (12c).$$

The coefficient A is calculated from Eqn. 12a, B is obtained from 12b, P_1 is the pressure at which a parental melt is segregated from its mantle source, in units of GPa, and F is melt fraction. We set $\left.\frac{\partial T}{\partial P}\right|_S$ = 13.3ºC/GPa (see Putirka 2005), which appears allowable in light Katsura et al.'s (2010) analysis of adiabatic ascent. Note that while most estimates of F are usually reported in weight proportions, attempts to reproduce F by mass balance from Walter (1998) show that the mole/weight conversion can be ignored: experimental error in determining F averages 40% and can range to 100%, depending upon which oxides are used for mass balance, or whether regression is used to average multiple oxides, and so is vastly greater than the mostly 1-5% contrasts between liquid fractions taken on a molar or weight basis.

To calculate $T^{\text{ol-liq}}$ in Eqn. 12c, most thermometers use $D_{\text{MgO}}^{\text{ol-liq}}$, which requires knowledge of both olivine and liquid compositions. However, Beattie (1993) provides a remarkably precise model for $T^{\text{ol-liq}}$ (his Eqn. 10) using a value of $D_{\text{MgO}}^{\text{ol-liq}}$ predicted from anhydrous liquid compositions only (his Eqn. 12; see Putirka 2008). This approach also means that $f\text{O}_2$, $X_{\text{Fe2O3}}^{\text{liq}}/X_{\text{FeO}}^{\text{liq}}$ and K_D can be obtained without knowing an equilibrium olivine composition. The Beattie (1993) model was not calibrated for hydrous systems, so we combine the Herzberg and O'Hara (2002) P-correction with a H_2O-correction:

$$T^{\text{ol-liq}}\ (^{\circ}\text{C}) = T_{1\ \text{atm}}^{\ (\text{Beattie, 1993})} + 54[\text{P(GPa)}] - 2[\text{P(GPa)}]^2 - 19.93[\text{H}_2\text{O(wt\%)}] \qquad (13)$$

This equation can be used as a consistency check on Eqn. 4 of Putirka et al. (2007).

Melt Fraction (F)

Once a mantle-equilibrated parental magma composition is obtained (from knowledge of K_D), it is necessary to estimate the fraction of melt (F) in the system. Here, we provide tests of various models that can be used to predict F.

The first of two possible approaches is that of Katz et al. (2003), where F is calculated from the proportional distance between the solidus and liquidus curves, and approach that is tested for accuracy in Fig. 8a. In this approach, a mantle composition is implicitly assumed, and T and P must be chosen. This method has an apparent disadvantage in that

it would seem to apply only to a single mantle composition. However, a number of different mantle compositions yield similar solidi (Hirschmann et al. 2000), so the method may have broader application. Using the Hirschmann et al. (2000) solidus, we obtain:

$F = (T^{\text{ol-liq}} + 5.14P^2 - 132.9P - 1120.7)/(465.3+233.7P^{0.5} + 5.14P^2 - 132.9P)$ (14a)

where T and P are in units of ºC and GPa. Equation (14a) uses a newly calibrated liquidus, $T(^{\circ}C) = 1596 + 233.7P^{0.5}$ (i.e., $F = [T^{\text{ol-liq}} - T^{\text{solidus}}]/[T^{\text{liquidus}} - T^{\text{solidus}}]$), obtained from Herzberg and Zhang (1998) and Fiquet et al. (2012) at pressures of 0.0001 to 137 GPa. The solidus, and hence Eqn. (14a), are only valid to P<10 GPa.

Another approach, is to calibrate F as a function of composition (Putirka et al. 2007; their Eqns. A1, A2). This obviates the need to assume a given mantle composition, but requires knowledge of a parental magma composition. Two new expressions were calibrated here from partial melting experiments using depleted and fertile mantle compositions (Takahashi et al. 1993; Baker and Stolper 1994; Baker et al. 1995; Robinson et al. 1998; Walter 1998; and Pickering-Witter and Johnston 2000), with compositional parameters only,

$F = -1.997 + 0.0316[SiO_2] - 0.041[FeOt] + 0.0458[MgO] + 0.0236[CaO]$ (14b),

and using T and P as input:

$F = -2.95 - 0.0556[FeOt] - 0.176[K_2O] + 0.00274[T^{\circ}C] - 0.1446[P(GPa)]$ (14c).

For Eqns. (14b) and (14c), all compositional parameters are in weight %, R^2 and SEE values are 0.92 and 0.91, and ±0.06 and ±0.05 respectively (Figures 8a-d compares these Eqns. to other models). The compositional corrections in Eqns. 14b and 14c account for the fact that at a given P and T, the value of F will be greater for a more fertile bulk composition (e.g., Pickering-Witter and Johnston 2000), compared to a depleted mantle composition (Baker et al. 1995).

The new models describe more data with greater accuracy (e.g., F is predicted to ±0.06 to ±0.08; Fig. 8c, d) compared to both Katz et al. (2003) and PRIMELTS3 (Herzberg and Asimow 2015) (Fig. 8d). The model of Lee and Chin (2014) works quite well at F<0.6 (Fig. 8e), and can be applied to test F estimates obtained from Eqn. 14b and A2 of Putirka et al. (2007) at such conditions.

For Mars, there are no experiments where F is constrained, so we return to the Katz et al. (2003) approach. Using the Ding and Dasgupta (2014) solidus measurements, we obtain: $T(^{o}C)^{solidus} = 927 + 261P^{0.5}$, and (using the peridotite liquidus):

$$F = (T^{ol\text{-}liq} - 927 - 261P^{0.5})/(669 - 27.3P^{0.5}) \quad (14d).$$

Equation 14d yields $F = 0.12$ to 0.43 for the various martian parental magma compositions. Equations 14a-14c are not applicable to Mars, yielding lower or negative values for F compared to 14d.

Figure 8 shows that any of these models can yield negative values for F for some experimental data, and for natural compositions as well. A recommended strategy is to predict F using Eqns. 14b, and 14c, and Eqns. A1 and A2 from Putirka et al. (2007); set F to 0 for any models that yield negative estimates; then average the results (including 0 values; Fig. 8d). This approach yields a SEE of ±0.07; the SEE is slightly lower (±0.06) if only Eqns. 14b and A2 are averaged.

FURTHER RESULTS AND DISCUSSION

Calculating Mantle-Equilibrated Parental Melt Compositions and T_p: Recommended Methods and Tests

A mantle-equilibrated parental magma composition is needed to calculate T_p from igneous compositions. A recommended approach uses Eqn. 9a (K_D^{FeOt}) to calculate a range of "candidate" parental magma compositions, which are then further tested for equilibrium, and consistency between various estimates of $T^{ol\text{-}liq}$, P, K_D, etc., and assumed Fo contents of olivine in the source region. Electronic Appendix A is a spreadsheet titled *Mantle Tp*, which performs all the above calculations, including outputs from other published models. *No knowledge of T, P, F or mantle composition (beyond Fo content) are required (an fO_2 is assumed later)*:

1a) For natural samples that fall on an olivine control line (a liquid line of descent, or LLD, where olivine controls major oxide variations): add or subtract olivine until a calculated liquid composition is in equilibrium with an assumed mantle olivine composition. The candidate liquids are determined by allowing K_D^{FeOt} (Eqn. 9a) to vary within its 1σ range: 0.24 to 0.34.

1b) Absent olivine control (liquids are saturated with other phases besides olivine), select a range of possible liquids that fall on, or extrapolate from, a LLD; use Eqn. 9a and its 1σ range to calculate liquids in equilibrium with an assumed mantle olivine composition.

In steps 1a) and 1b), *we assume only that the parental magma composition lies along a LLD, rather than outside it, and that the mantle olivine composition is known.*

2) Calculate $T^{ol\text{-}liq}$ and P for the candidate compositions (step 1a, b), simultaneously or iteratively, using Putirka et al. (2007; Eqn. 4), Eqn. 13, and Putirka (2008; Eqns. 41-42). Use D_{Mg} from Beattie (1993; his Eqn. 12) for $T^{ol\text{-}liq}$. P and T are thus obtained from the calculated parental liquid composition only.

3) Calculate $X_{Fe2O3}^{liq}/X_{FeO}^{liq}$ from Eqn. 6b and K_D from Eqn. 8b, for each candidate liquid, using $T^{ol\text{-}liq}$ and P from 2), and an assumed fO_2.

4) <u>*The Tests:*</u> (a) Use the new value of K_D from 3), and the calculated $X_{Fe2O3}^{liq}/X_{FeO}^{liq}$, to calculate an equilibrium olivine composition for each of the candidate liquid compositions. (b) Calculate $T^{ol\text{-}liq}$ using Putirka et al. (2007) Eqn. 4, but now using the calculated olivine composition from 4a) to obtain D_{Mg}. The successful candidate liquid yields a calculated olivine that matches what is observed or expected for the mantle source, and a value for $T^{ol\text{-}liq}$ that matches the value from step 2). The preferred values of $T^{ol\text{-}liq}$, P and $X_{Fe2O3}^{liq}/X_{FeO}^{liq}$ are those for the successful candidate liquid.

If the olivines calculated for a given candidate liquid in 4) do not match the assumed mantle olivine composition from step 1), then the candidate liquid composition fails. One might broaden the range of values of K_D^{FeOt} from Eqn. 9a, but moving out of that range represents inconsistency between K_D and K_D^{FeOt}, which may indicate an invalid LLD.

5) <u>*To obtain T_p*</u>, let the above-calculated P (step 2) = P_1 (in Eqns. 2 and Eqn. 12c) and calculate the average value of F from Eqn. 14b, and Eqn. A2 from Putirka et al. (2007). For F, all negative estimates are taken as 0, and the 0 values are used in the average. Then, use $T^{ol\text{-}liq}$ from 2) or 4) to obtain ΔH_{fus} and C_p using Eqns. 12a and 12b (which yield coefficients A and B respectively in Eqn. 12c). The values of P_1, F, ΔH_{fus} and C_p are then inserted into Eqn. 12c.

$T^{ol\text{-}liq}$ and fO_2 of Basalt Source Regions from Natural Basalt Samples

The contents of Fe_2O_3 and FeO have been measured in various hydrous arc, hot spot and spreading ridge basalts (Allan and Carmichael 1984; Wallace and Carmichael 1989; Luhr et al. 1989; Lange et al. 1993; Feldstein and Lange 1999; Carmichael et al. 1996; Rhodes and Vollinger 2005; Bezos and Humler 2005; Cottrell and Kelley 2011; Kelley and Cottrell 2012). Most of these samples contain sufficiently high MgO (median MgO = 7.8 wt. %) so as to have olivine at or near the liquidus, which allows T, P and fO_2 to be calculated as above (see Table 2, Method 1). Estimates of $T^{ol\text{-}liq}$ for 54 hydrous and 218 nearly anhydrous samples (<1% H2O) are the same within model error using Putirka et al. (2007; Eqn. 4) and Eqn. 13 (all <29ºC apart; mostly <10ºC apart) except for two leucitites from Wallace and Carmichael (1989; samples 161 and 156). These temperatures can thus be used to infer mantle fO_2.

Calculated fO_2 values vary greatly, from ~0.5 log units below magnetite-wüstite, or MW ($10^{-10.3}$ bars) to ~0.2 log units above magnetite-hematite, or MH ($10^{-1.6}$ bars) (Fig. 7A) as expected (Carmichael and Ghiorso 1990; Carmichael 1991). The results do not parallel putative O_2-buffers except for MORB, consistent with the findings of Canil et al. (1994) for peridotites. MORB and Hawaiian samples also mostly fall within ± 1 log unit relative to QFM, the range of peridotites determined by Canil et al. (1994).

The calculated fO_2 values for MORB yield different results depending on the modeling used compared to measurements (Cottrell and Kelley 2011). Two aspects of the Cottrell and Kelley (2011) data are of special interest. First, not only do different models yield different results for fO_2 (Figs. 7b, c), but the relative magnitudes can vary with P. At P = 1 atm, for example, fO_2 is near NNO using Eqn. 7, and equation from Kilinc et al. (1983), but closer to QFM using Kress and Carmichael (1991; their Eqn. 7) and Jayasuriya et al. (2005) (Fig. 9a). When fO_2 is calculated at the higher P expected for the melt source region (1.0 ± 0.2 GPa), the fO_2 values for Kilinc et al. (1983), Jayasuriya et al. (2005) and Eqn. 7 each maintain their positions relative to QFM and NNO (which range form QFM to NNO), whereas the Kress and Carmichael (1991) values shift from near QFM to 0.5 log units above NNO. This shift is not due to intrinsic P-sensitivity but rather because Kress and Carmichael (1991) utilize additional T-dependent terms, which make their model more sensitive to the changes in T that accompany changes in P. Clearly, the positions of MORB relative to the solid-state buffers are model-dependent. But all four

models mostly overlap within 1σ model error and so supply a measure of agreement that sub-oceanic fO_2 is between QFM and NNO.

The data of Cottrell and Kelley (2011) are precise enough to exhibit an interesting parallelism relative to the QFM and NNO buffers, regardless of which of the four models are applied to calculate log[fO_2]. The phase assemblages required to buffer fO_2 are absent, so the parallelism is a coincidence. But as Carmichael (1991) recognized, the ΔH_r across the solid-state buffers (coefficients to the $1/T$ terms; see Fegley 2013) are similar to one another, and probably also to the equilibria that control $Fe^{3+} \Leftrightarrow Fe^{2+}$ (e.g., Eqn. 6a). This parallelism further reveals the long-recognized and overwhelming control of T on fO_2 compared to other parameters (Eugster and Wones 1962). For example, contrary to intuition, $X_{Fe2O3}^{liq}/X_{FeO}^{liq}$ ratios *increase* in the down-T, down-fO_2 direction, from about 0.40 at 1220ºC, to 0.97 at 1170ºC. Moreover, $X_{Fe2O3}^{liq}/X_{FeO}^{liq}$ ratios for the MORB data are uncorrelated with fO_2, no matter how calculated ($R^2 = 0.01$ using Kress and Carmichael 1991; $R^2 = 0.17$ using Eqn. 7; $R^2 = 0.08$ using Jayasuriyra et al. 2005) and negatively correlated with MgO ($R^2 = 0.44$) and T ($R^2 = 0.46$). From the MgO- $X_{Fe2O3}^{liq}/X_{FeO}^{liq}$ relationships, Cottrell and Kelley (2011) convincingly posit that $X_{Fe2O3}^{liq}/X_{FeO}^{liq}$ ratios increase with fractionation. But this implies that O_2 partial pressures decrease, even as $X_{Fe2O3}^{liq}/X_{FeO}^{liq}$ ratios increase—due to the overriding control of T on fO_2.

Errors Related to fO_2 and Parental Melt Reconstructions

There are different ways in which $fO_2 \rightarrow X_{Fe2O3}^{liq}/X_{FeO}^{liq}$ relationships can be handled, which we now use to explore errors on T_p. Cottrell and Kelley (2011) show that MORB-source mantle may be more oxidized than previously thought, and their results are important in the reconstruction of parental magma compositions. This is not because olivine-liquid thermometers (e.g., Beattie 1993; Putirka et al. 2007) are intrinsically sensitive to fO_2 or $X_{Fe2O3}^{liq}/X_{FeO}^{liq}$: an increase in fO_2 of 10^3 may decrease $T^{ol\text{-}liq}$ by only 10ºC if a fixed K_D is assumed. Rather, assumptions of fO_2, $X_{Fe2O3}^{liq}/X_{FeO}^{liq}$, and K_D, affect the fractionation vector when calculating a parental magma composition.

Figure 10 illustrates the issue, with $T^{ol\text{-}liq} - fO_2$ estimates for six different fractionation vectors (Table 2; Method 2), derived using a primitive Mauna Loa basalt (HSDP-2; sample SR0061-0.00; Rhodes and Vollinger 2004). These estimates are compared with

$T^{ol\text{-}liq} - fO_2$ for primitive MORB compositions from Cottrell and Kelley (2011). The Mauna Loa sample, without correction, would be in equilibrium with ~Fo82 olivine. But Mauna Loa lavas carry phenocrysts that range to Fo90.7 to Fo91.3 (Garcia et al. 1995; Baker et al. 1996; Putirka et al. 2007). Since HSDP samples projects towards Fo86, this composition olivine is added until equilibrium with Fo90.5-Fo91.3 is reached. It makes only a small difference (a few ºC) whether one adds Fo91.3 or Fo86, but the assumed K_D and fO_2 values matter greatly. Table 2 (Method 2, E1 –E7) shows the various assumptions applied regarding fO_2, $X_{Fe2O3}^{liq}/X_{FeO}^{liq}$ and Fo_{max}. For example, in option E3 we let $fO_2^{Hawaii} = fO_2^{MORB}$ (option E3), while in E4, we extrapolate $X_{Fe2O3}^{liq}/X_{FeO}^{liq}$ vs. MgO relationships from Cottrell and Kelley (2011) to predict $X_{Fe2O3}^{liq}/X_{FeO}^{liq}$ at Mauna Loa.

One may take issue with any of these six Mauna Loa $T^{ol\text{-}liq}$-fO_2 estimates (Fig. 8), but except for option E1, none are probably grossly unreasonable (option E1 preserves the 1-atm fO_2 determinations of Rhodes and Vollinger (2005) at high T, and implies that $X_{Fe2O3}^{liq}/X_{FeO}^{liq}$ in the Mauna Loa source is ~0.008). Together, these estimates (except E1) define error bounds on T-fO_2 beneath Mauna Loa, where $\log[fO_2] = -4.1 \pm 0.6$, $T^{ol\text{-}liq} = 1560 \pm 30$ºC, and $T_p^{Hawaii} = 1670 \pm 51$ºC. Note that even in the extreme case E1, $T^{ol\text{-}liq}$ estimates are mostly within the range of $T^{ol\text{-}liq}$ estimates obtained at fO_2>QFM (Fig. 8). Whether such fO_2- related error is acceptable depends upon the questions one asks. Small differences in fO_2 may determine whether Mauna Loa has a similar or different calculated T_p compared to Kilauea; but even large fO_2 differences are unimportant when comparing Mauna Loa to MORB, or Mars.

Error on Mantle Potential Temperatures (T_p)

Our T_p estimates for MORB provide additional examples of how T_p is sensitive to other inputs and assumptions. Mantle potential temperatures are extremely sensitive to the Fo content of olivine assumed for the mantle source. At NNO for example, T_p^{MORB} is approximately:

$$T_p^{MORB} = 74.225[Fo] - 5316.4 \qquad (15)$$

Equation 15 is derived using primitive MORB compositions (Cottrell and Kelley 2011; Putirka et al. 2007) to equilibrate with different mantle olivine compositions; the SEE for Eqn. (15) is ±44ºC (remarkably close to the error determined by Herzberg and Asimow

2015). But each Fo in Eqn. 15 implies a different parental magma, created at a different F. If we let $F = 0.08$, the Cottrell and Kelley (2011) "primary melt" compositions yield a mean $T_p = 1338\pm42$ºC (1285-1418ºC). But the F predicted for these compositions is mostly <0.03 (which lowers T_p further), and these liquids equilibrate with Fo88.8±0.04 (at $K_D = 0.34$; $P = 0.96\pm0.26$ GPa; and at fO_2 of 0.2 log units below NNO). These T_p estimates are lower than Putirka (2008) and Putirka (2007), where T_p = 1390-1450ºC, and where $F = 0.08$, and mantle olivine = Fo91.5. The Cottrell and Kelley (2011) compositions yield T_p = 1441ºC, when corrected so as to equilibrate with Fo91.5 (P=1.7 GPa; fO_2 = NNO; $F = 0.08$; K_D=0.34).

A T_p^{MORB} nearer to 1400ºC is here preferred. First, Fo91.5 olivines appear to be common in MORB; second, the East Pacific Rise segment that yields Fo91.5 olivines is not hot-spot related, and has FeOt contents typical of MORB (Putirka et al. 2007). But global MORB olivine variations are too poorly documented to declare whether T_p^{MORB} is in some places near 1330ºC, or if all estimates reflect fractionated systems.

More generally, we find that 1σ error on T_p, is ~ ±77ºC, on the high end of errors reported by Putirka (2005; his Fig. 8). This error includes that related to estimating (a) a parental magma composition from fO_2 vs. $X_{Fe2O3}^{liq}/X_{FeO}^{liq}$ relationships (±30ºC, as illustrated above; Table 2), (b) melt fraction, F (±63ºC), (c) pressure, P (±30ºC), and (d) uncertainty in ΔH_{fus} and C_p (±13ºC). Error from P uncertainty is interestingly low, and derives from a remarkably close comparison of T_p estimates for compositions from Herzberg et al. (2010), where T_p is calculated at 1-atm (open symbols in Fig. 9b) and at calculated equilibrium pressures (using Putirka 2008; Eqns. 41-42). The close agreement stems from the fact that at 1-atm, F is greater (by +0.17 avg.) to achieve a given liquid MgO content (e.g., Stolper 1980), which compensates for lower 1-atm $T^{ol\text{-}liq}$ in Eqn. 2c.

There is yet another possible source of error not included in the above accounting, and embedded in the question: what does a parental magma represent? Herzberg and Asimow (2008) express concern that T_p estimates depend upon whether a parental magma is an isobaric batch melt (T_p^{batch}), or more realistically, as an "accumulated" melt (T_p^{acc}) i.e., the sum of a series of smaller, polybaric, fractional or incremental melts that are later pooled. Hirose and Kushiro (1998) suggest that liquid MgO contents are affected by such

processes (higher MgO at a lower F for an accumulated melt compared to a batch melt), which implies that T_p based on an isobaric batch assumption may be overestimated.

Fortunately, $T_p^{batch} \approx T_p^{accumulated}$. Potential temperatures are calculated for the incremental, accumulated and isobaric batch melt compositions of Hirose and Kushiro (1998) and Hirose and Kawamura (1994) (Fig. 9), using Table 2, Method 2 (fO_2 = QFM). Equations 14b, c and Eqn. A2 from Putirka et al. (2007) are used to estimate F. These experiments were not used for calibration of any model, so the data provide a true test of our ability to predict T_P. Not only is there no systematic error between accumulated, incremental and isobaric batch melt cases (Fig. 11), but T_p estimates are remarkably small (standard errors of estimates, or SEEs, for the 12 observations are ±16-18ºC; Figs. 11A, B), and in agreement with Asimow et al.'s (1997) findings.

Cooling Rates on Earth, Moon, Mars and Vesta

Pressure Estimates, Planet Size and Archean Temperatures

Here we compare T_p estimates across planetary bodies through time, mostly using published parental magma compositions. For reference, mean calculated pressures (P_1) are as follows: 0.5±0.2 GPa for eucrites, 1.6±0.5 GPa for Mars (except for Nakhla, at 0.0±0.5 GPa—effectively atmospheric pressure) and 2.2±0.8 GPa, for high MgO lunar samples. These are mostly similar and within error to estimates of Lee et al. (2009), although slightly higher pressures are obtained for Mars and eucrites. For primitive MORB and Hawaiian (Mauna Loa) compositions, mean pressures are 1.0±0.3 GPa, and 2.8±0.3 GPa respectively. For eucrites, P = 0.05 GPa is used.

Certain of our inter-planetary thermal comparisons are as expected. In the 4500 to 4300 Ma range, T_p increases with planet size from Vesta to Moon to Mars to Earth (Fig. 10). This ordering may be anticipated for at least two reasons: smaller planets have smaller accretion energies (Consolmagno and Schaefer 1994, p. 95-97), and lower temperatures should be expected for smaller planets due to the positive Clausius-Clapeyron slope for melting of silicates or Fe-Ni alloys. Estimates by Herzberg et al. (2010), though, place this sequence in doubt. For their parental magmas (circles in Fig. 10) there is an apparent decrease in T_p from 2700 to 3700 Ma. If valid, Earth would then be *cooler* than either its Moon, or Mars at 3700 Ma.

We surmise, though, that Earth was indeed much hotter at 2700-3700 Ma, and earlier. As acknowledged by Herzberg et al. (2010), MgO contents for Archean magmas can be quite high. For example, Green et al. (1975) show that some komatiites are possibly liquids, with up to 30 wt. % MgO, and in equilibrium with ~Fo94 olivine. Bernstein et al. (2007) and Herzberg and Rudnick (2012) further show that Fo92-94 olivines characterize the Archean mantle, representing the residues of partial melting when $F = 0.4$-0.5.

As a test, we calculate $T^{\text{ol-liq}}$ and olivine compositions for the Green et al. (1975) anhydrous composition (49J) at 1 GPa (their experimental P; and we let $X_{Fe2O3}^{liq}/X_{FeO}^{liq} = 0$ since Green et al. (1975) use graphite capsules). Our new models yield K_D=0.36, $T^{\text{ol-liq}}$ = 1676±30ºC, and olivine of Fo94.0, which match the Green et al. experimental results of 1650ºC, and Fo93.6 remarkably well. If we instead assume that fO_2 = QFM and use P calculated from Si-activity, then K_D is still 0.36, but P=5.7 GPa, $T^{\text{ol-liq}}$ =1858ºC, $X_{Fe2O3}^{liq}/X_{FeO}^{liq} = 0.247$, and the equilibrium olivine is Fo96. The higher Fo content is not intrinsically due to P (note that K_D, though P-dependent, is the same within error) but rather because higher P requires a higher T of equilibration, which in turn affects, $X_{Fe2O3}^{liq}/X_{FeO}^{liq}$, and hence the equilibrium olivine composition.

Given the Bernstein et al. (2007) results, perhaps any composition that yields Fo96 olivine should be rejected (see Keiding et al. (2011) for a word of caution on high Fo olivines). We thus remove 25% olivine from 49J to obtain Fo94, at K_D =0.36, with P=4.2 GPa, $T^{\text{ol-liq}}$ =1743ºC, and $X_{Fe2O3}^{liq}/X_{FeO}^{liq} = 0.186$. Note how a simple assumption of elevated P fundamentally alters the assessment of equilibrium—the Green et al. (1975) bulk composition only reproduces observed olivine compositions at 1 GPa, but is far too MgO-rich to yield the observed olivine composition at P>4 GPa. It is not at all clear which of these cases is valid. Olivines of Fo94 may have formed from the most primitive melts entering a chamber at 1 GPa or less, say at the base of the crust—validating the Green et al. (1975) results, and their use of 1 GPa to perform their experimental tests. In this case Archean T_p is 2178ºC. But if Fo 94 olivines are relict from the inferred depth of melt segregation from the mantle (4-6 GPa), there ensues a cascading sequence of inter-connected relationships that yield a T_p that is >200ºC lower, at 1959ºC! These two calculations for the Green et al. composition are plotted in Fig. 9B as red squares, and in either case, indicate much higher terrestrial T_p at 3500 Ma. What's more, the Green et al.

(1975) composition is not unique (e.g., Nisbet et al. 1993; Robin-Popieul et al. 2012). Using Bernstein et al. (2007) as a guide, GEOROC contains 270 Archean-age samples (out of ~5200 Archean samples with >10% MgO) that are in equilibrium with Fo92-94, at F = 0.4-0.5 (at P = 3.5±1.1 GPa; Fig. 12a; see red open squares for T_p), and these yield a distinct mode for Archean T_p at 1940ºC. This mode is preserved if we include samples where F is as low as 0.1, or where mantle olivine is as low as Fo90 (Fig. 12b). This high T_p mode is remarkably close to the Green et al. (1975) case at P =4-6 GPa. Mean Archean T_p^{plume} is thus estimated to be ~1940-1960ºC, and perhaps as high as 2030ºC (Fig. 12b).

This is not to say that Archean T_p is without alternative viewpoints (e.g., Parman et al. 1997; Keiding et al. 2011). But these high T_p estimates are not unprecedented. Archean temperatures approach those of Nisbet et al (1993), and our inferred plume-cooling curve is practically identical to that of Herzberg (1995; his Fig. 8 for T_{ex} = 300ºC). There is also modest thermal overlap with recent T estimates derived from Archean peridotites. Lee and Chin (2014) obtain melting temperatures of 1400-1750ºC at 1-5 GPa, compared to 1500-1910ºC and 2-5 GPa here. Perhaps it should not be unexpected that peridotite-derived temperatures are lower, but Lee and Chin (2012) do not attempt to reproduce the Fo92-94 olivines (Bernstein et al. 2007; Herzberg and Rudnick 2012), and might have obtained higher temperatures had they done so.

Secular Cooling And The Cooling of Plumes

By accepting high Fo olivines and high MgO Archean compositions as magmatic, then Earth, like Mars, exhibits monotonic cooling through its recorded history (see Abbott et al. 1994). These results are in concert with recent numerical modeling efforts. For example, the magnitude and thermal trend of Fig. 12a agrees with the high-T initial state of Nakagawa and Tackley (2012), which shows monotonic cooling from 4.5 Ga to the present (Nakagawa and Tackley 2012, their Fig. 2). They also find a modern T_{avg} of 2027ºC (=2300 K), which is remarkably close to T_{avg} = 1992-2042ºC, based on T_p^{MORB} = 1400-1450ºC (Putirka et al. 2007, and confirmed here), when using the adiabat of Katsura et al. (2010). Davies (2008), and Nakagawa and Tackley (2010; 2014) also infer near monotonic cooling of Earth's ambient mantle, and the thermal boundary layer (TBL) above the core-mantle boundary (CMB).

Figure 12a would appear to be in contention with Korenaga (2008), or Herzberg et al. (2010), who suggest that T_p should increase from 4.5 to 3.7 or 2.7 Ga, and whose cooling histories are tied to the Urey ratio (Ur = heat production/heat flow). However, the higher temperatures inferred here would appear to lessen the apparent Ur-related problem: low Ur estimates imply high temperatures in the Archean (Korenaga 2008; Silver and Behn 2008), and such temperatures are realized here (Fig. 12a). But Nakagawa and Tackley (2012) also show that modern estimates of Ur seem to be uninformative regarding thermal history. In support of Herzberg et al. (2010), though, T_p estimates in Fig. 12a are only slightly greater at 3200-3710 Ma (1870±113ºC) compared to 2680-3000 Ma samples (1827±143ºC) (Fig. 12) indicating very subdued cooling in the Archean.

No less interesting is that our modern plume T_p estimates (1700 ºC today; ~1940-2030ºC in the Archean), which are high compared to Lee et al. (2009) and Herzberg et al. (2010), extrapolate to CMB depths of just 2380ºC (and to 3015ºC in the Archean if maximum T_p = 2000ºC). A T_{CMB} of 2380ºC, based on Mauna Loa, does not even reach low-end CMB-TBL temperatures of 2500-3000ºC estimated by Nomura et al. (2014). This mismatch may mean that T_P^{plume} is still underestimated, but could also mean that the mantle is super-adiabatic or, as Korenaga (2005) suggests, that plumes do not reflect the hottest parts of CMB-TBL.

Earth and Mars may also reveal similar secular cooling rates. For Mars, maximum temperatures are ~1700ºC at 4300 Ma (Yamato 980459; Eqn. 14d yields F =0.38) and ~1320ºC at 1300 Ma (if we exclude Nakhla D), which bracket Filberto and Dasgupta's (2011) mean T_p for Mars of 1445-1475ºC. Nakhla D (Longhi and Pan 1989; Treiman 1986) is problematic as it owes its high T_P estimate (1602ºC) to its uniquely high MgO content of 12% (which yields F = 0.43 from Eqn. 14d), compared to <6% MgO for all other parental Nakhla compositions (Treiman 1993; Goodrich et al. 2013). Ignoring Nakhla D, and connecting maximum T_p estimates from 4.3 to 1.3 Ga, yields a martian cooling rate of ~110-130ºC/Ga; this rate drops to 33ºC/Ga if we use Nakhla D. Mars also reveals non-linear cooling, with early rates as high as 275-550ºC/Ga. If Mars exhibits a "stagnant lid" (Fig. 1c), then the long term averaged rates there should be compared to the cooling of terrestrial mantle plumes.

For terrestrial plume cooling rates, we assume that Archean maximum T_p estimates of ~1950ºC to 2030ºC are plumes (e.g., Herzberg et al. 2010), and compare these to Mauna Loa, where mean T_p = 1560±51ºC (Putirka 2008b) and maximum T_p =1670ºC (Fig. 12a). Long-term terrestrial plume cooling rates are thus between 111ºC/Ga (= [1950-1560ºC]/3.5 Ga) to 103ºC/Ga (= [2030-1670ºC]/3.5 Ga)—at the low end of martian cooling rates, but perhaps not surprisingly so, since Earth does not capture early post-accretion cooling. These overlapping cooling rates for Earth and Mars support Stevenson's (2003) idea that smaller planetary bodies cool at roughly similar rates as larger bodies, but at lower T (see also Papuc and Davies 2008).

Bi-modal Mantle Potential Temperatures and the Inception of Plate Tectonics

The prior section delimits cooling rates for terrestrial plumes; what about cooling rates for ambient terrestrial mantle? Silver and Behn (2008) propose that a stagnant lid, or an approximation thereof, may have characterized the Archean Earth, implying uni-modal (plume) volcanic activity at that time. But Archean volcanism is thermally bi-modal, with modes at T_p = 1940ºC and 1740ºC (Fig. 12b). The faintness of the mode at 1740ºC may be due to sampling or preservation bias—or perhaps lack of substantial low-T_p volcanism. In any case, the implied excess temperatures ($T_{ex} = T^{plume} - T^{ambient}$) are 200-290ºC—quite close to modern values of 220-320 ºC (Fig. 12a). Moreover, if T_p^{MORB} is between 1400ºC-1350ºC, then using 1740ºC for the Archean ambient mantle, we obtain ambient mantle cooling rates that are quite similar to terrestrial plumes, falling between 97-111ºC/Ga.

IMPLICATIONS

Error on Mantle Potential Temperatures

A key motivation of this study was to better ascertain propagated errors on estimates of T_p, and we find that 1σ = ±77ºC, although 1σ may be <±42ºC, as determined in places here, and also by Herzberg and Asimow (2015). The latter's PRIMELT3 model provides at least two temperatures for $T^{ol\text{-}liq}$, reported as "T(C)" and "Old T(C)". The apparently preferred "T(C)" estimates under-predict experimental $T^{ol\text{-}liq}$ (Fig. 12c), but their "Old T(C)" and the Putirka (2008; Eqn. 22) model (identical to Putirka et al. (2007) Eqn. 4) have much less systematic error. These tests of $T^{ol\text{-}liq}$ (Fig. 12c) use experimental P as input; but solving for P and T simultaneously, using Putirka (2008; Eqns. 22, 41-42)

introduces little additional error on $T^{ol\text{-}liq}$ (Fig. 12c). However, T_p, P, fO_2, K_D and $X_{Fe2O3}^{liq}/X_{FeO}^{liq}$, are highly interconnected, and as illustrated using the Green et al. (1975) komatiite composition, assumptions of P can fundamentally alter interpretations of equilibrium, $X_{Fe2O3}^{liq}/X_{FeO}^{liq}$, etc, which significantly impact T_p.

Planetary Temperatures & Cooling Rates

This reanalysis also shows that T_p estimates capture monotonic secular cooling histories for Earth and Mars, and a positive relationship between planet-size and early maximum T_p. The Archean exhibits thermally bi-modal volcanism, albeit heavily weighted towards the mantle plume end of the spectrum (T_p = 1940ºC-2000ºC). The Archean Earth thus did not act as a stagnant lid, but these results do not preclude "intermittent" tectonic modes (Silver and Behn 2008).

These high Archean temperatures are not unprecedented. Earlier studies (Miller et al. 1991; Nisbet et al. 1993; Herzberg 1995) concluded that Archean mantle melting should reach the transition zone, or the top of the lower mantle. Here, a $T_p^{ambient}$ of 1740ºC would intersect the solidus at ~8.5 GPa, or ~260 km (Fig. 12d), whereas Archean plumes (T_p = 1940ºC) would begin melting at 19 GPa, or ~535 km, effectively matching the 500 km estimate of Nisbet et al. (1993). At higher T_p (~2000ºC), initial melting depths are almost unconstrained, ranging from the mid-mantle (58 GPa, 1330 km; solidus of Nomura et al. 2014), to the transition zone (20-22 GPa, 560-610 km; using the solidi of Zerr et al. 1998; Fiquet et al. 2010).

Perhaps more importantly, the surmised Archean "thermal catastrophe" (Silver and Behn 2008) at low Urey ratio (Ur) appears to be exaggerated. The new Archean T_p^{plume} and $T_p^{ambient}$ values allow for lower Ur values. More interestingly, Nakagawa and Tackley's (2012) findings appear to divorce any given Ur from a particular thermal history. But there is also misunderstanding: O'Neil and Debaille (2012) express concern that T_p = 1800ºC would cause the "whole mantle [to be] molten" (p. 55)—but nothing of the sort is true. First, it should be noted that T_p^{plume} estimates are irrelevant to such discussion, as they do not reflect ambient mantle temperatures; but even a T_p of 2000ºC is insufficient to melt the entire mantle (Fig. 12d), and Archean $T_p^{ambient}$ is closer to 1740ºC.

Evolution of Earth-like Planets?

A key finding is that terrestrial Archean volcanism appears to be thermally bi-modal. Since the onset of thermally bi-modal volcanism is a likely harbinger of plate tectonics, we conclude that plate tectonics began on Earth at least by 3.5 Ga. This finding allows an early-plate-tectonic explanation by Blichert-Toft et al. (2015) for long-term Lu/Hf enrichments in some Archean volcanics, and other geochemical evidence of early tectonic activity (e.g., Shirey et al. 2008). Intriguingly, Mars, at 1300 Ma, might also approach thermal bi-modality (Fig. 12). But this highly tentative conclusion hinges upon whether Nakhla D (Treiman 1986; Longhi and Pan 1989) is a magmatic composition. If Nakhla D is not errant, then Mars may have experienced an internal shift from stagnant lid to plate tectonics, at least momentarily before its apparent thermal shutdown. Although uncertain, this interpretation implies that the timings and persistence of a stagnant lid-to-plate tectonic transition are controlled by planet size. Investigation of young martian volcanic features should be a top priority for new rover missions, as these may provide even greater insight as to why Earth is unique, compared to the present focus on sedimentary basins.

Mantle Source Mineralogy

A final implication concerns the mineralogy of the modern terrestrial mantle. That hotter, deeper, Hawaiian lavas have equal or lower $X_{Fe2O3}^{liq}/X_{FeO}^{liq}$ compared to MORB (Figs. 7 and 8) (even at higher absolute fO_2) is a compelling argument that (a) pyroxenite does not exist in the Hawaiian mantle source and (b) that the deep mantle is not as reduced as implied by Frost and McCammon (2008). Pyroxene-rich lithologies have the capacity to carry considerably more Fe^{3+} than their olivine-rich counterparts, and if they reflect recycled, fractionated, near-surface materials, then pyroxenite sources should be well oxidized. This result seems to have been anticipated by Carmichael (1991), who hypothesized that high fO_2 arc-lavas may have a pyroxenite source, since properly analyzed peridotites had fO_2 levels far too low to be appropriate. Canil et al.'s (1994) work supports this idea, as they see a positive correlation between Fe_2O_3 and both of CaO and Al_2O_3, in natural peridotites and pyroxenites. Modern volcanic products should thus yield $X_{Fe2O3}^{liq}/X_{FeO}^{liq}$ in proportion to the amounts of pyroxenite predicted for their sources (e.g., Sobolev et al. 2007), if indeed such sources exist.

Acknowledgments

Special and sincere thanks are owed to Cin-Ty Lee, Claude Herzberg, and Mike Garcia, Each provided thorough and thoughtful reviews—amongst the most helpful received on any paper. I greatly appreciate Mike Garcia's attention to detail, which saved the manuscript from being published with even more errors than it likely already has, and for making the paper a much better read than the original. Reviews by Lee and Herzberg were also invaluable, as they prompted serious re-evaluation of several key issues, including Lee's concerns about reconstruction of mantle geotherms, and Claude's recognition of possible bi-modal volcanism in the Archean. I also thank the National Science Foundation for their generous support. This work grew out of two broadly related projects funded by NSF, 1250322 and 1250323.

Figure Captions

FIGURE 1. (a) Illustrates calculations to convert a magmatic temperature, T^{m}, to a mantle potential temperature, T_p. The conversion involves two corrections: the first accounts for the heat of fusion, and so recovers the T the solid mantle (T^{sol}) would have had, had it not partitioned some of its energy in converting solidus to liquids. The second correction projects T^{sol}, as if the solid mantle were transported to the surface along an isentropic adiabat (see discussion of Eqns. 1-2 in the text for details). The black solid line is the geotherm. If the mantle does not rise along an isentrope, then T_p would not project downwards to yield a convective geotherm (but still may be used as a useful reference T to compare heat contents of mantle parcels, as in (b), which compares the adiabatic geotherms and T_ps for passive upwelling of ambient mantle, as beneath terrestrial ridges or arcs, and active upwelling from a thermal boundary layer (TBL), as in terrestrial plumes. In (c), "plate mode" (e.g., plate tectonics) and "stagnant lid" cases are compared (see Stevenson 2003). Planets that do not have plate tectonic should yield a uni-modal distribution of T_p, since volcanism only occurs by the action of plumes from a TBL. In contrast, sufficiently large planets, with plate tectonics, may exhibit a bi-modal distribution of T_p, as on Earth, since volcanic rocks also sample cooler ambient mantle, which upwells beneath spreading ridges and arcs.

FIGURE 2. (a) K_D (= ($X_{FeO}^{ol}/X_{MgO}^{ol}$)/($X_{FeO}^{liq}/X_{MgO}^{liq}$)) is calculated for 1270 experiments (where fO_2 is constrained) using two different methods to calculate $X_{Fe2O3}^{liq}/X_{FeO}^{liq}$: Kress and Carmichael (1991; Eqn. 7) and Jayasuriya et al. (2005; Eqn. 12); X_{Fe2O3}^{liq} = $[X_{FeOt}^{liq}][X_{Fe2O3}^{liq}/X_{FeO}^{liq}]/(1+2[X_{Fe2O3}^{liq}/X_{FeO}^{liq}])$; $X_{FeO}^{liq} = X_{FeOt}^{liq} - 2[X_{Fe2O3}^{liq}]$. (b). The $X_{Fe2O3}^{liq}/X_{FeO}^{liq}$ ratios, used as input for (a), are compared. Higher $X_{Fe2O3}^{liq}/X_{FeO}^{liq}$ by Jayasuriya et al. (2005) in (b) leads to lower $X_{FeO}^{liq}/X_{MgO}^{liq}$, and thus higher K_D in (a). Note that some experiments that would have $K_D = 0.30$ using Kress and Carmichael (1991) could have a K_D of nearly 0.4 using Jayasuriya et al. (2004).

FIGURE 3. (a) $X_{Fe2O3}^{liq}/X_{FeO}^{liq}$ and (b) K_D are calculated over a range of temperatures, at fO_2 = 1.5 log units below QFM (QFM – 1.5; see Rhodes and Vollinger 2004), for HSDP-2 whole rock composition SR0641-1 (Putirka et al. 2011). Values for $X_{Fe2O3}^{liq}/X_{FeO}^{liq}$ and K_D are from Eqn. 6b, Jayasuriya et al. (2005) (J), Kress and Carmichael (1991; Eqn. 7) (KC91) and Kress and Carmichael (1988) (KC88). T-fO_2 relationships for QFM are from Myers and Eugster (1983) (M&E (1983)), Schwab and Kustner (1981) (S&K (1981)) and Hewitt (1978) (H (1978)). $X_{Fe2O3}^{liq}/X_{FeO}^{liq}$ ratios in (a) are used to obtain $X_{FeO}^{liq}/X_{MgO}^{liq}$ ratios and K_D in (b). Note that different solid-state buffer calibrations, used to determine fO_2 from T, yield trivial error, but models used to calculate $X_{Fe2O3}^{liq}/X_{FeO}^{liq}$ from fO_2 yield contrasting fO_2- $X_{Fe2O3}^{liq}/X_{FeO}^{liq}$ relationships: Jayasuriya et al. (2004), for example, predicts decreasing $X_{Fe2O3}^{liq}/X_{FeO}^{liq}$ as fO_2 increases along a solid-state buffer (with increased T), while KC91, KC88, and Eqn. 6b are more neutral in this regard. (c) A comparison of $X_{Fe2O3}^{liq}/X_{FeO}^{liq}$ as in panel (a), but using Fegley's (2013) model for QFM (calculations are at 1-atm). Contrasts are small at QFM-2, but increase with increased fO_2 and are quite significant at QFM+2, especially at low T.

FIGURE 4. Panels (a) through (h) compare $X_{Fe2O3}^{liq}/X_{FeO}^{liq}$ ratios calculated from different models, using experimental results where $X_{Fe2O3}^{liq}/X_{FeO}^{liq}$ ratios are measured, mostly by "wet chemistry" (data sets DS1 and DS2) but also by Mossbauer spectroscopy (DS3; see Table 1). All statistics are for predictions of $X_{Fe2O3}^{liq}/X_{FeO}^{liq}$, not the log of such ratios. Equation 6b is calibrated using (DS1 and DS3). (h) is the same as (g), except that the log

scale is removed, so as to illustrate the error on calculations of $X_{Fe2O3}^{liq}/X_{FeO}^{liq}$, which increase at higher $X_{Fe2O3}^{liq}/X_{FeO}^{liq}$, as measurement errors appear to scale with X_{Fe203}^{liq}.

FIGURE 5. Panels (a) through (d) compare predicted vs. measured values of fO_2 using Eqn. 7, and the commonly-used models of Kress and Carmichael (1991) and Kilinc et al (1983), as well as Jayasuriya et al. (2004). Equation 7 is calibrated using DS1 (see Fig. 3 caption) only; DS2 and DS3 are test data. All regression statistics are for the combined data sets DS1, DS2 and DS3. Note that use of Eqn. 7 increases both accuracy and precision.

FIGURE 6. (a) K_D is calculated for experimental data, using $X_{Fe2O3}^{liq}/X_{FeO}^{liq}$ from Eqn. 6b. The distribution is nearly Gaussian with a mean of 0.33. (b) Plot of $\ln K_D$ vs. 10^4/T(K) shows that K_D is nearly independent of T, at least when there is accounting for $X_{Fe2O3}^{liq}/X_{FeO}^{liq}$. K_D is compared to (c) wt. % $Na_2O + K_2O$, (d) wt. % SiO_2, and (e) P(GPa). None explain more than a small fraction of the total observed variation in K_D, but each are still useful in predicting systematic shifts in K_D, compared to use of the mean in (a).

FIGURE 7. K_D is predicted for experimental data (Fig. 1) using (a) Toplis (2005), (b) Eqn. 8b, (c) Eqn. 8d, and (d) Eqn. 9b; in (a) – (c), Eqn. 6b us used to calculate $X_{Fe2O3}^{liq}/X_{FeO}^{liq}$; in (d) all Fe in the liquid is treated as FeO. All but Toplis (2005) predict K_D from liquid compositions only. Eqn. 9b (d) explains half the variation of K_D, but the lower R^2 values for the other models are not necessarily defects, as they account for fO_2-dependencies through the use of Eqn. 6b, that are simply made explicit in Eqn. 9b, where all Fe is FeO.

FIGURE 8. Melt fraction is predicted, for experimental data (Takahashi et al. 1993; Baker and Stolper 1994; Baker et al. 1995; Robinson et al. 1998; Walter 1998; and Pickering-Witter and Johnston 2000) where F is measured, in (a) as a fractional distance between liquidus and solidus, as in Katz et al. (2003), and Eqn. 14a, which uses the Hirschmann et al. (2000) solidus, in (b) using the composition-dependent equations A1 and A2 of Putirka et al. (2007), and (c) using the new composition dependent models 14b, c. Each of these models may predict F to be <0 or >1 for a number of experimental data. This

effect can be mitigated by taking the mean of multiple estimates, and taking $F = 0$ for all cases where F is predicted to be <0 (using zeros as part of the average). The most successful mean values (d) use a combination of Eqns. 14b, 14c, A1 and A2, or just 14b and A2 alone. (e) Lee and Chin (2014) model for F; their model is calibrated from Walter (1998). (f) Predicted F from PRIMELTS3 (Herzberg and Asimow 2015), using "F(proj)", which is their best and apparently preferred model.

FIGURE 9. (a) fO_2 v. T for natural magma compositions where $X_{Fe2O3}^{liq}/X_{FeO}^{liq}$ ratios are measured; fO_2 buffer curves are from Fegley (2013). All fO_2 v. T conditions are calculated as in Method 1 of Table 2 (using Putirka et al. 2007; Eqn. 4 for T). (b) fO_2 v. T is calculated assuming 1-atm pressure for the Cottrell and Kelley (2011) natural compositions, using Putirka et al. (2007; Eqn. 4 for T) and various models to obtain fO_2 from measured $X_{Fe2O3}^{liq}/X_{FeO}^{liq}$ as in the legend. (c) The same as in (b) except P is calculated from Putirka (2008) Eqns. 41-42 (Si-activity). Note that 1σ model error of ±0.75 to ±1.0 log units fO_2 (Fig. 4) covers the range of fO_2 from QFM to NNO; also, all models yield parallel fO_2 v. T trends, which also parallel the reference solid-state buffers, since all such equilibria appear to have similar heats of reaction, ΔH_r (i.e., similar regression coefficients for 1/T terms).

FIGURE 10. fO_2 v. T relationships for parental MORB compositions (Cottrell and Kelley 2011), and Hawaiian (Mauna Loa) magma compositions (where $X_{Fe2O3}^{liq}/X_{FeO}^{liq}$ is predicted). All calculations follow Method 2 of Table 2. For MORB at Step E, two calculations methods are illustrated, by preserving from the natural compositions either mean $X_{Fe2O3}^{liq}/X_{FeO}^{liq}$, or fO_2 v. $1/T$ relationships. For Mauna Loa, we employ five different assumptions regarding $X_{Fe2O3}^{liq}/X_{FeO}^{liq}$ and fO_2 to explore how such assumptions affect the range of resulting $T^{ol\text{-}liq}$ estimates; see text and Table 2, Methods 2, Step E for details.

FIGURE 11. Calculated vs. experimental mantle potential temperatures, for incremental, accumulated and batch partial melts, from Hirose and Kawamura (1994) and Hirose and Kushiro (1998) using melt fraction, F, from (a) Eqn. 14a and (b) Eqn. A2 of Putirka et al. (2007). All estimates are within 1σ model error of T_p.

FIGURE 12. (a) A comparison of time vs. mantle potential temperatures, T_p, estimates for published parental magma compositions from Earth, Moon, Mars and Vesta, and possible high MgO Archean magma compositions. Non-terrestrial T_p estimates use parental magma compositions from published sources noted in the Methods section. T_p estimates for Hawaii are from Mauna Loa, as shown in Figure 10. MORB estimates use Cottrell and Kelley (2011) primitive magmas. Terrestrial Phanerozoic T_p estimates use parental magmas for the Cretaceous komatiites from Gorgona Island of Herzberg and O'Hara (2002), and plumes and Large Igneous Provinces from Herzberg and Gazel (2009) and Hole (2015). Precambrian T_p estimates use parental magma compositions of non-arc magmas (Herzberg et al. 2010), shown using calculated P (1.7-4.1 GPa), and P = 1atm. Also shown is the Green et al. (1975) Archean composition, equilibrated (at fO_2 = QFM) with Fo96 (P =5.7 GPa; $T^{ol\text{-}liq}$ = 1996ºC) and Fo94 (P =4.2 GPa, $T^{ol\text{-}liq}$ = 1814ºC), and Archean volcanic bulk compositions (from GEOROC) that allow equilibrium with olivine of Fo91-94, at F = 0.4-0.5, as in Bernstein et al. (2007) (at P =1.2-6.0 GPa, $T^{ol\text{-}liq}$ = 1470-1855ºC, and fO_2 = QFM). For the Herzberg et al. (2010) parental compositions, calculated $Fe^{3+}/\Sigma Fe$ ranges from 0.08-0.22, bracketing measured values of 0.1 from Berry et al. (2008), but ranging to higher ratios since we allow that $X_{Fe2O3}/X_{FeO} = f(T)$. **(b)** A histogram of T_p estimates for Archean magmas in equilibrium with Fo92-94 olivine (at F = 0.40-0.50) and Fo90-94 olivine (at F = 0.10-0.55). Both distributions appear bi-modal, with modes at 1740ºC and 1940ºC, perhaps reflecting partial melting of ambient mantle and mantle plumes respectively. (c) Comparison of $T^{ol\text{-}liq}$ for PRIMLET3 outputs and Eqn. from Putirka (2008) using data as in Fig. 8, excepting Takahashi et al. (1993), whose temperatures were more poorly predicted by all models. The PRIMELT3 "Old T(C)" model is nearly identical to Putirka (2008), and both have little systematic error. Blue circles show that using calculated P (from Putirka 2008; Eqns. 41-42) as input has only a small effect: the SEE is ±36ºC when the Takahashi et al. (1993) data are excluded. (d) Comparison of mantle solidi with adiabatic paths of Katsura et al. (2010) for T_p values of 1740ºC, 1940ºC and 2000ºC. The solidus at P<19 GPa is from Putirka et a. (2007; their Eqn. 6; the same as the Hirschmann et al. (2000) at low P, except calibrated to avoid quadratic behavior). At P>19 GPa, we use the solidus of Nomura et al. (2014) (T(ºC) =

1990.73+9.918*P*(GPa)) and Zerr et al. (1998) (*T*(ºC) = -391+872.8ln(P(GPa)), the latter of which is quite similar to Fiquet et al. (2010) (*T*(ºC) = -578.4+918.65ln(P(GPa)). The Nomura et al. (2014) solidus implies initial melting depths in the mid-mantle, but this is not a robust result given non-trivial uncertainties in both the adiabat path, and the mantle solidus. The Katsura et al. (2010) isentropic adiabat (their Fig. 2) dT(ºC)/dz(/km) is approximated as follows:

if z(km)<500, $dT/dz = -0.32+9.762\times10^{-4}[z(km)] +1.25\times10^{-6}[z(km) - 882.3]^2$;

if 500<z(km)<670, $dT/dz = 0.042+6.2\times10^{-4}[z(km)]$;

if z(km)>670, $dT/dz = (1.44+9.8\times10^{-4}[z(km)])^{-1}$.

References Cited

Abbott, D., Burgess, L., Longhi, J. and Smith, W.H.F. (1994) An empirical thermal history of Earth's upper mantle. Journal of Geophysical Research, 99, 13835-13850.

Agee, C.B. and Walker, D. (1993) Olivine flotation in mantle melt. Earth and Planetary Science Letters, 114, 315–324.

Allan, J. F. & Carmichael, I. S. E. (*1984*) Lamprophyric lavas in the Colima graben, SW Mexico. Contributions to Mineralogy and Petrology, 88, 203–216.

Ariskin, A.A. (2007) Parental magmas of lunar troctolite: genetic problems and estimated original compositions. Geochemistry International, 45, 413-427.

Asimow, P.D., Hirschmann, M.M. and Stolper, E.M. (1997) An analysis of variations in isentropic melt productivity. Philosophical Transactions of the Royal Society, 355, 255-281.

Baker, M.B., Alves, S., and Stolper, E. M. (1996) Petrography and petrology of the Hawaii scientific drilling project lavas: inferences from olivine phenocryst abundances and compositions. Journal of Geophysical Research, 101, 11715-11727.

Baker, M.B., Hirschmann, M.M., Ghiorso, M.S., and Stolper, E.M. (1995) Compositions of near-solidus peridotite melts from experiments and thermodynamic calculations, Nature, 375, 308-311.

Baker, M.B., and Stolper, E.M. (1994) Determining the composition of high-pressure mantle melts using diamond aggregates. Geochimica et Cosmochimica Acta 58, 2811-2827.

Barr, J.A., and Grove, T.L. (2013) Experimental petrology of the Apollo 15 group A green glasses: melting primordial lunar mantle and magma ocean cumulate assimilation. Geochimica et Cosmochimica Acta, 106, 216-230.

Beattie, P. (1993) Olivine-melt and orthopyroxene-melt equilibria. Contributions to Mineralogy and Petrology 115, 103-111.

Bernstein, S., Kelemen, P.B., and Hanghø, K. (2007) Consistent olivine Mg# in cratonic mantle reflects Archean mantle melting to the exhaustion of orthopyroxene. Geology, 35, 459-462.

Berry. A.J., Danyushevsky, L.V., O'Neill, H.St.C., Newville, M., and Sutton, S.R. (2008) Oxidation state of iron in komatiitic melt inclusions indicates hot Archean mantle. Nature, 455, 960-963.

Bezos, A., Humler, E. (2005) The Fe^{3+}/Fe ratios of MORB glasses and their implications for mantle melting. Geochimica et Cosmochimica Acta 69, 711–725.

Bickle, M.J., Ford, C.E., and Nisbet, E.G. (1977) The petrogenesis of peridotitic komatiites: evidence from high-pressure melting experiments. Earth and Planetary Science Letters, 37, 97-106.

Blichert-Toft, J., Arndt, N.T., Wilson, A., and Coetzee, G. (2015) Hf and Nd isotopic systematics of early Archean komatiites from surface sampling and ICDP drilling in the Barberton Greenstone Belot, South Africa. American Mineralogist, 100, 2396-2411.

Bolton, D. (1980) The computation of equivalent potential temperature. Monthly Weather Review, 108, 1046-1053.

Botcharnikov, R.E., Koepke, J., Holtz, F., McCammon, C., and Wilke, M. (2005): The effect of water activity on the oxidation and structural state of Fe in a ferrobasaltic melt, Geochimica et Cosmochimica Acta, 69 (21), 5071-5085

Borisov, A.A. (2010) Ferric-ferrous ratio in liquid iron oxides: analysis and applications to natural basaltic melts. Petrology, 18, 471-481.

Bouvier, A., Blichert-Toft, J., and Albarede, F. (2009) Martian meteorite chronology and the evolution of the interior of Mars. Earth and Planetary Science Letters, 280, 285-295.

Brown, J.M. and Shankland, T.J. (1981) Thermodynamic parameters in the Earth as

determined from seismic profiles. Geophysical Journal of the Royal Astronomical Society, 66, 579-596.

Bunge, H-P. (2005) Low plume excess temperature and a high core heat flux inferred form non-adiabatic geotherms in internally heated mantle circulation models. Physics of the Earth and Planetary Interiors, 153, 3-10.

Canil, D., O'Neill, H.S.C., Pearson, D.G., Rudnick, R.L., McDonough, W.F., and Carswell, D.A. (1994) Ferric iron in peridotites and mantle oxidation states Earth and Planetary Science Letters, 123, 205-220.

Carmichael, I.S.E. (1991) The redox state of basic and silicic magmas: a reflection of their source regions? Contributions to Mineralogy and Petrology, 106, 129-141.

Carmichael, I.S.E., Ghiorso, M.S. (1990) The effect of oxygen fugacity on the redox state of natural liquids and their crystallizing phases, in, Nicholls J, Russell JK, eds., Modern Methods of Igneous Petrology: Understanding Magmatic Processes, Mineralogical Society of America Reviews in Mineralogy, 24, 191-212.

Carmichael, I. S. E., Lange, R. A. & Luhr, J. F. (1996) Minettes and related lavas in the Mascota Volcanic Field, Jalisco, Mexico. Contributions to Mineralogy and Petrology *124*, *304*–323.

Castellan, G.W. (1971) Physical Chemistry, 2nd. Ed. Addison-Wesley, Reading MA. 866 p.

Cawthorn, R.G. (1975) Degrees of melting in mantle diapers and the origin of ultrabasic liquids. Earth and Planetary Science Letters 27, 113–120.

Cottrell, E. and Kelley, K.A. (2011) The oxidation state of Fe in MORB glasses and the oxygen fugacity of the upper mantle. Earth and Planetary Science Letters, 305, 270-282.

Consolmagno, G.J. and Schaefer, M.W. (1994) Worlds Apart: a textbook in planetary sciences. Prentice Hall, Englewood Cliffs, NJ, 0-13-964131-9, 323 p.

DaSilva, C.R.S., Wentzcovitch, R.M. Patel, A., Price, G.D., and Karato, S.I. (2000) The composition and geotherm of the lower mantle: constraints from the elasticity of silicate perovskite. Physics of Earth and Planetary Materials, 188, 103-109.

Davies, G.F. (1988) Ocean bathymetry and mantle convection 1. Large-scale flow and hotspots. Journal of Geophysical Research, 93, 10467-10480.

Davies, G.F. (2009) Reconciling the geophysical and geochemical mantles: plume flows, heterogeneities, and disequilibrium. Geochemistry, Geophysics, Geosystems, doi:10.1029/2009GC002634

Deschamps F. and Trampert (2004) Towards a lower mantle reference temperature and composition. Earth and Planetary Science Letters, 222, 161-175.

Delano, J.W. (1986) Pristine lunar glasses: criteria, data and implications. Lunar and Planetary Science Conference Proceedings 17, D201-213.

Ding, S.D. and Dasgupta, R.D. (2015) Solidus of martian mantle constrained by new high pressure-temperature experiments at nominally anhydrous conditions. 46th Lunar and Planetary Science Conference, Contribution number 1832, p. 2079.

Eugster, H.P. and Wones, D.R. (1962) Stabiliity relation of the ferruginous biotite, annite Journal of Petrology, 3, 82-125.

Fegley, B. Jr. (2013) Practical chemical thermodynamics for geoscientists. Academic press, ISBN 978-0-12-251100-4.

Feldstein, S.N. and Lange, R.A. (1999) Pliocene potassic magmas from the Kings River region, Sierra Nevada, California: evidence for melting of a subduction-modified mantle. Journal of Petrology, 40, 1301-1320.

Filberto, J., and Dasgupta, R. (2011) Fe^{2+}-Mg partitioning between olivine and basaltic melts: applications to genesis of olivine-phyric shergottites and conditions of melting in the martian interior. Earth and Planetary Science Letters, 304, 527-537.

Filberto, J., and Dasgupta, R. (2015) Constraints on the depth and thermal vigor of melting in the martian mantle. Journal of Geophysical Research: Planets, 10.1002/2014JE004745.

Filberto, J. Treiman, A.H., and Le, L. (2008) Crystallization experiments on a Gusev Adirondack basalt composition. Meteoritics and Planetary Science, 43, 1137-1146.

Fiquet, G., Auzende, A.L., Siebert, J., Corgne, A., Bureau, H., Ozawa, H. and Barbarino, G. (2010) Melting of peridotite to 140 GPa. Science, 329, 1516-1518.

Frost, D.J., and McCammon, C.A. (2008) The redox state of Earth's mantle, Annual Reviews in Earth and Planetary Science, 36, 389-420.

Gaillard, F., Scaillet, B., Pichavant, M., and Bény, J.-M. (2001) The effect of water and fO_2 on the ferric-ferrous ratio of silicic melts. Chemical Geology, 174, 255.273.

Galton, F. (1886) Regression towards mediocrity in hereditary stature. The Journal of the Anthropological Institute of Great Britain and Ireland, 15, 246-263.

Ganguly, J. (2005) Adiabatic decompression and melting of mantle rocks: an irreversible thermodynamic analysis. Geophysical Research Letters, 32, L06312, doi:10.1029/2005GL022363.

Garcia, M.O., and Hulsebosch, T.P. and Rhodes, J.M. (1995) Olivine-rich submarine basalts form the southwest Rift Zone of Mauna Loa Volcano: implications for magmatic processes and geochemical evolution, in Rhodes, M.J. and Lockwood, JP. Eds., Mauna Loa Revealed, American Geophysical Union Washington, D.C., 219-239.

Gillet, P., Richet, P., Guyot, F., and Fiquet, G. (1991) High-temperature thermodynamic properties of forsterite. Journal of Geophysical Research, 96, 11805-11816.

Gee, L.L., Sack, R.O. (1988) Experimental petrology of melilite nephelinites. Journal of Petrology 29, 1233–1255.

Goodrich, C.A., Treiman, A.H., Filberto, J., and Jercinovic, M.J. (2010) The Nakhla parent magma: old problems, new approaches. 41st Lunar and Planetary Science Conference, 1387.

Goodrich, C.A., Treiman, A.H., Filberto, J., Gross, J., and Jercinovic, M.J. (2013) The K_2O-rich trapped melt in olivine in the Nakhla meteorite: implications for petrogenesis of nakhlites and evolution of the martian mantle. Meteoritics and Planetary Science, 48, 2371-2405.

Greeley, R., Foing, B.H., McSween, H.Y., Neukum, G., Pinet, P., van Kan, M., Werner, S.C., Williams, D.A., and Zegers, T.E. (2005) Fluid lava flows in Gusev crater, Mars. Journal of Geophysical Research, 110, E05008, doi:10.1029/2005JE002401.

Green, D.H., Nicholls, I.A., Vilojen, M., and Vilojen, R. (1975) Experimental demonstration of the existence of peridotitic liquids in earliest archean magmatism, Geology, 3, 11-14.

Herd, C. (2006) Insights into the redox history of the NWA 1068/1110 martian basalt from mineral equilibria and vanadium oxybarometry. American Mineralogist, 91, 1616-1627.

Herzberg, C. (1995) Generation of plume magmas through time: an experimental perspective. Chemical Geology, 126, 1-16.

Herzberg, C., and Asimow, P.D. (2008) Petrology of some oceanic island basalts: PRIMELT2.XLS software for primary magma calculation. Geochemistry, Geophysics, Geosystems, doi: 10.1029/2008GC002057.

Herzberg, C., and Asimow, P.D. (2015) PRIMELT3 MEGA.XLSM software for primary magma calculation: Peridotite primary magma MgO contents from the liquidus to the solidus. Geochemistry, Geophysics, Geosystems, doi: 10.1002/2014GC005631.

Herzberg, C., Condie, K., and Korenaga, J. (2010) Thermal history of the Earth and its petrological expression. Earth and Planetary Science Letters, 292, 79-88.

Herzberg, C. and Gazel, E. (2009) Petrological evidence for secular cooling in mantle plumes. Nature, 458, 619-623.

Herzberg, C., O'Hara, M.J. (1998) Phase equilibrium constraints on the origin of basalts, picrites and komatiites. Earth-Science Reviews 44, 39–79.

Herzberg, C. and O'Hara, M.J. (2002) Plume-associated ultramafic magmas of Phanerozoic age. Journal of Petrology, 43, 1857-1883.

Herzberg, C., and Rudnick, R. (2012) Formation of cratonic lithosphere: an integrated thermal and petrological model. Lithos, 149, 4-15.

Herzberg, C., and Zhang, J. (1996) Melting experiments on anhydrous peridotite KLB-1; composition of magmas in the upper mantle and transition zone. Journal of Geophysical Research, 101, 8271-8295.

Hess. H. (1962) History of the ocean basins. In: Petrologic Studies: A Volume in Honor of A.F. Buddington. Engle AE, James HL, Leonard BF (eds) p 599-620

Hewitt, D.A. (1978) A redetermination of the fayalite-magnetite-quartz equilibrium between 650 and 850ºC. American Journal of Science, 278, 715-724.

Hirose, K. and Kawamura, K. (1994) A new experimental approach for incremental batch melting of peridotite at 1.5 GPa. Geophysical Research Letters, 19, 2139-2142.

Hirose, K., and Kushiro, I. (1998) The effect of melt segregation on polybaric mantle melting: estimation from the incremental melting experiments. Physics of Earth and Planetary Interiors, 107, 111-118.

Hirschmann, M.M. (2000) Mantle solidus: experimental constraints and the effects of peridotite composition. Geochemistry, Geophysics, Geosystems 1 (2000GC000070).

Hirschmann, M.M., Asimow, P.D., Ghiorso, M.S. and Stolper, E.M. (1999) Calculation

of peridotite partial melting from thermodynamic models of minerals and melts III. Controls on isobaric melt production and the effect of water on melt production. Journal of Petrology, 40, 831-851.

Hirschmann, M. M., Ghiorso, M. S., Davis, F. A., Gordon, S. M., Mukherjee, S., Grove, T. L., Krawczynski, M., Medard, E. & Till, C. B. (2008). Library of experimental phase relations (LEPR): a database and web portal for experimental magmatic phase equilibria data. Geochemistry, Geophysics, Geosystems 9, Q03011, doi:10.1029/2007GC001894.

Hole, M.J. (2015) The generation of continental flood basalts by decompression melting of internally heated mantle. Geology, dpi:10.1130G36442.1.

Holland, T.J.B., and Powell, R. (1998) An internally consistent thermodynamic data set for phases of petrological interest. Journal of Metamorphic Geology, 16, 309-343.

Jayasuriya, K. O'Neill, H.St., Berry, A.J., and Campbell, S.J. (2004) A Mössbauer study of the oxidation state of Fe in silicate melts. American Mineralogist, 89, 1597-1609.

Katsura, T. Yoneda, A., Yamazaki, D., Yoshino, T., and Ito, E. (2010) Adiabatic temperature profile in the mantle. Physics of the Earth and Planetary Interiors, 183, 212-218.

Katz, R.F., Spiegelman, M. and Langmuir, C.H. (2003) A new parameterization of hydrous mantle melting. Geochemistry, Geophysics, Geosystems, 4, doi:10.1029/2002GC000433.

Keiding, J.K., Trumbull, R.B., Veksler, I.V., Jerram, D.A. (2011) On the significance of ultra-magnesian olivines in basaltic rocks. Geology, 39, 1095-1098.

Kelley, K.A., and Cottrell, E. (2012) The influence of magmatic differentiation on the oxidation state of Fe in a basaltic arc magma. Earth and Planetary Science Letters, 329-330, 109-121.

Kilinc, A., Carmichael, I.S.E., Rivers, M.L., and Sack, R.O. (1983) The ferric-ferrous ratio of natural silicate liquids equilibrated in air. Contributions to Mineralogy and Petrology, 83, 136-140.

Kojitani, H. and Akaogi, M. (1997) Melting enthalpies of mantle peridotite: calorimetric determinations in the system CaO-MgO-Al_2O_3-SiO_2 and application to magma generation. Earth and Planetary Science Letters, 153, 209-222.

Korenaga, J. (2005) Firm mantle plumes and the nature of the core-mantle boundary region. Earth and Planetary Science Letters, 232, 29-37.

Korenaga, J. (2008) Urey ratio and the structure and evolution of Earth's mantle. Reviews in Geophysics, 46, 1-32, paper # 2007RG000241.

Kress, V.C. and Carmichael, I.S.E. (1988) Stoichiometry of the iron oxidation reaction in silicate melts. American Mineralogist, 73, 1267-1274.

Kress, V.C. and Carmichael, I.S.E. (1991) The compressibility of silicate liquids containing Fe_2O_3 and the effect of composition, temperature, oxygen fugacity, and pressure on their redox states. Contributions to Mineralogy and Petrology, 108, 82-92.

Lange, R. L. & Carmichael, I. S. E. (1990) Thermodynamic properties of silicate liquids with emphasis on density, thermal expansion and compressibility. In: Nicholls, J. & Russell, J. K. (eds) Modern Methods of Igneous Petrology. Mineralogical Society of America, Reviews in Mineralogy 24, 25-64.

Lange, R.A., Carmichael, I.S.E., and Renne, P.R. (1993) Potassic volcanism near Mono basin, California: evidence for high water and oxygen fugacities inherited from subduction. Geology, 21, 949-952.

Lee, C-T., and Chin, E.J. (2014) Calculating melting temperatures and pressure of peridotite protoliths: implications for the origin of cratonic mantle. Earth and Planetary Science Letters, 403, 273-286.

Lee, C-T., Luffi, P., Plank, T., Dalton, H., and Leeman, W.P. (2009) Constraints on the depths and temperatures of basaltic magma generation on Earth and other terrestrial planets, using new thermobarometers for mafic magmas. Earth and Planetary Science Letters, 279, 20-33.

Longhi, J. and Pan, V. (1989) The parent magmas of the SNC meteorites. Proceedings of the 19th Lunar and Planetary Science Conference, 451-464.

Luhr, J. F., Allan, J. F., Carmichael, I. S. E., Nelson, S. A. & Hasenaka, T. (1989) Primitive calc-alkaline and alkaline rock types from the western Mexican Volcanic Belt. Journal of Geophysical Research 94, 4515–*4530*.

Mandler, B.E. and Elkins-Tanton, L.T. (2013) The origin of eucrites, diogenites, and olivine diogenites: magma ocean crystallization and shallow magma chamber processes on Vesta. Meteoritics and Planetary Science, 48, 2333-2349.

Mattern, E., Matas, J., Ricard, Y., and Bass, J. (2005) Lower mantle composition and temperature from mineral physics and thermodynamic modeling. Geophysical Journal International, 160, 973-990.

Matzen, A.K., Baker, M.B., Beckett, J.R., and Stolper, E.M. (2011) Fe-Mg partitioning between olivine and high-magnesian melts and the nature of Hawaiian parental liquids. Journal of Petrology, doi:10.1093/petrology/egq089.

McCallum, I.S. and Schwartz, J.M. (2001) Lunar Mg suite: thermobarometry and petrogenesis of parental magmas. Journal of Geophysical Research, 106, 27969-27983.

McKenzie, D.P. (1967) Some remarks on heat flow and gravity anomalies. Journal of Geophysical Research, 72, 6261-6273.

McKenzie, D.P. and Bickle, M.J. (1988) The volume and composition of melt generated by extension of the lithosphere. Journal of Petrology, 29, 625-679.

Miller, G.H., Stolper, E.M., and Ahrens, T.J. (1991) The equation of state of a molten komatiite: 2. Application to komatiite petrogenesis and the Hadean mantle. Journal of Geophysical Research, 96, 11849-11864.

Monders, A.G., Médard, E. and Grove, T.L. (2007) Phase equilibrium investigations of the Adirondak class basalts from the Gusev plains, Gusev crater, Mars. Meteoritics and Planetary Science, 42, 131-148.

Moore, G., Righter, K. and Carmichael, I.S.E. (1995) The effect of dissolved water on the oxidation state of iron in natural silicate liquids. Contributions to Mineralogy and Petrology, 120, 170-179.

Morgan, W.J. (1971) Convection plumes in the lower mantle. Nature 230:42-43.

Musselwhite, D.S., Dalton, H.A., Kiefer, W.S., and Treiman, A.H. (2006) Experimental petrology of the basaltic shergottite Yamato-980459: implications for the thermal structure of the martian mantle. Meteoritics and Planetary Science, 41, 1271-1290.

Myers, J., and Eugster, H.P. (1983) The system Fe-Si-O: Oxygen buffer calibrations to 1500 K. Contributions to Mineralogy and Petrology, 82, 75-90.

Mysen, B.O. (1991) Relations between structure, redox equilibria of iron, and properties of magmatic liquids, in Perchuk, L.L., and Kushiro, I., eds., Physical Chemistry of Magmas, Springer-Verlag, NY, NY, 41-98.

Nakagawa, T. and Tackley, P.J. (2010) Influence of initial CMB temperature and other parameters on the thermal evolution of Earth's core resulting from thermochemical and spherical mantle convection. Geochemistry, Geophysics, Geosystems, 11, 10.1029/2010GC003031.

Nakagawa, T. and Tackley, P.J. (2012) Influence of magmatism on mantle cooling, surface heat flow and Urey ratio. Earth and Planetary Science Letters, 329-330, 1-10.

Nakagawa, T. and Tackley, P.J. (2014) Influence of combined primordial layering and recycled MORB on the coupled thermal evolution of Earth's mantle and core. Geochemistry, Geophysics, Geosystems, 10.1002/2013GC005128.

Navrotsky, A. Ziegler, D. Oestrike, R. and Maniar, P. (1989) Calorimetry of silicate melts at 1773 K: measurement of enthalpies of fusion and of mixing I the systems diopside-anorthite-albite and anorthite-forsterite. Contribution to Mineralogy and Petrology, 101, 122-130.

Nisbet, E.G., Cheadle, M.J., Arndt, N.T., and Bickle, M.J. (1993) Constraining the potential temperature of the Archean mantle; a review of the evidence from komatiites. Lithos, 30, 291-307.

Nomura, R., Hirose, K., Usegui, K., Ohishi, Y., Tsuchiyama, A., Miyake, A., and Ueno, Y. (2014) Low core-mantle boundary temperature inferred from the solidus of pyrolite. Science, 343, 522-525.

O'Neill, C., and Debaille, V. (2014) The evolution of Hadean-Eoarchean geodynamics. Earth and Planetary Science Letters, 406, 49-58.

O'Rourke, J.G. and Korenaga, J. (2012) Terrestrial planet evolution in the stagnant-lid regime: size effects and the formation of self-destabilizing crust. Icarus, 221, 1043-1060.

Papuc, A.M. ad Davies, G.F. (2008) The internal activity and thermal evolution of Earth-like planets. Icarus, 195, 447-458.

Parman, S.W., Dann, J.C., Grove, T.L., deWit, M.J. (1997) Emplacement conditions of komatiite magmas from the 3.49 Ga Komati Formation, Barberton Greenstone Belt, South Africa. Earth and Planetary Science Letters, 150, 303-323.

Partsch, G.M., Lattard, D., and McCammon, C. (2004) Mossbauer spectroscopic

determination of Fe3+/Fe2+ in synthetic basaltic glass: a test of empirical fO_2 equations under superliquidus and subliquidus conditions. Contributions to Mineralogy and Petrology, 147, 565-580.

Pickering-Witter, J., and Johnston, A.D. (2000) The effects of variable bulk composition on the melting systematics of fertile peridotitic assemblages. Contributions to Mineralogy and Petrology, 140, 190-211.

Putirka, K. D. (2005). Mantle potential temperatures at Hawaii, Iceland, and the mid-ocean ridge system, as inferred from olivine phenocrysts: Evidence for thermally driven mantle plumes. Geochemistry, Geophysics Geosystems 6, doi:10.1029/005GC000915.

Putirka, K. D. (2008a) Thermometers and barometers for volcanic systems. In: Putirka, K. D. & Tepley, F. (eds) Minerals, Inclusions and Volcanic Processes. Mineralogical Society of America and Geochemical Society, Reviews in Mineralogy and Geochemistry 69, 61-120.

Putirka, K. (2008b) Excess temperatures at ocean islands: implications for mantle layering and convection. Geology, 36, 283-286.

Putirka, K. D., Perfit, M., Ryerson, F. J. & Jackson, M. G. (2007) Ambient and excess mantle temperatures, olivine thermometry, and active vs. passive upwelling. Chemical Geology 241, 177-206.

Putirka, K. D., Ryerson, F.J., Perfit, M., and Ridley, W.I. (2011) Mineralogy and composition of the oceanic mantle. Journal of Petrology, 52, 279-313.

Ramburg, H. (1971) Temperature changes associated with adiabatic decompression in geological processes. Nature, 234, 539-540.

Rhodes, J.M., and Vollinger, M.J. (2004) Composition of basaltic lavas sampled by phase-2 of the Hawaii Scientific Drilling Project: Geochemical stratigraphy and magma types. Geochemistry, Geophysics, Geosystems, 5, doi:10.1029/2002GC000434.

Rhodes, J.M., and Vollinger, M.J. (2005) Ferric/ferrous ratios in 1984 Mauna Loa lavas: a contribution to understanding the oxidation state of Hawaiian magmas. Contributions to Mineralogy and Petrology, 149, 666-674.

Richet, P. and Bottinga, Y. (1986) Thermochemical properties of silicate glasses and

liquids: a review. Reviews in Geophysics, 24, 1-25.

Righter, K., Yang, H., Costin, G., and Downs, R.T. (2008) Oxygen fugacity in the martian mantle controlled by carbon: new constraints from the Nakhlite MIL 03346. Meteoritics and Planetary Sciences, 43, 1709-1723.

Robie, R.A., and Hemingway, B.S. (1995) Thermodynamic properties of minerals and related substances at 298.15 K and 1 bar (10^8 Pascals) pressure and at higher temperatures. U.S. Geological Survey Bulletin 2131, U.S. Government Printing Office, Washington, D.C.

Robin-Popieul, C.C.M., Arndt, N.T., Chauvel, C., Byerly, G.R., Sobolev, A.V., and Wilson, A. (2012) A new model for Barberton Komatiites: deep critical melting with high melt retention. Journal of Petrology, 53, 2191-2229.

Robinson, J.A.C., Wood, B.J., and Blundy, J.D. (1998) The beginning of melting of fertile and depleted peridotite at 1.5 GPa. Earth and Planetary Science Letters, 155, 97-111.

Roeder, P.L. and Emslie, R.F. (1970) Olivine-liquid equilibrium. Contributions to Mineralogy and Petrology, 29, 275-289.

Sack, R.O., Carmichael, I.S.E., Rivers, M., and Ghiorso, M.S. (1980) Ferric-ferrous equilibria in natural silicate liquids at 1 bar. Contributions to Mineralogy and Petrology, 75, 369-376.

Saunders, P.M. (1957) The thermodynamics of saturated air: a contribution to the classical theory. Quarterly Journal of the Royal Meteorological Society, 83, 342-350.

Schmidt, B.C., and Behrens, H. (2008) Water solubility in phonolite melts: influence of melt composition and temperature. Chemical Geology, 256, 259-268.

Schuessler, J.A., Botcharnikov, R.E., Behrens, H., Misiti, V., and Freda, C. (2008) Oxidation state of iron in hydrous phono-tephritic melts. American Mineralogist, 93, 1493-1504.

Schwab, R.O., and Küstner, D. (1981) Die Gleichgewichtsfugazitäten technologisch und petrologisch wichtiger Sauerstoffpuffer. Neues Jahrbuch für Mineralogie Abhandlungen, 140, 111-142.

Shirey, S.B., Kamber, B.S., Whitehouse, M.J., Mueller, P.A., and Basu, A.R. (2008) A

review of the isotopic and trace element evidence for mantle and crustal processes in the Hadean and Archean: implications for the onset of plate tectonic subduction. In: Condie, K.C. and Pease, V. eds., When Did Plate Tectonics Begin on Planet Earth?, GSA Special Paper 440, 1-29.

Silver, P.G. and Behn, M.D. (2008) Intermittent plate tectonics. Science, 319, 85-88.

Sobolev, A. V., Hofmann, A. W., Kuzmin, D. V., Yaxley, G. M., Arndt, N. T., Chung, S.-L., Danyushevsky, L. V., Elliott, T., Frey, F. A., Garcia, M. O., Gurenko, A. A., Kamenetsky, V. S., Kerr, A. C., Krivolutskaya, N. A., Matvienkov, V. V., Nikogosian, I. K., Rocholl, A., Sigurdsson, I. A., Sushchevskaya, N. M. & Teklay, M. (2007). The amount of recycled crust in source of mantle-derived melts. Nature 316, 412-417.

Sparks, D.W., and Cheadle, M.J. (1993) Thermodynamic modeling of melting in mantle plumes: komatiites, the ultimate test. Eos, Transactions of the American Geophysical Union, 74, 594.

Stebbins, J.F., Carmichael, I.S.E., and Moret, L.K. (1984) Heat capacities and entropies of silicate liquids and glasses. Contributions to Mineralogy and Petrology, 86, 131-148.

Stevenson, D. J. (2003) Styles of mantle convection and their influence on planetary evolution. Comptes Rendus Geoscience, 335, 99-111.

Stolper, E. (1980) A Phase Diagram for Mid-Ocean Ridge Basalts: Preliminary Results and Implications for Petrogenesis. Contributions to Mineralogy and Petrology, 74, 13-27.

Takahashi, E., Shimazaki, T., Tsuzaki, Y., and Yoshida, H. (1993) Melting study of a peridotite KLB-1 to 6.5 GPa, and the origin of basaltic magmas. Philosophical Transactions of the Royal Society of London, 342, 105-120.

Thieblot, L., Tequi, C., and Richet, P. (1999) High-temperature heat capacity of grossular ($Ca_3Al_2Si_3O_{12}$), enstatite ($MgSiO_3$), and titanite ($CaTiSi_{O5}$). American Mineralogist, 84, 848-855.

Tirone, M. (2015) On the thermal gradient in the Earth's deep interior. Solid Earth, 7, 2501-2525.

Toplis M.J. (2005) The thermodynamics of iron and magnesium partitioning between

olivine and liquid: criteria for assessing and predicting equilibrium in natural and experimental systems. Contributions to Mineralogy and Petrology, 149, 22-39.

Treiman, A.H. (1986) The parental magmas of the nakhla achondrite meteorite: ultrabasic volcanism on the shergottite parent body. Geochimica et Cosmochimica Acta, 50, 1061-1070.

Treiman, A. H. (1993) The parent magma of the Nakhla (SNC) meteorite, inferred from magmatic inclusions. Geochimica et Cosmochimica Acta, 57, 4753-4767.

Treiman, A.H. (1997) The parent magmas of the cumulate eucrites: a mass balance approach. Meteoritics and Planetary Science, 32, 217-230.

Turcotte, D.L. and Oxburgh, E.R. (1972) Mantle convection and the new global tectonics. Annual Reviews in Fluid Mechanics, 4, 33-66.

Wadhwa, M. (2008) Redox conditions on small bodies, the Moon and Mars, in Oxygen in the solar system, MacPherson, G.J., Mittlefehldt, D.W., Jones, H.H., and Simon, eds., Reviews in Mineralogy and Geochemistry, 68, 493-510.

Wallace, P. & Carmichael, I. S. E. (1989) Minette lavas and associated leucitites from the western front of the Mexican Volcanic Belt: petrology, chemistry and origin. Contributions to Mineralogy and Petrology, 103, 470–492.

Walter, M. J. (1998) Melting of garnet peridotite and the origin of komatiite and depleted lithosphere. Journal of Petrology, 39, 29-60.

Werner, S.C., Ody, A., and Poulet, F. (2014) The source crater of martian shergottite meteorites. Science, 343, 1343-1346.

Wilke, M., Behrens, H. Burkhard, D.J.M., and Rossano, S. (2002) The oxidation state of iron in silicic melt at 500 MPa water pressure. Chemical Geology, 189, 55-67.

Zerr, A., Diegeler, A., Boehler, R. (1998) Solidus of Earth's Deep Mantle. Science, 281, 243-246.

Zhang, J. and Herzberg, C. (1994) Melting experiments on anhydrous peridotite KLB-1 from 5.0-22.5 GPa. Journal of Geophysical Research, 99, 17729-17742.

Table 1. Sources of Experimental Data of measured Fe_2O_3/FeO, with P, T and weight % compositional ranges

Source (1)	*n*	Method (2)	logf_{O_2}	*P*(MPa)	*T*(°C)	SiO_2	FeOt	MgO (wt. %)	TA (3)	H_2O
1) Botcharnikov et al. (2005)	16	M, XANES	-7.21 to -3.97	200	1200 - 1204	46.6 - 49.7	5.9 - 17.5	6.0 - 6.3	2.8 - 3.1	0.7 - 4.8
2) Gaillard et al. (2001)	33	W	-12.8 to -4.97	201 - 228	923 - 927	73 - 79.1	0.2 - 4.4	0 - 0.2	6.2 - 10.5	6.2 - 8.6
3) Kilinc et al. (1983)	46	W	-0.678	0.1	1613-1727	38.7 - 74.4	1.6 - 15.1	0 - 12.0	2.9 - 13.3	0 - 2.4
4) Kress and Carmichael (1988)	63	W	-10.23 to -0.68	0.1	1249 - 1636	38.7 - 58.6	2.3 - 25	5.8 - 7.4	0.7 - 7.4	0
5) Moore et al. (1995)	53	W	-10.4 to -0.67	0.1 - 807	950 - 1557	51.6 - 78.8	1.2 - 10.7	0 - 6.7	2.3 - 10.1	0 - 8.3
6) Partzsch et al. (2004)	16	M	-10.3 to -6.56	0.1	1183 - 1222	47.6 - 48.6	9.7 - 17.6	3.2- 6.4	3.0 - 5.8	1.3 - 2.4
7) Sack et al. (1980)	57	W	-8.46 to -6.77	0.1	1201 - 1330	39 - 77.6	1.9 - 16.2	0 - 11.3	2.5 - 14.6	0
8) Schmidt & Behrens (2008)	35	W	-4.68 to -4.46	52 - 469	180 - 1200	48.8 - 56.3	4.7 - 6.0	0.5 - 0.6	10.1 - 17.0	2.2 - 9.7
9) Schuessler et al. (2008)	21	W	-9.26 to -4.29	50 - 500	1200 - 1250	44.4 - 48.5	4.5 - 7.1	4.9 - 5.6	8.3 - 9.6	9.0 - 16.1
10) Wilke et al. (2002)(4)	6	M	-5.6 to -6.35	500	850 - 950	67.6 - 68.5	0.8 - 1.7	0	1.9 - 2.1	10.7 - 11.2

(1) Data Set 1 (DS1) are the "W" calibration data for Eqn. 3b, which are all data but 6) and 9), which are reserved for testing. DS2 = 6) and 9); DS3 = 1) and these data are also used to calibrate Eqn. 3b. (2) Method by which Fe3+/Fe2+ ratios were measured: W = Wet chemistry analysis; M = Mossbauer; XANES = X-ray absorption near-edge structures. (3) TA = total alkalis (Na2O + K2O) in weight %. (4) No exiting or new model was able to predict data by Wilke et al. (2004) and including these data into regression models weakened the prediction of other experimental observations; these data are not used for regression or test purposes.

Table 2. Outline of calculation methods

Step	*Method 1: $X_{Fe2O3}^{liq}/X_{FeO}^{liq}$ is measured*	*Method 2: $X_{Fe2O3}^{liq}/X_{FeO}^{liq}$ is calculated*	
A	Use parental magmas from Cottrell and Kelley (2011); *P* is set to 0.0001 GPa;	Use parental magmas from Cottrell and Kelley (2011); Calculate a range of Mauna Loa parental magma candidates assuming mantle olivine = Fo90-91.5, and adding olivine to SR0061 until equilibrium is reached using Eqn. 9A; *P* is set to 2.4 GPa at Hawaii, 1 GPa for MORB	
B	K_D is estimated using Eqn. 8b[1] and used to calculate mantle olivine composition.	K_D is estimated using Eqn. 8b	
C	$D_{MgO}^{ol\text{-}liq}$ obtained from (a) bulk composition, which we denote as D_{Mg1} (Beattie 1993; his Eqn. 12) and (b) using olivine from B, which we denote as D_{Mg2}.	$D_{MgO}^{ol\text{-}liq}$ obtained from bulk composition only (from Beattie 1993; his Eqn. 12); denote as D_{Mg1}	
D	Calculate *T* from Eqn. 11 using D_{Mg1}, and from Putirka et al. (2007; their Eqn. 4) using D_{Mg2}. Compare *T*	Calculate *T* from Eqn. 11 using D_{Mg1}	
E	Calculate *T* and *P* by iteration from Putirka et al. (2007, Eqn. 4, D_{Mg2}), and Putirka (2008; Eqns. 41-42); compare with *T* from D.	Hawaii[2]: Establish fO_2 and $X_{Fe2O3}^{liq}/X_{FeO}^{liq}$ by 7 different methods:	1. Preserve low-*T* fO_2 conditions of Rhodes and Vollinger (2005)
			2. Use fO_2 of Rhodes and Vollinger (2005) (near MW) but apply *T*-fO_2 relationship ($\log[fO_2] = 10.726 - 22151.8/T(^oC)$) of MORB data (Cottrell and Kelley 2011)
			3. Apply fO_2 of MORB-source mantle (as in 2., use MORB *T*-fO_2 slope)
			4. Assume equilibrium with Fo90.5, and use $X_{Fe2O3}^{liq}/X_{FeO}^{liq} = f(\text{MgO})$ from Cottrell and Kelley (2011), where $X_{Fe2O3}^{liq}/X_{FeO}^{liq} = 0.2466 - 0.00728$ [MgO wt. %])[3]
			5. Increase $X_{Fe2O3}^{liq}/X_{FeO}^{liq}$ measured by Rhodes and Vollinger (2005), by 31.7%, i.e., the fractional increase in this ratio discovered by Cottrell and Kelley (2011) relative to Bezos and Humler (2005)
			6. Preserve mean of $X_{Fe2O3}^{liq}/X_{FeO}^{liq}$ ratios of Rhodes and Vollinger (2005) with fO_2 calculated from

			Eqn. 4
			7. Same as 6., except each liquid is matched with Fo91.3; no iterations required to obtain T and fO_2
F	Calculate fO_2 from Eqn. 7	MORB: Preserve mean $X_{Fe2O3}^{liq}/X_{FeO}^{liq}$ from Cottrell and Kelley (2011), and obtain fO_2 from T-fO_2 slope of the natural compositions of MORB at lower T: $\log[fO_2] = 10.726\text{-}22151.8/T(^oC)$	
G		Olivine composition is calculated from steps B & E	
H		D_{Mg2} is obtained by calculating olivine composition using K_D (Eqn. 8b) and $X_{Fe2O3}^{liq}/X_{FeO}^{liq}$ from E-F, and bulk composition	
I		Calculate T and P by iteration from Putirka et al. (2007; their Eqn. 4, D_{Mg2}), and Putirka (2008; Eqns. 41-42)	
J	Calculate T_p from Eqns. 12a,b,c; mean F is from Eqns. 14,b, c, and Putirka et al. (2007; Eqns. A1, A2); $F = 0$ for any model that yields $F < 0$		

[1] Cottrell and Kelley (2011) report atomic $Fe^{3+}/\sum Fe$ and so their compositions are converted to wt. % Fe_2O_3 and FeO (anhydrous), from which $X_{Fe2O3}^{liq}/X_{FeO}^{liq}$ are calculated.

2. Plotted $T^{ol\text{-}liq}$-fO_2 results are those conditions that yield observed maximum Fo contents at Mauna Loa (90.5-91.3) when a value for K_D (calculated from 5b) is imposed. Exceptions are options 5 and 7, where an olivine composition is assumed. In these cases, the preferred $T^{ol\text{-}liq}$-fO_2 conditions are those where the K_D obtained from the assumed olivine composition matches the value calculated from Eqn. 5b.

3. The motivation behind this reconstruction is that while Cottrell and Kelley (2011) present a convincing case that $X_{Fe2O3}^{liq}/X_{FeO}^{liq}$ varies with fractionation, MgO may act as a proxy for an intrinsic T effect on Eqn. $3a_3$: since Fe^{2+} appears on the high entropy side of Eqn. 3a, $X_{Fe2O3}^{liq}/X_{FeO}^{liq}$ ratios should decrease with increased T, as Cottrell and Kelley (2011) observe.

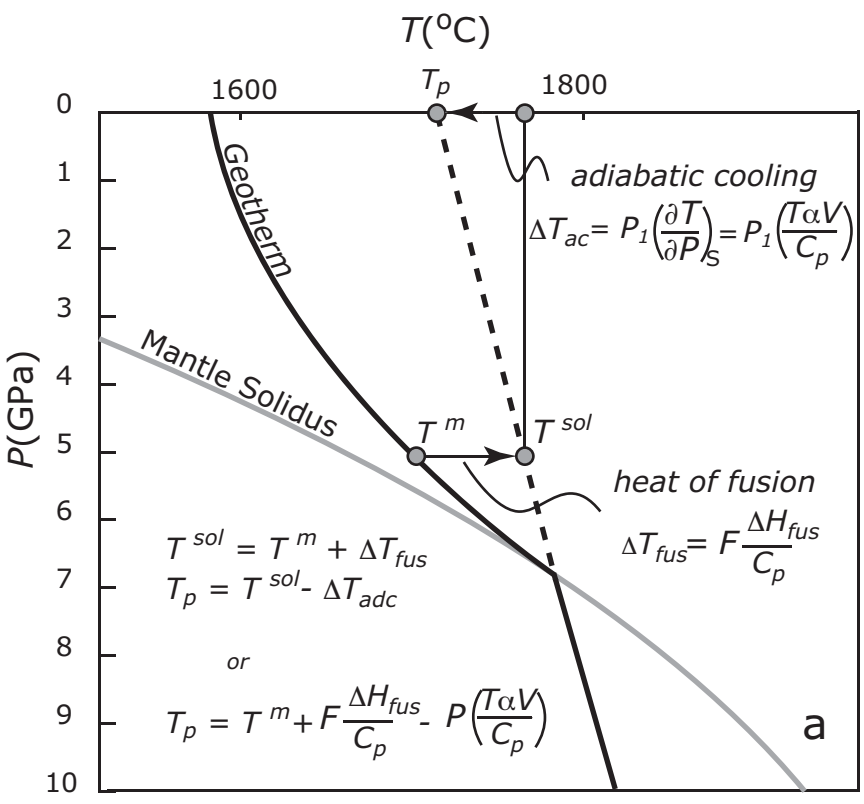
T(°C)
1600
Tp
1800
0
1
2
3
4
5
6
7
8
9
10
P(GPa)
Geotherm
Mantle Solidus
adiabatic cooling
$\Delta T_{ac} = P_1\left(\frac{\partial T}{\partial P}\right)_S = P_1\left(\frac{T\alpha V}{C_p}\right)$
T^m
T^{sol}
heat of fusion
$\Delta T_{fus} = F\frac{\Delta H_{fus}}{C_p}$
$T^{sol} = T^m + \Delta T_{fus}$
$T_p = T^{sol} - \Delta T_{adc}$
or
$T_p = T^m + F\frac{\Delta H_{fus}}{C_p} - P\left(\frac{T\alpha V}{C_p}\right)$
a

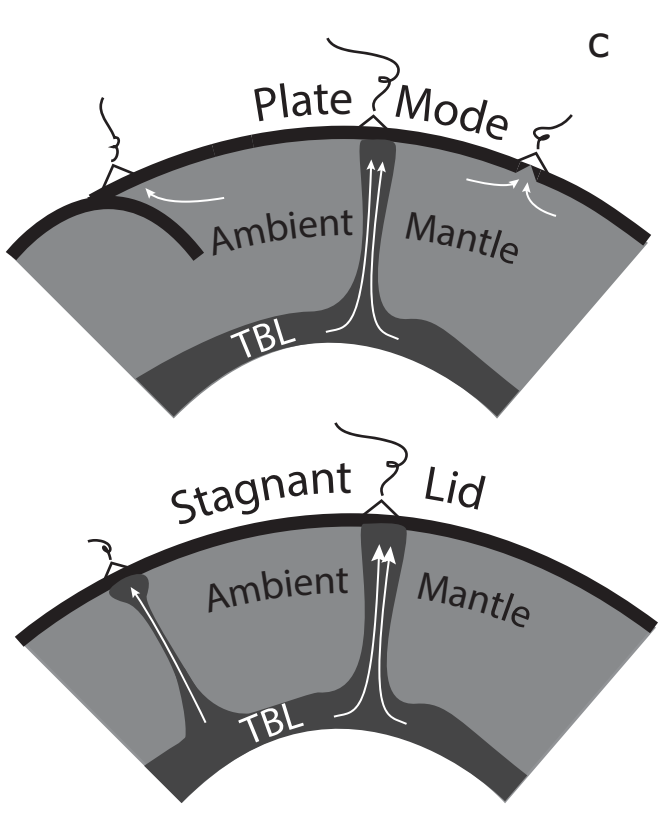
c
Plate Mode
Ambient
Mantle
TBL
Stagnant Lid
Ambient
Mantle
TBL

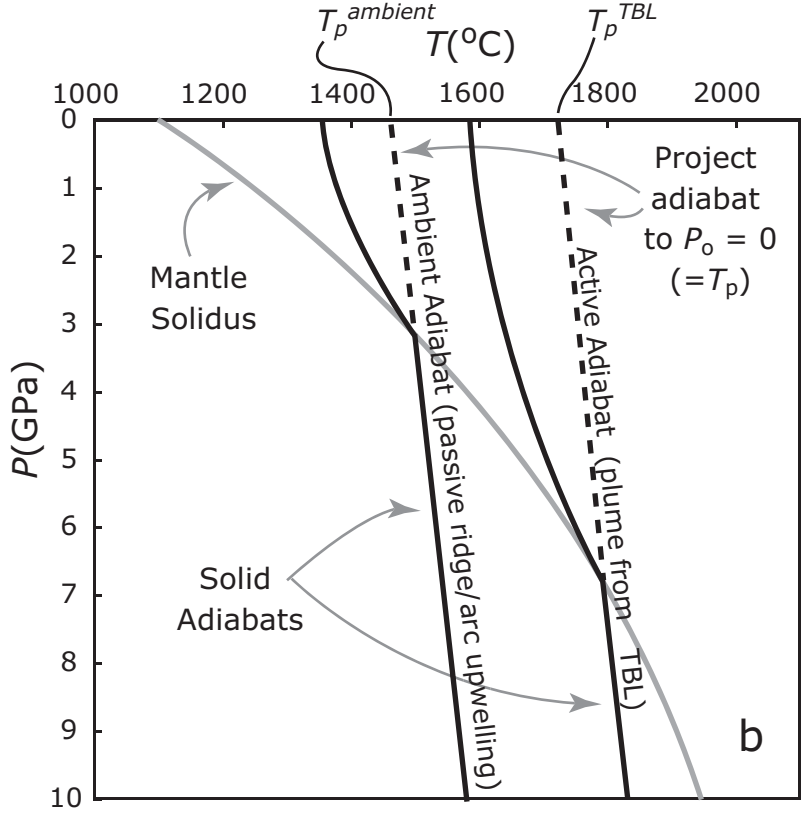
$T_p^{ambient}$
T(°C)
T_p^{TBL}
1000
1200
1400
1600
1800
2000
0
1
2
3
4
5
6
7
8
9
10
P(GPa)
Mantle Solidus
Ambient Adiabat (passive ridge/arc upwelling)
Active Adiabat (plume from TBL)
Project adiabat to $P_o = 0$ ($=T_p$)
Solid Adiabats
b

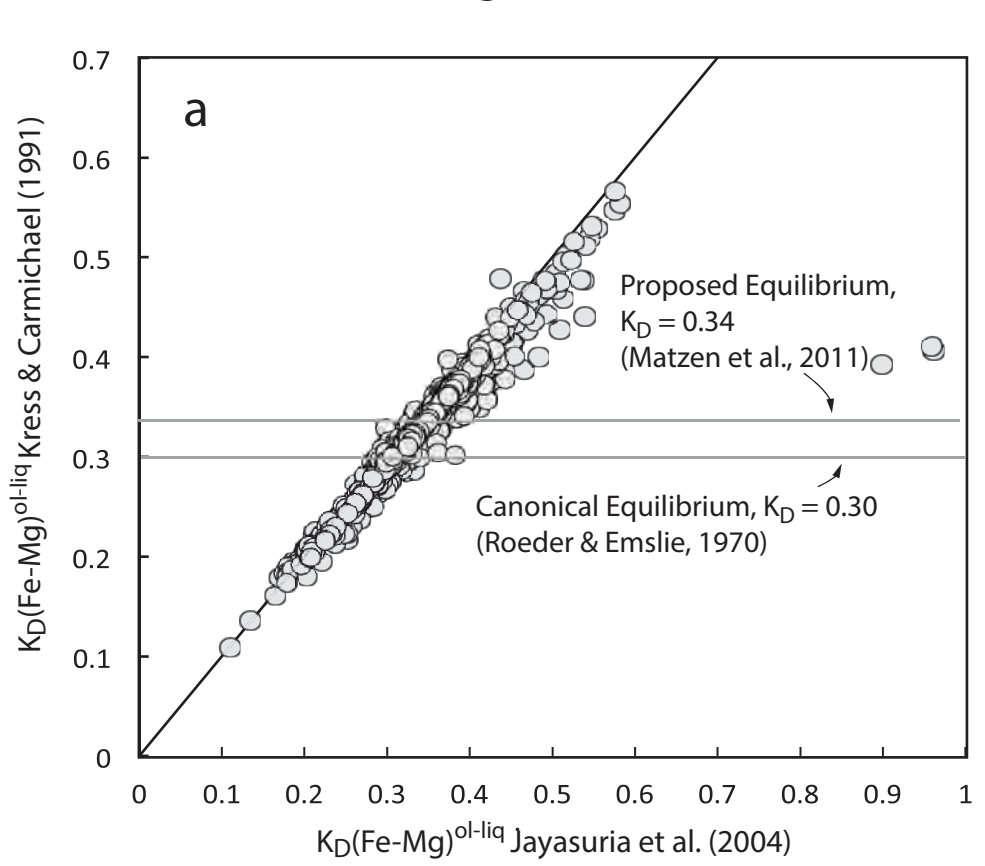
a
Proposed Equilibrium,
K_D = 0.34
(Matzen et al., 2011)
Canonical Equilibrium, K_D = 0.30
(Roeder & Emslie, 1970)
$K_D(Fe\text{-}Mg)^{ol\text{-}liq}$ Kress & Carmichael (1991)
$K_D(Fe\text{-}Mg)^{ol\text{-}liq}$ Jayasuria et al. (2004)

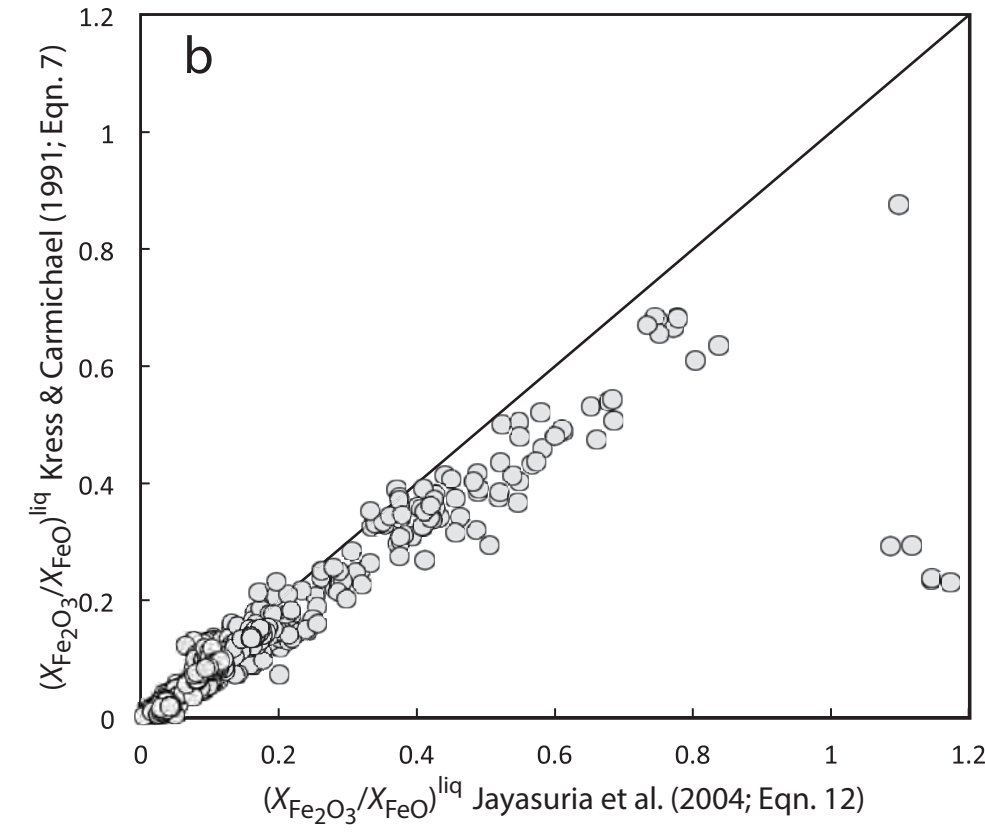
b
$(X_{Fe_2O_3}/X_{FeO})^{liq}$ Kress & Carmichael (1991; Eqn. 7)
$(X_{Fe_2O_3}/X_{FeO})^{liq}$ Jayasuria et al. (2004; Eqn. 12)

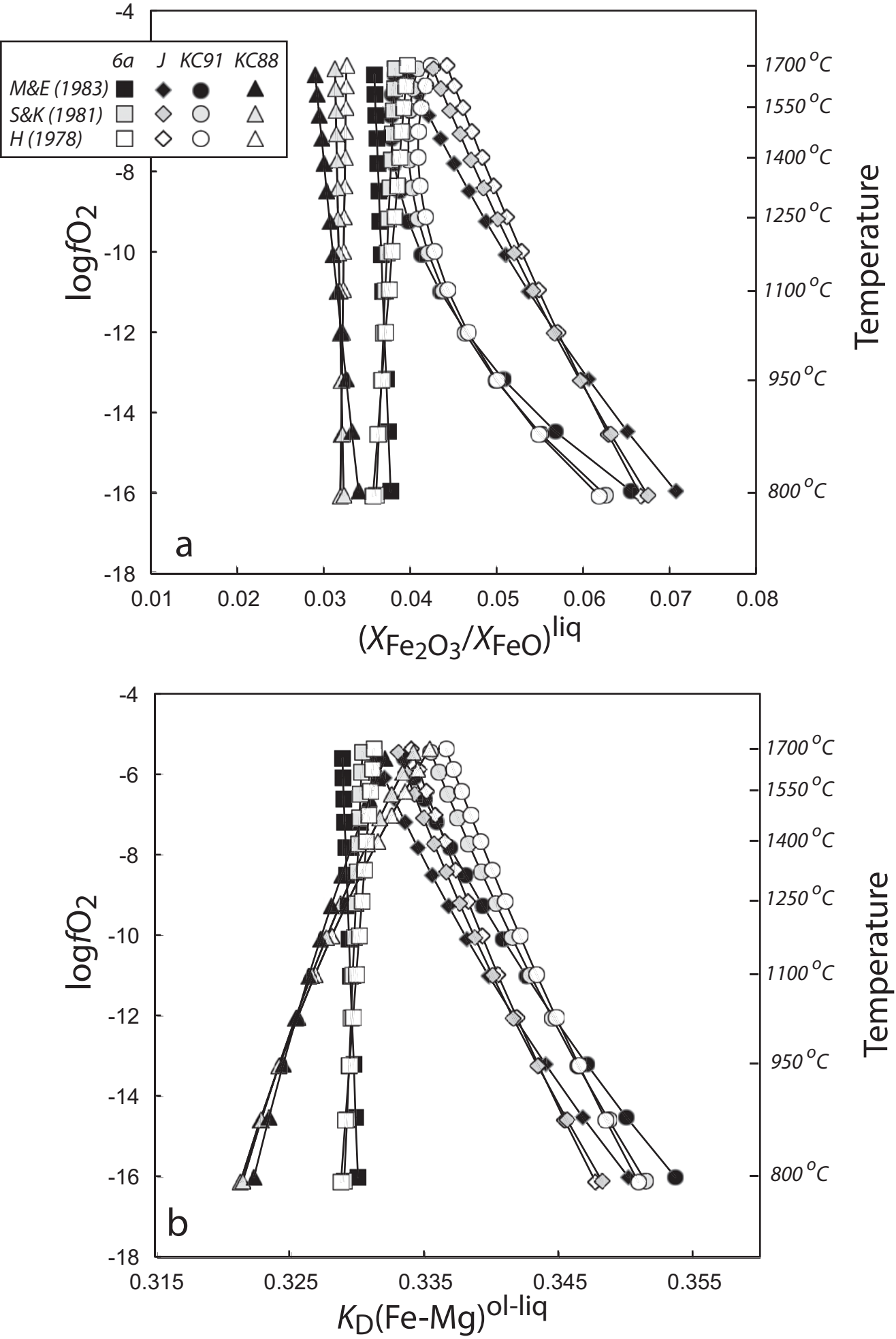
6a
J
KC91
KC88
M&E (1983)
S&K (1981)
H (1978)
-4
-8
-10
-12
-14
-16
-18
logfO2
1700 °C
1550 °C
1400 °C
1250 °C
1100 °C
950 °C
800 °C
Temperature
a
0.01
0.02
0.03
0.04
0.05
0.06
0.07
0.08
(XFe2O3/XFeO)liq
-4
-6
-8
-10
-12
-14
-16
-18
logfO2
1700 °C
1550 °C
1400 °C
1250 °C
1100 °C
950 °C
800 °C
Temperature
b
0.315
0.325
0.335
0.345
0.355
KD(Fe-Mg)ol-liq

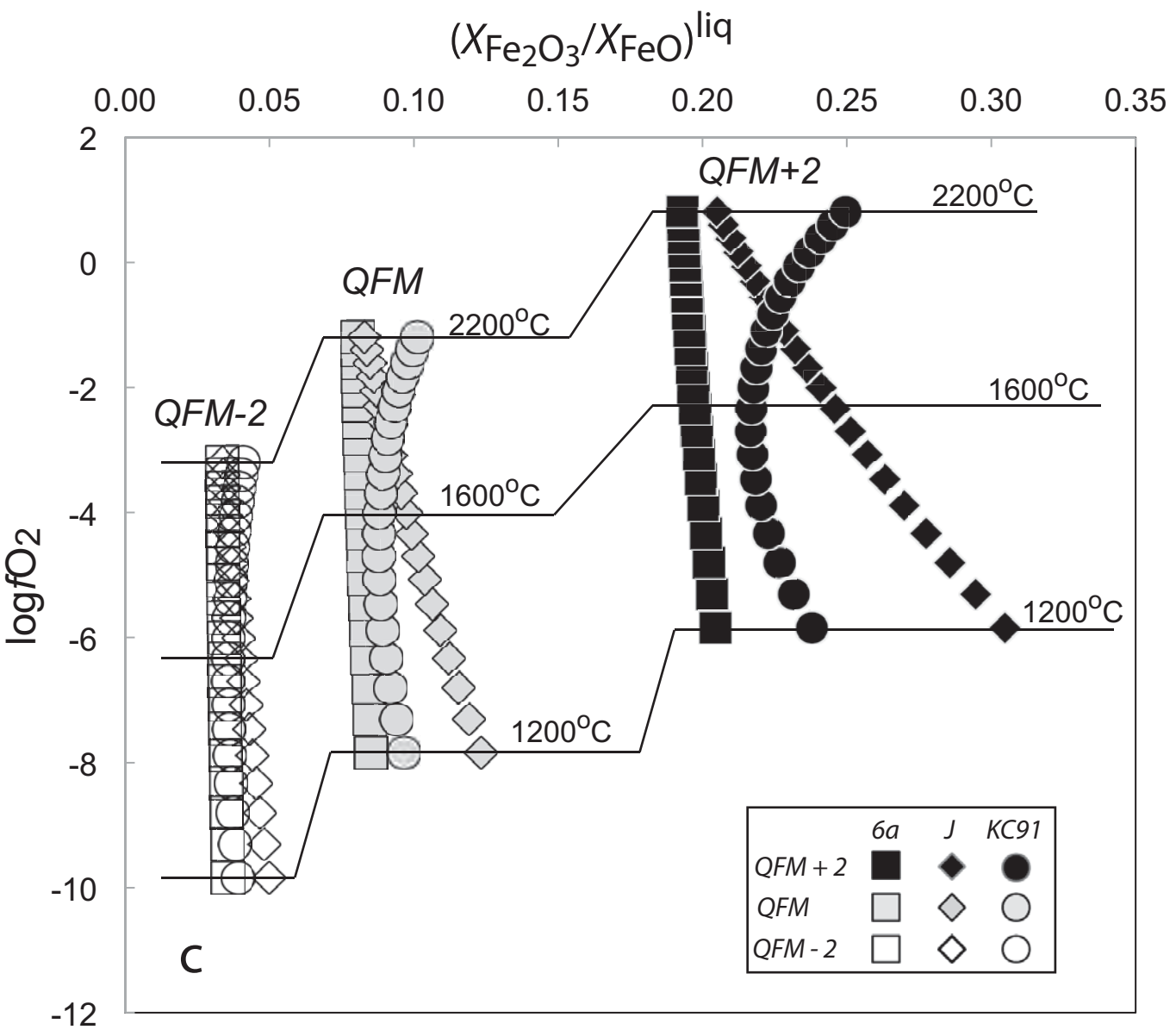
$(X_{Fe_2O_3}/X_{FeO})^{liq}$
0.00
0.05
0.10
0.15
0.20
0.25
0.30
0.35
2
0
-2
-4
-6
-8
-10
-12
$\log fO_2$
QFM+2
QFM
QFM-2
2200°C
1600°C
1200°C
2200°C
1600°C
1200°C
6a
J
KC91
QFM + 2
QFM
QFM - 2
C

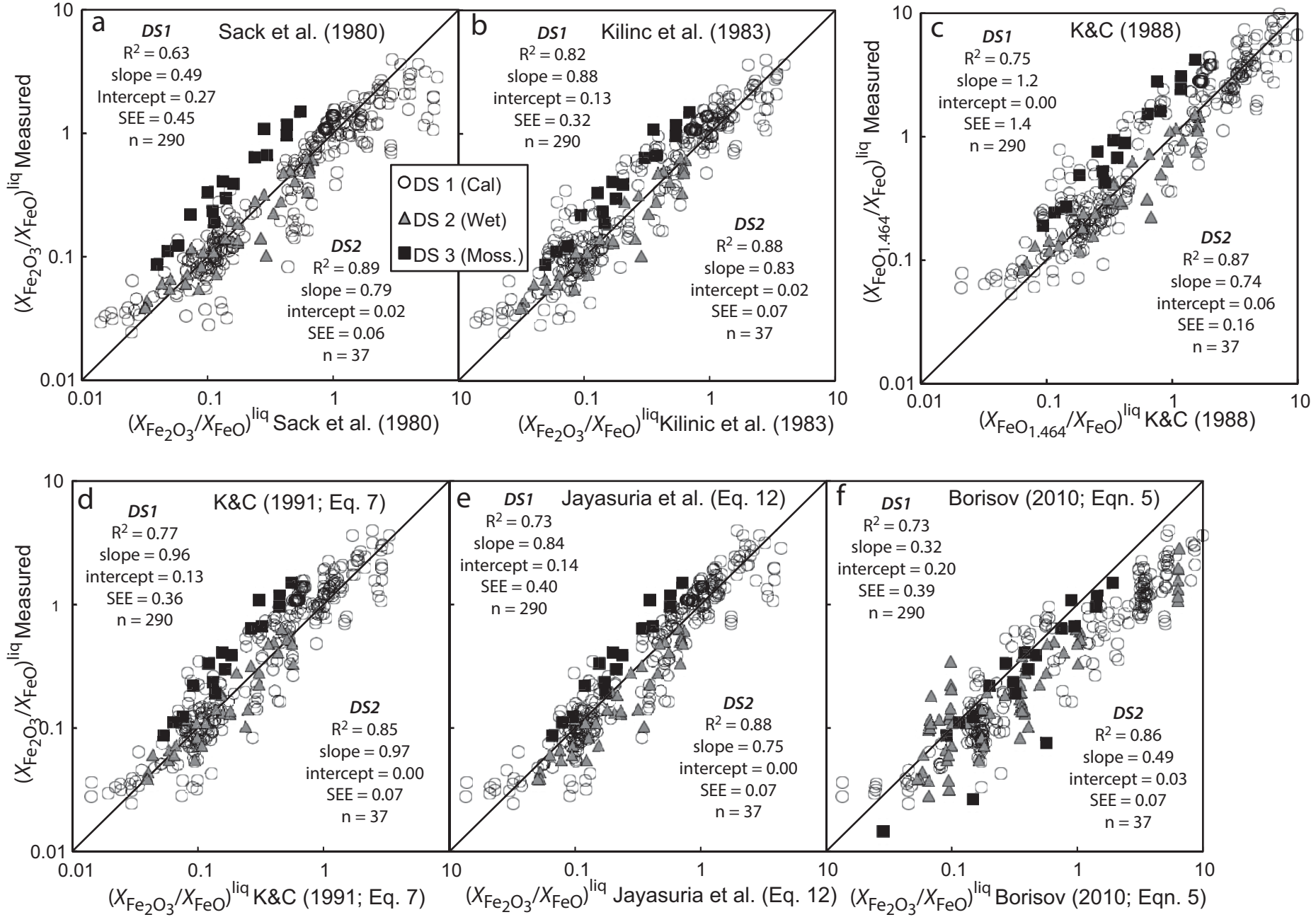
a
DS1
Sack et al. (1980)
R2 = 0.63
slope = 0.49
Intercept = 0.27
SEE = 0.45
n = 290
DS2
R2 = 0.89
slope = 0.79
intercept = 0.02
SEE = 0.06
n = 37
DS 1 (Cal)
DS 2 (Wet)
DS 3 (Moss.)
b
DS1
Kilinc et al. (1983)
R2 = 0.82
slope = 0.88
intercept = 0.13
SEE = 0.32
n = 290
DS2
R2 = 0.88
slope = 0.83
intercept = 0.02
SEE = 0.07
n = 37
c
DS1
K&C (1988)
R2 = 0.75
slope = 1.2
intercept = 0.00
SEE = 1.4
n = 290
DS2
R2 = 0.87
slope = 0.74
intercept = 0.06
SEE = 0.16
n = 37
d
DS1
K&C (1991; Eq. 7)
R2 = 0.77
slope = 0.96
intercept = 0.13
SEE = 0.36
n = 290
DS2
R2 = 0.85
slope = 0.97
intercept = 0.00
SEE = 0.07
n = 37
e
DS1
Jayasuria et al. (Eq. 12)
R2 = 0.73
slope = 0.84
intercept = 0.14
SEE = 0.40
n = 290
DS2
R2 = 0.88
slope = 0.75
intercept = 0.00
SEE = 0.07
n = 37
f
DS1
Borisov (2010; Eqn. 5)
R2 = 0.73
slope = 0.32
intercept = 0.20
SEE = 0.39
n = 290
DS2
R2 = 0.86
slope = 0.49
intercept = 0.03
SEE = 0.07
n = 37
(XFe2O3/XFeO)liq Measured
(XFeO1.464/XFeO)liq Measured
(XFe2O3/XFeO)liq Sack et al. (1980)
(XFe2O3/XFeO)liq Kilinic et al. (1983)
(XFeO1.464/XFeO)liq K&C (1988)
(XFe2O3/XFeO)liq K&C (1991; Eq. 7)
(XFe2O3/XFeO)liq Jayasuria et al. (Eq. 12)
(XFe2O3/XFeO)liq Borisov (2010; Eqn. 5)

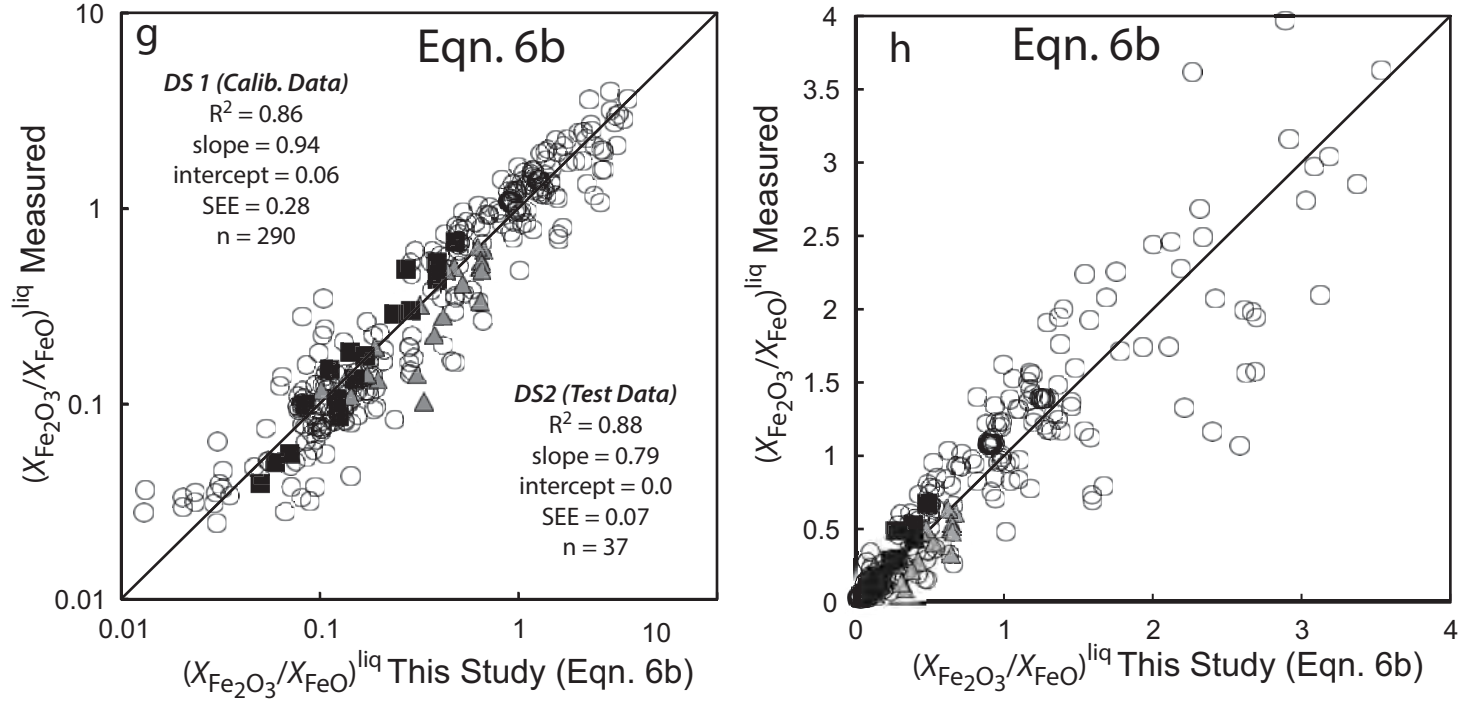
g
Eqn. 6b
DS 1 (Calib. Data)
R2 = 0.86
slope = 0.94
intercept = 0.06
SEE = 0.28
n = 290
DS2 (Test Data)
R2 = 0.88
slope = 0.79
intercept = 0.0
SEE = 0.07
n = 37
(XFe2O3/XFeO)liq Measured
(XFe2O3/XFeO)liq This Study (Eqn. 6b)
h
Eqn. 6b
(XFe2O3/XFeO)liq Measured
(XFe2O3/XFeO)liq This Study (Eqn. 6b)

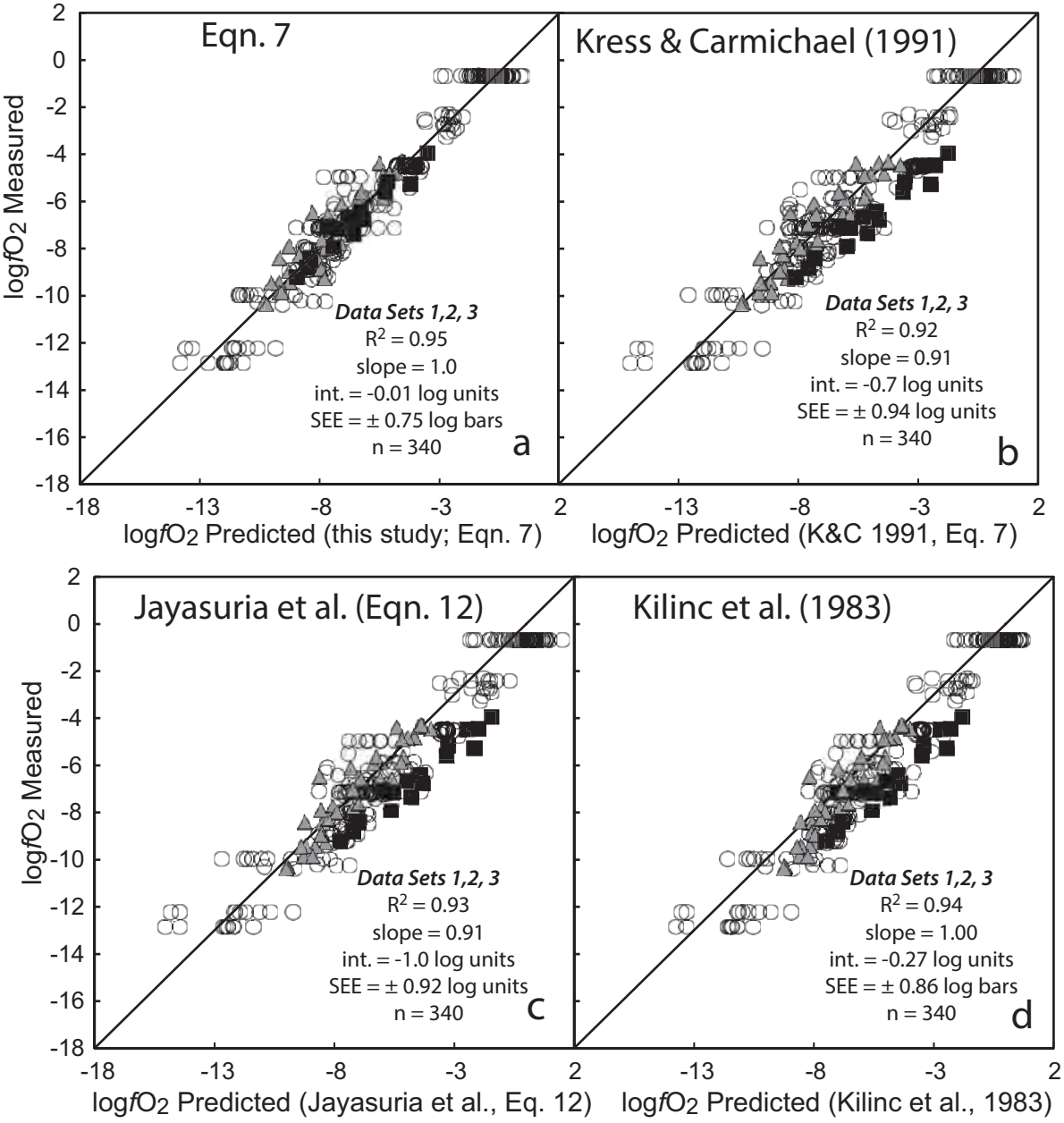
Eqn. 7
Data Sets 1,2, 3
R2 = 0.95
slope = 1.0
int. = -0.01 log units
SEE = ± 0.75 log bars
n = 340
a
Kress & Carmichael (1991)
Data Sets 1,2, 3
R2 = 0.92
slope = 0.91
int. = -0.7 log units
SEE = ± 0.94 log units
n = 340
b
Jayasuria et al. (Eqn. 12)
Data Sets 1,2, 3
R2 = 0.93
slope = 0.91
int. = -1.0 log units
SEE = ± 0.92 log units
n = 340
c
Kilinc et al. (1983)
Data Sets 1,2, 3
R2 = 0.94
slope = 1.00
int. = -0.27 log units
SEE = ± 0.86 log bars
n = 340
d
logfO2 Measured
logfO2 Predicted (this study; Eqn. 7)
logfO2 Predicted (K&C 1991, Eq. 7)
logfO2 Predicted (Jayasuria et al., Eq. 12)
logfO2 Predicted (Kilinc et al., 1983)
2
0
-2
-4
-6
-8
-10
-12
-14
-16
-18
-18
-13
-8
-3
2

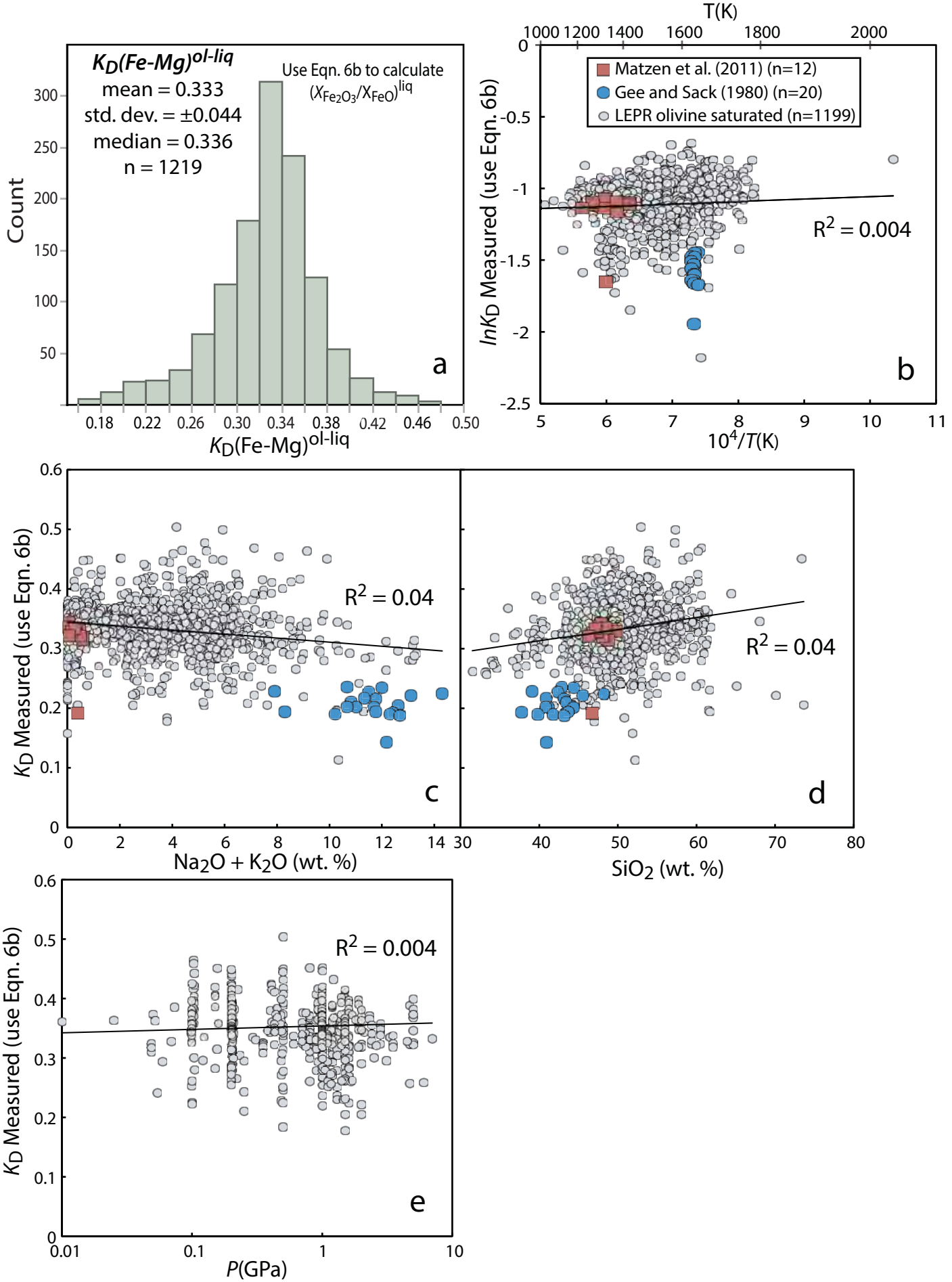
$K_D(Fe\text{-}Mg)^{ol\text{-}liq}$
mean = 0.333
std. dev. = ±0.044
median = 0.336
n = 1219
Use Eqn. 6b to calculate $(X_{Fe_2O_3}/X_{FeO})^{liq}$
Count
$K_D(Fe\text{-}Mg)^{ol\text{-}liq}$
a
T(K)
Matzen et al. (2011) (n=12)
Gee and Sack (1980) (n=20)
LEPR olivine saturated (n=1199)
R^2 = 0.004
lnK_D Measured (use Eqn. 6b)
$10^4/T(K)$
b
R^2 = 0.04
K_D Measured (use Eqn. 6b)
$Na_2O + K_2O$ (wt. %)
c
R^2 = 0.04
SiO_2 (wt. %)
d
R^2 = 0.004
K_D Measured (use Eqn. 6b)
P(GPa)
e

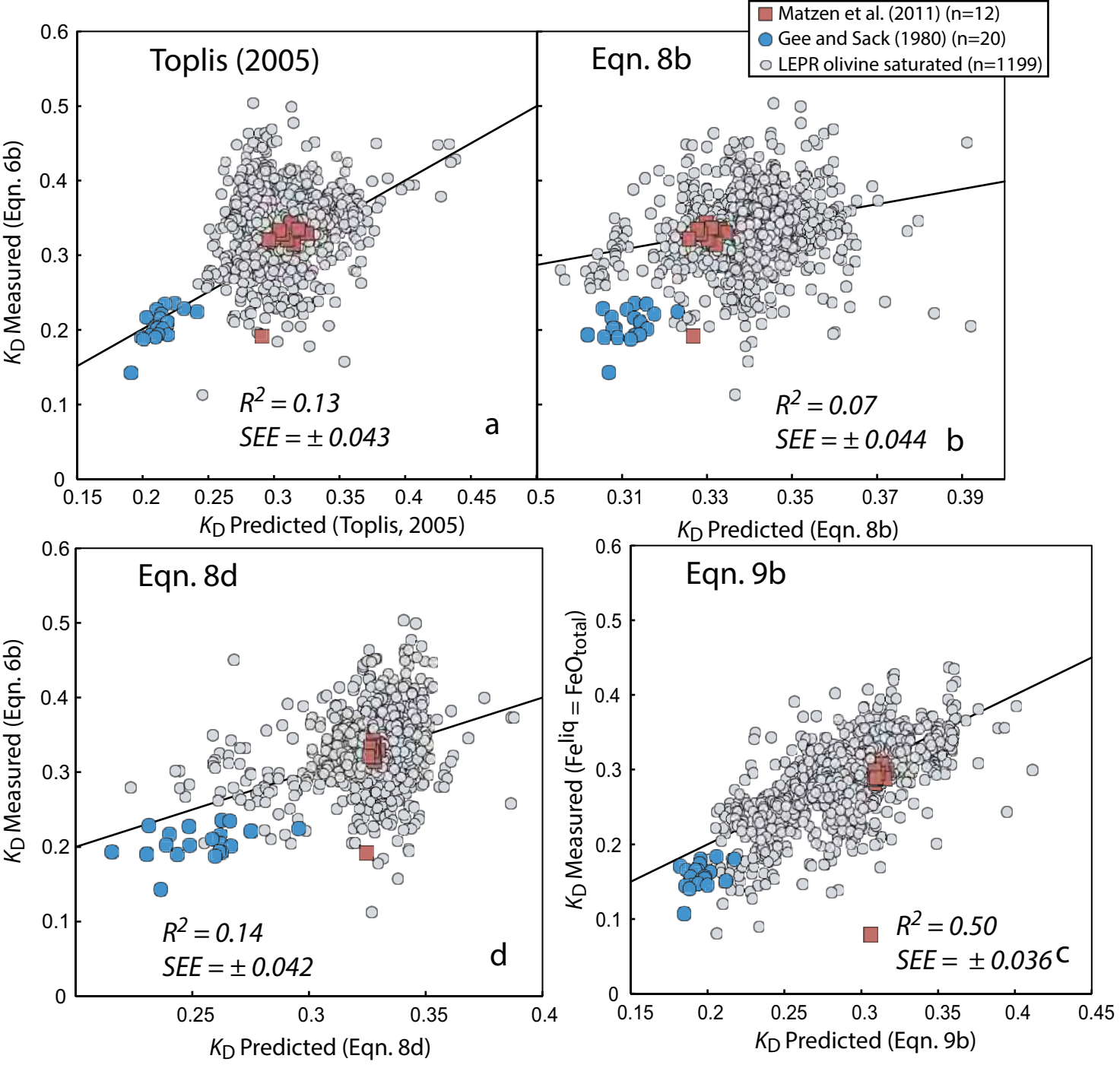
Matzen et al. (2011) (n=12)
Gee and Sack (1980) (n=20)
LEPR olivine saturated (n=1199)
Toplis (2005)
Eqn. 8b
Eqn. 8d
Eqn. 9b
K_D Measured (Eqn. 6b)
K_D Predicted (Toplis, 2005)
K_D Predicted (Eqn. 8b)
K_D Predicted (Eqn. 8d)
K_D Measured ($Fe^{liq} = FeO_{total}$)
K_D Predicted (Eqn. 9b)
$R^2 = 0.13$
$SEE = \pm 0.043$
a
$R^2 = 0.07$
$SEE = \pm 0.044$
b
$R^2 = 0.14$
$SEE = \pm 0.042$
d
$R^2 = 0.50$
$SEE = \pm 0.036$
c

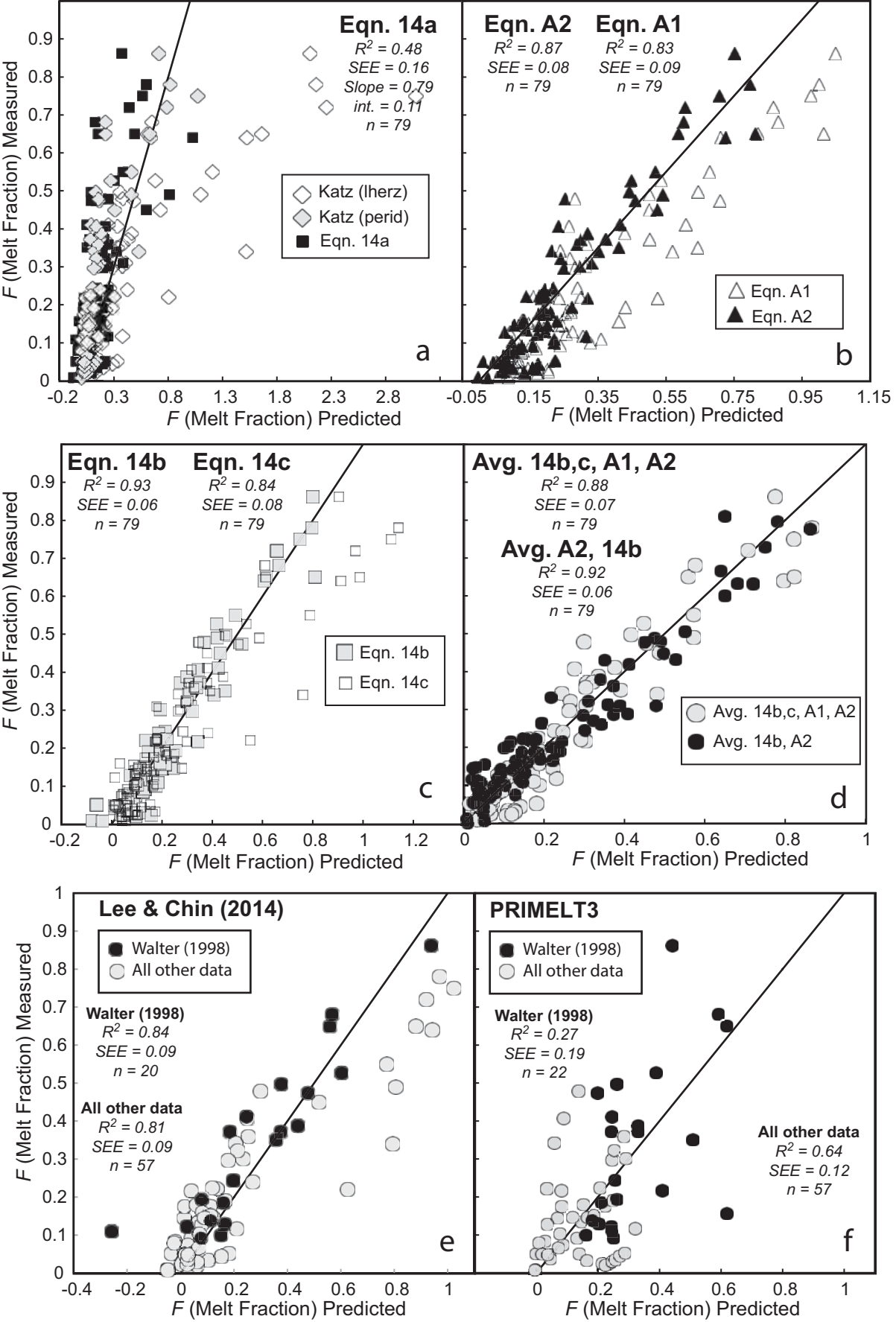
Eqn. 14a
R2 = 0.48
SEE = 0.16
Slope = 0.79
int. = 0.11
n = 79
Katz (lherz)
Katz (perid)
Eqn. 14a
a
Eqn. A2
R2 = 0.87
SEE = 0.08
n = 79
Eqn. A1
R2 = 0.83
SEE = 0.09
n = 79
Eqn. A1
Eqn. A2
b
F (Melt Fraction) Measured
F (Melt Fraction) Predicted
Eqn. 14b
R2 = 0.93
SEE = 0.06
n = 79
Eqn. 14c
R2 = 0.84
SEE = 0.08
n = 79
Eqn. 14b
Eqn. 14c
c
Avg. 14b,c, A1, A2
R2 = 0.88
SEE = 0.07
n = 79
Avg. A2, 14b
R2 = 0.92
SEE = 0.06
n = 79
Avg. 14b,c, A1, A2
Avg. 14b, A2
d
Lee & Chin (2014)
Walter (1998)
All other data
Walter (1998)
R2 = 0.84
SEE = 0.09
n = 20
All other data
R2 = 0.81
SEE = 0.09
n = 57
e
PRIMELT3
Walter (1998)
All other data
Walter (1998)
R2 = 0.27
SEE = 0.19
n = 22
All other data
R2 = 0.64
SEE = 0.12
n = 57
f

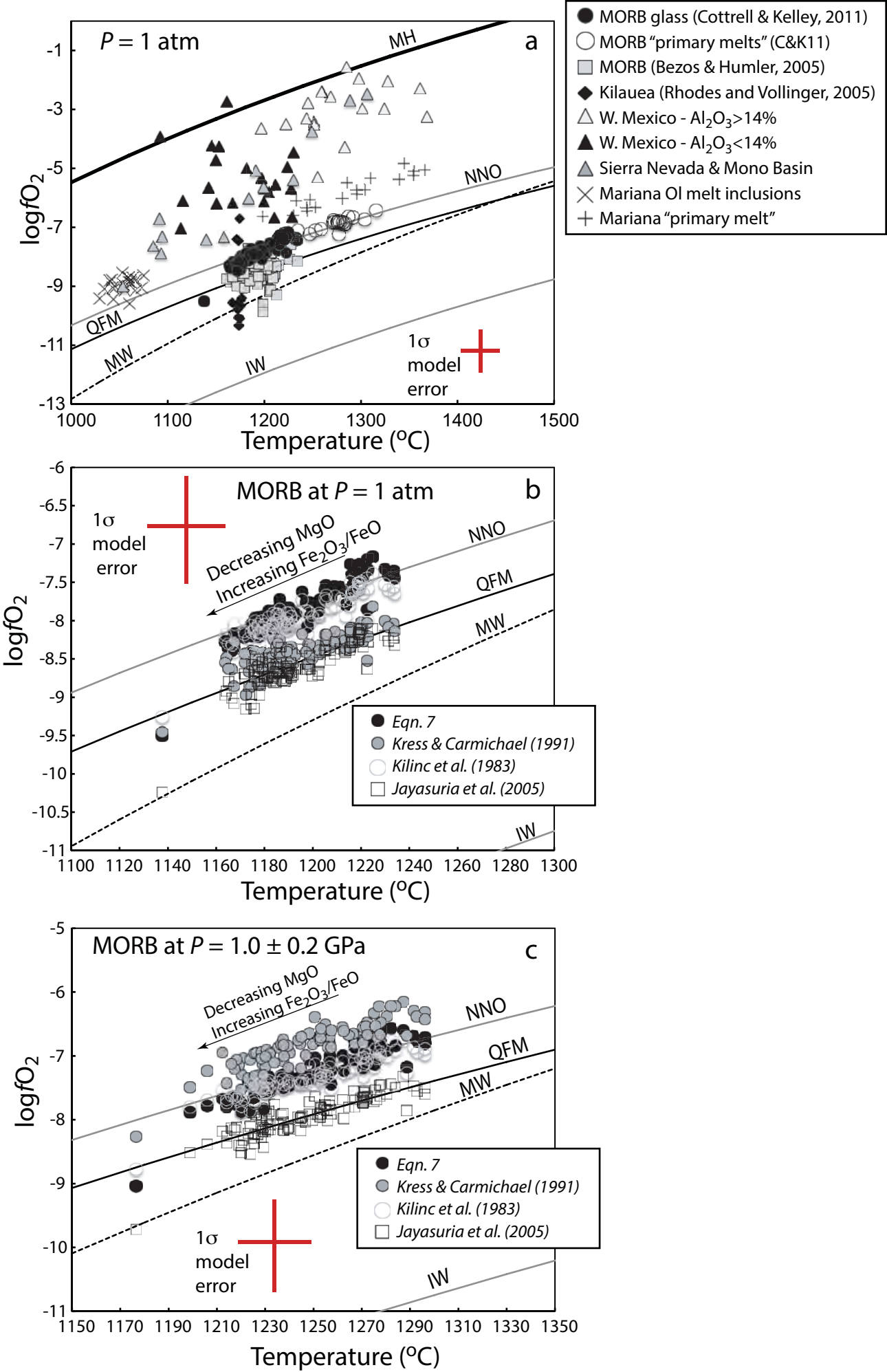
MORB glass (Cottrell & Kelley, 2011)
MORB "primary melts" (C&K11)
MORB (Bezos & Humler, 2005)
Kilauea (Rhodes and Vollinger, 2005)
W. Mexico - Al2O3>14%
W. Mexico - Al2O3<14%
Sierra Nevada & Mono Basin
Mariana Ol melt inclusions
Mariana "primary melt"
P = 1 atm
a
MH
NNO
QFM
MW
IW
1σ model error
logfO2
Temperature (°C)
MORB at P = 1 atm
b
1σ model error
Decreasing MgO
Increasing Fe2O3/FeO
Eqn. 7
Kress & Carmichael (1991)
Kilinc et al. (1983)
Jayasuria et al. (2005)
MORB at P = 1.0 ± 0.2 GPa
c

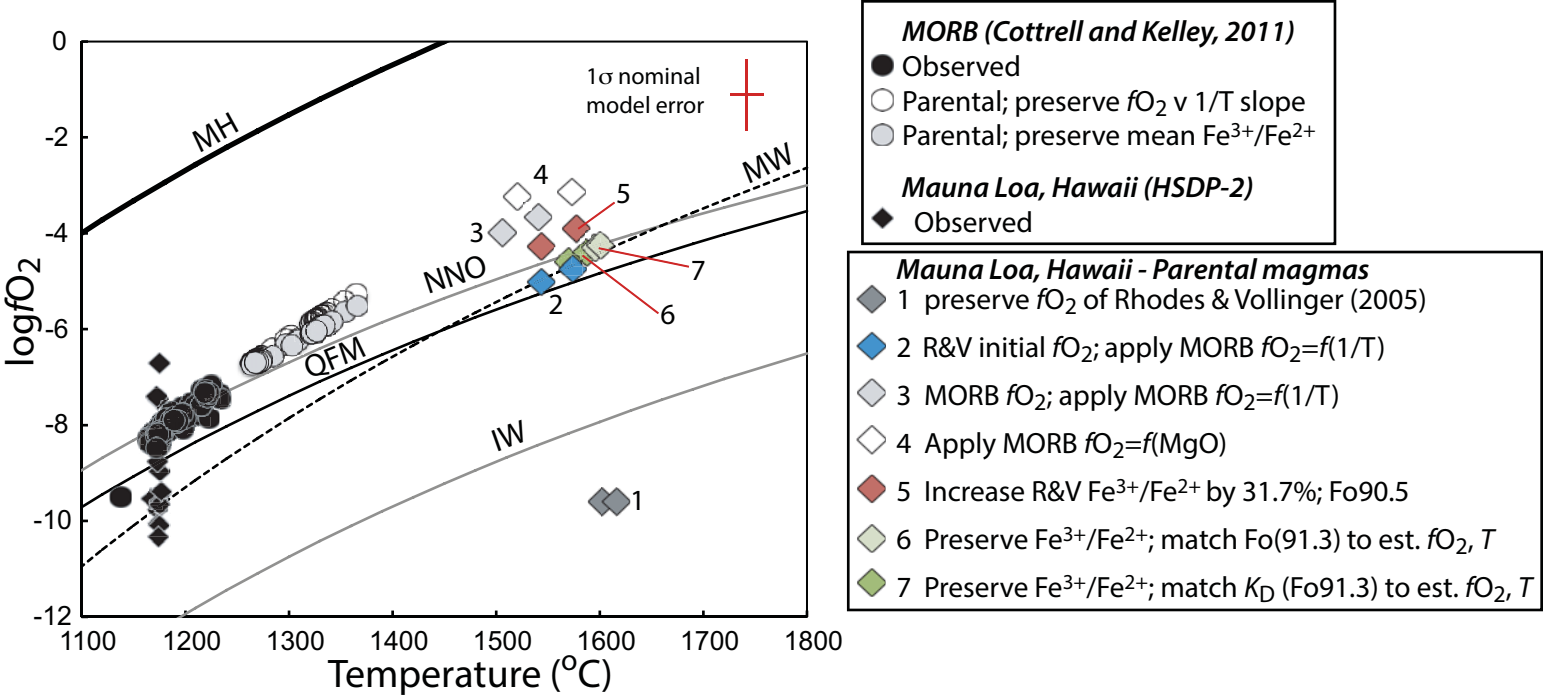
0
-2
-4
-6
-8
-10
-12
logfO2
1100
1200
1300
1400
1500
1600
1700
1800
Temperature (°C)
1σ nominal model error
MH
MW
NNO
QFM
IW
1
2
3
4
5
6
7
MORB (Cottrell and Kelley, 2011)
Observed
Parental; preserve fO2 v 1/T slope
Parental; preserve mean Fe3+/Fe2+
Mauna Loa, Hawaii (HSDP-2)
Observed
Mauna Loa, Hawaii - Parental magmas
1 preserve fO2 of Rhodes & Vollinger (2005)
2 R&V initial fO2; apply MORB fO2=f(1/T)
3 MORB fO2; apply MORB fO2=f(1/T)
4 Apply MORB fO2=f(MgO)
5 Increase R&V Fe3+/Fe2+ by 31.7%; Fo90.5
6 Preserve Fe3+/Fe2+; match Fo(91.3) to est. fO2, T
7 Preserve Fe3+/Fe2+; match KD (Fo91.3) to est. fO2, T

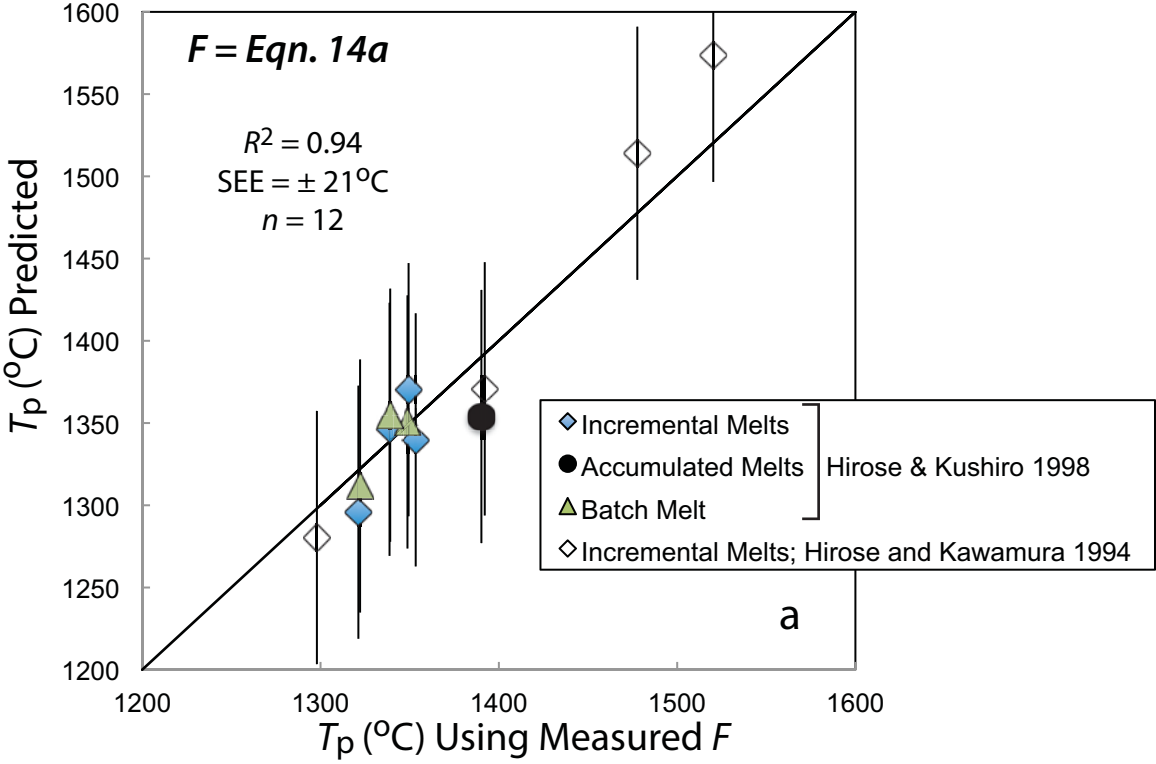
F = Eqn. 14a
R2 = 0.94
SEE = ± 21°C
n = 12
Incremental Melts
Accumulated Melts
Batch Melt
Hirose & Kushiro 1998
Incremental Melts; Hirose and Kawamura 1994
a
Tp (°C) Predicted
Tp (°C) Using Measured F
1200
1250
1300
1350
1400
1450
1500
1550
1600

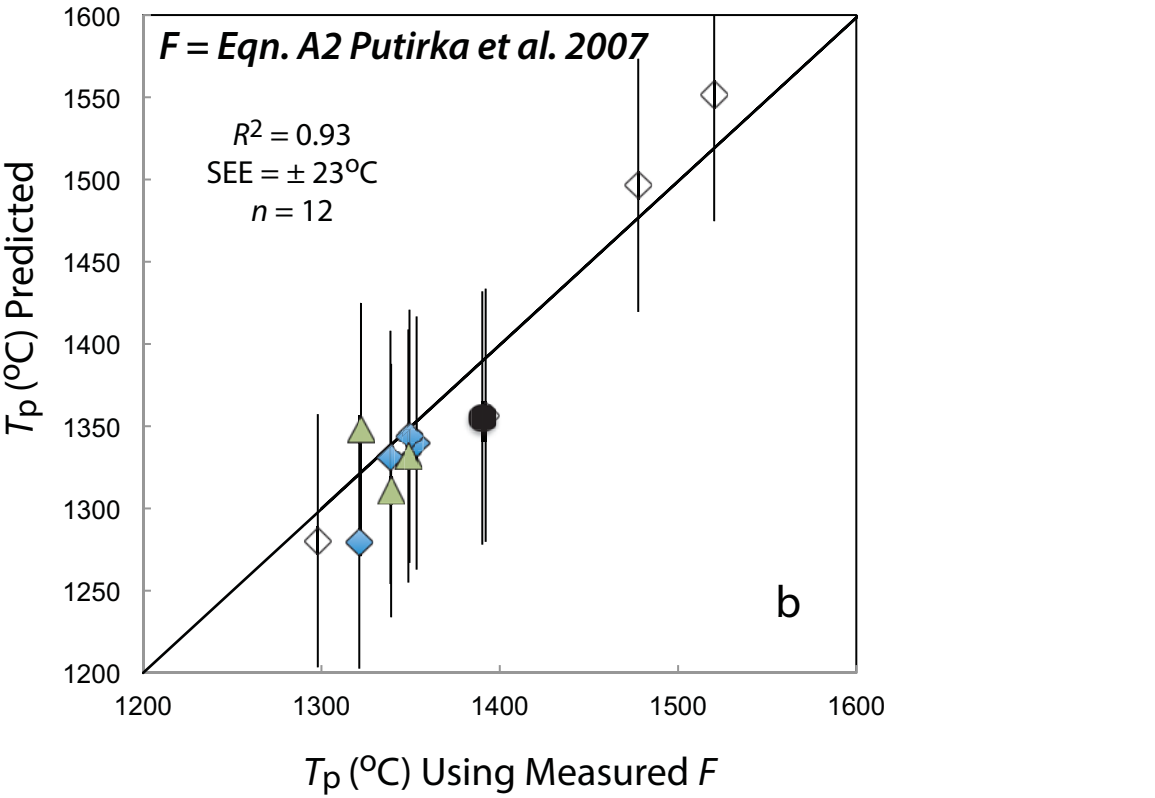
F = Eqn. A2 Putirka et al. 2007
R2 = 0.93
SEE = ± 23°C
n = 12
b
Tp (°C) Predicted
Tp (°C) Using Measured F
1200
1250
1300
1350
1400
1450
1500
1550
1600

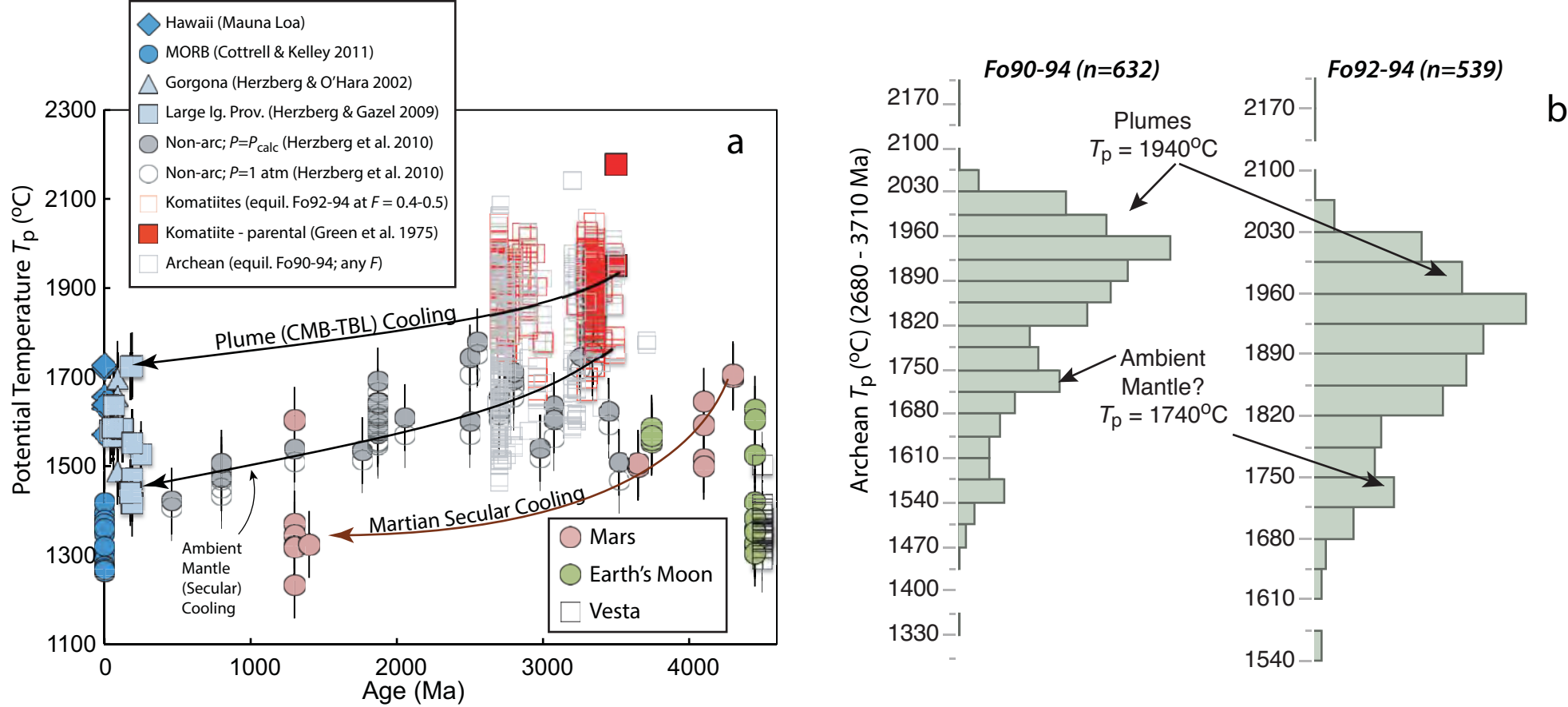
Hawaii (Mauna Loa)
MORB (Cottrell & Kelley 2011)
Gorgona (Herzberg & O'Hara 2002)
Large Ig. Prov. (Herzberg & Gazel 2009)
Non-arc; P=Pcalc (Herzberg et al. 2010)
Non-arc; P=1 atm (Herzberg et al. 2010)
Komatiites (equil. Fo92-94 at F = 0.4-0.5)
Komatiite - parental (Green et al. 1975)
Archean (equil. Fo90-94; any F)
a
Plume (CMB-TBL) Cooling
Martian Secular Cooling
Ambient Mantle (Secular) Cooling
Mars
Earth's Moon
Vesta
Potential Temperature Tp (°C)
Age (Ma)
2300
2100
1900
1700
1500
1300
1100
0
1000
2000
3000
4000
Fo90-94 (n=632)
Fo92-94 (n=539)
b
Archean Tp (°C) (2680 - 3710 Ma)
Plumes
Tp = 1940°C
Ambient Mantle?
Tp = 1740°C
2170
2100
2030
1960
1890
1820
1750
1680
1610
1540
1470
1400
1330

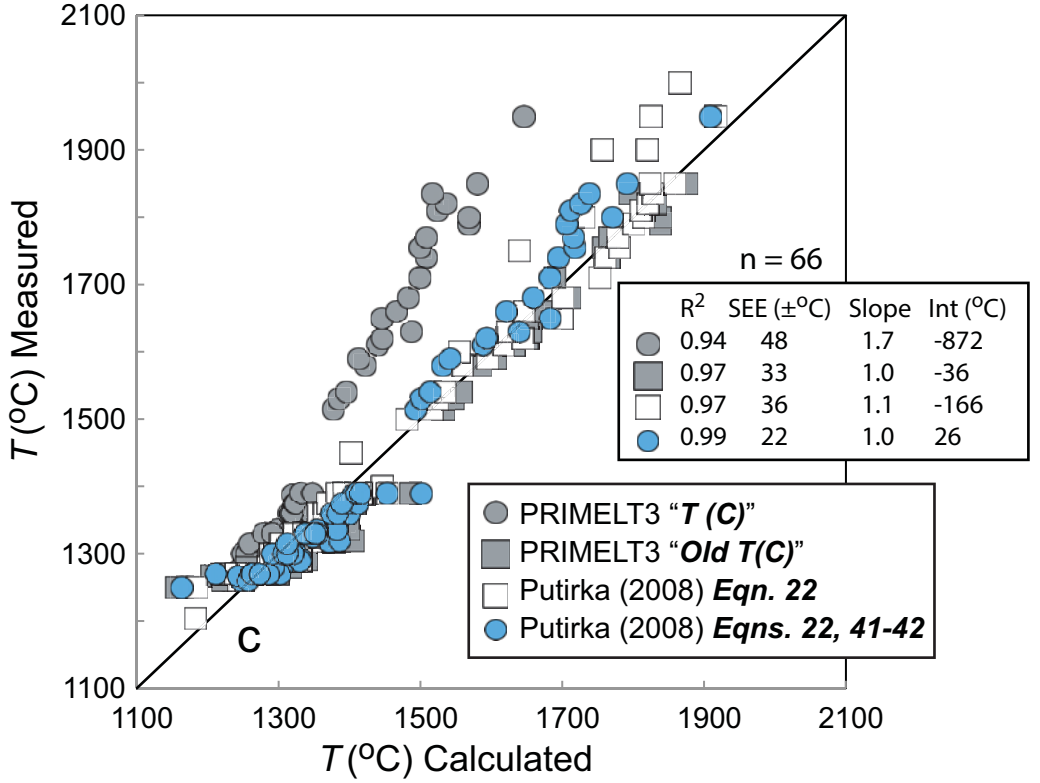
2100
1900
1700
1500
1300
1100
T (°C) Measured
1100
1300
1500
1700
1900
2100
T (°C) Calculated
n = 66
R2 SEE (±°C) Slope Int (°C)
0.94 48 1.7 -872
0.97 33 1.0 -36
0.97 36 1.1 -166
0.99 22 1.0 26
PRIMELT3 "T (C)"
PRIMELT3 "Old T(C)"
Putirka (2008) Eqn. 22
Putirka (2008) Eqns. 22, 41-42
c

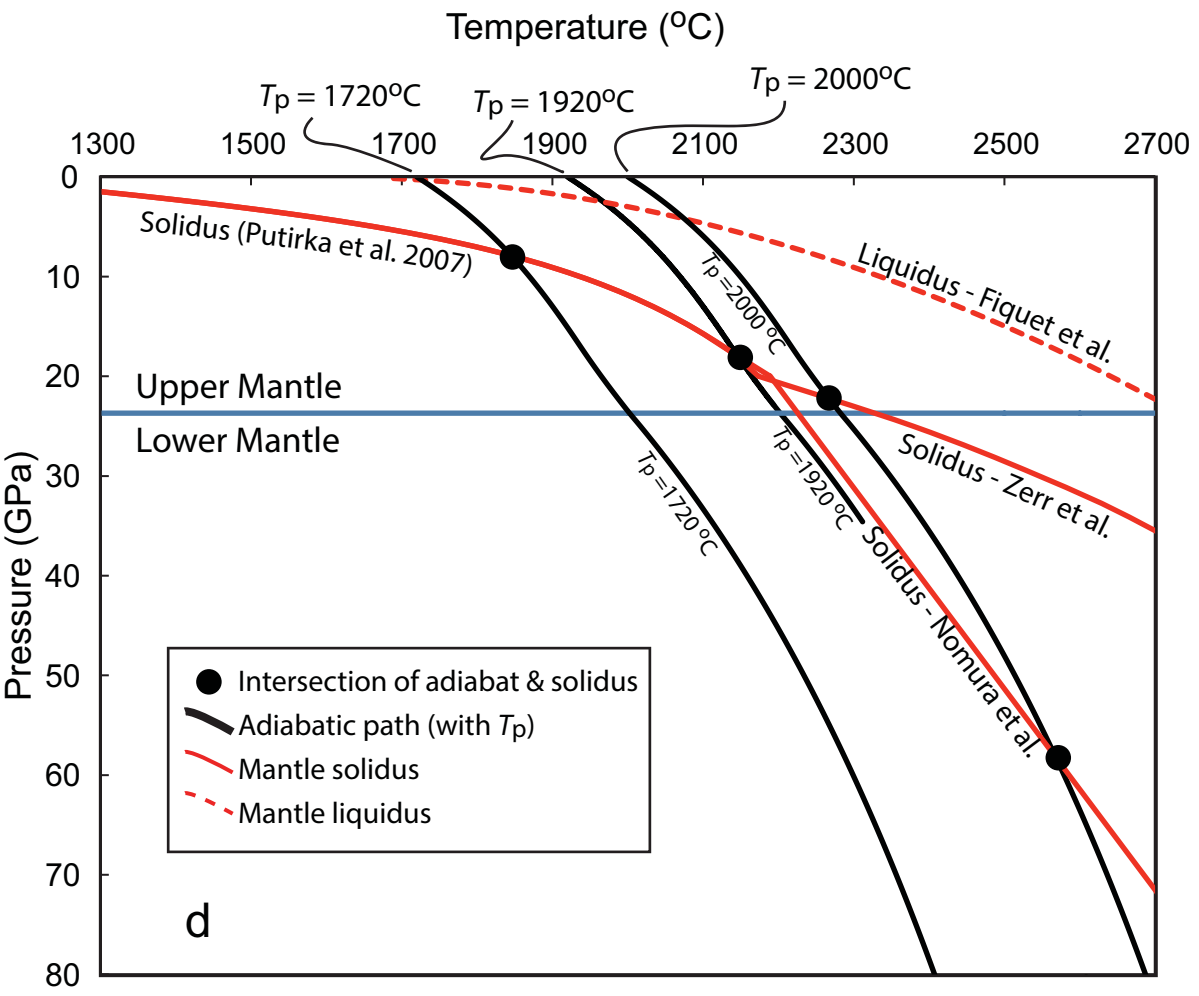
Temperature (°C)
Tp = 1720°C
Tp = 1920°C
Tp = 2000°C
1300
1500
1700
1900
2100
2300
2500
2700
0
10
20
30
40
50
60
70
80
Pressure (GPa)
Solidus (Putirka et al. 2007)
Liquidus - Figuet et al.
Tp =2000 °C
Upper Mantle
Lower Mantle
Solidus - Zerr et al.
Tp =1920 °C
Tp =1720 °C
Solidus - Nomura et al.
Intersection of adiabat & solidus
Adiabatic path (with Tp)
Mantle solidus
Mantle liquidus
d